

EXPERIMENTAL SLOT FILM COOLING EFFECTIVENESS
MEASUREMENTS FOR VARYING INJECTION ANGLES
IN ACCELERATING AND NON-ACCELERATING FLOWS

by

BRUNO PHILIPPE MEHLMAN

SUBMITTED TO THE DEPARTMENT OF
MECHANICAL ENGINEERING
IN PARTIAL FULFILLMENT OF THE
REQUIREMENTS FOR THE COMBINED DEGREE OF

MASTER OF SCIENCE IN MECHANICAL ENGINEERING

and

BACHELOR OF SCIENCE IN MECHANICAL ENGINEERING

at the

MASSACHUSETTS INSTITUTE OF TECHNOLOGY
February, 1990

© Bruno Philippe Mehlman, 1990. All rights reserved.

The author hereby grants to MIT permission to reproduce and to
distribute copies of this thesis document in whole or in part.

Signature of Author _____

Department of Mechanical Engineering
February 1, 1990

Certified by _____

Bora Mikic
Professor of Mechanical Engineering
Thesis Supervisor

Accepted by _____

Ain A. Sonin
Chairman, Department Committee

MASSACHUSETTS INSTITUTE
OF TECHNOLOGY

AUG 13 1990

LIBRARIES
ARCHIVES

EXPERIMENTAL SLOT FILM COOLING EFFECTIVENESS
MEASUREMENTS FOR VARYING INJECTION ANGLES
IN ACCELERATING AND NON-ACCELERATING FLOWS

by

Bruno Philippe Mehlman

Submitted to the Department of Mechanical Engineering
on February 1, 1990 in partial fulfillment of the
requirements for the combined Degree of Bachelor and
Master of Science in Mechanical Engineering

ABSTRACT

A parametric study is performed to investigate the effects of slot injection to mainstream flow angle on adiabatic film cooling effectiveness for an accelerating and non-accelerating mainstream flow. Five different injection angles are investigated ($\alpha = 0.0^\circ, 5.0^\circ, 8.5^\circ, 11.5^\circ$ and 15.0°). The accelerating mainstream flow test is performed with the 8.5° injection angle configuration. Acceleration factors at the slot breakout location are equal to $Ka = 5.7-7.5 \cdot 10^6$. Correlations are realized for the film effectiveness (η) in terms of the non-dimensionalized downstream distance (x/Ms). An optimum injection angle equal to 8.5° is observed for (x/Ms) values less than 60. Lower film effectiveness values are observed when acceleration is introduced into the mixing region. A numerical study using FLUENT is performed for a two-dimensional slot configuration with tangentially injected coolant into a mainstream flow. Computational results indicate a much higher increase in effectiveness values as a function of mass-velocity ratio compared to the experimental results.

Thesis Supervisor: Prof. Bora Mikic

Title: Professor of Mechanical Engineering

ACKNOWLEDGEMENTS

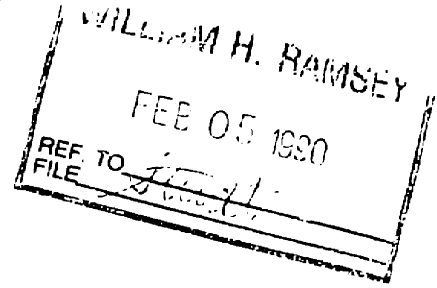
I would like to thank Professor Bora Mikic who has been my advisor ever since my early days at MIT. He provided advice, encouragement, enthusiasm and support along with his witty humor.

I would like to thank the support and the patience of the members of the Heat Transfer group in particular that of Dave Kercher, Sam Spring and Mo Taslim.

Financial support of the General Electric Company, Aircraft Engines, Lynn Massachusetts is gratefully acknowledged.

Dept. of Mechanical Engineering
for Graduates
Company File
Summary File
Student File

ENGINEERING INTERNSHIP PROGRAM
SCHOOL OF ENGINEERING
MASSACHUSETTS INSTITUTE OF TECHNOLOGY
CAMBRIDGE, MA 02139



THESES REVIEW LETTER

ATTENTION: William H. Ramsey Director, Room 1-211

SUBJECT: Master's Thesis of _____

(Student Name)

The attached thesis, Experimental Rot Film Cooling Effectiveness
Measurements for varying injection angles
in accelerating and non-accelerating flows has been
(Title)

reviewed by the undersigned _____

(Company Name)

representatives and confirmed that it does not contain details
objectionable from the standpoint of _____

(Company Name)

In addition, we understand that the aforementioned thesis report
becomes the permanent property of M.I.T., will be placed in the
M.I.T. Library within one month of the date of submission and may
not be published wholly or in part except by the authorization
of the Department of _____, in which the

(Department Name)

student is enrolled. (It is understood that authorization is
granted to the Company for such limited publication as the
Company's prior contractual obligations may require.)

General Electric Company Name

Company Supervisor
2-1-90

Student Name

Approved By (for Company)

Title: _____

Date: 2/1/90

Date: 2-1-90

Date: _____

TABLE OF CONTENTS

Nomenclature	5
List of Figures	6
List of Tables	8
I. Introduction	9
I.1 The Need for Advanced Cooling Techniques in Gas Turbines.....	9
I.2 Film Cooling Applied to Gas Turbine Airfoil Designs	11
I.3 Previous Work	11
I.3 Objectives of the Investigation.....	15
II. Experimental Program	17
II.1 Introduction.....	17
II.2 Test Apparatus.....	17
II.3 Test Procedure.....	27
II.4 Data Reduction	29
II.5 Error Analysis.....	31
III. Experimental Results.....	34
III.1 Introduction.....	34
III.2 Effect of Injection Angle on Film Effectiveness.....	34
III.2.1 Non-Accelerating Mainstream Flow.....	34
III.2.2 Accelerating Mainstream Flow	38
III.3 Correlation of Film Effectiveness Data	40
III.4 Summary of Correlations	44
III.5 Comparison with Previous Work	46
IV. Numerical Investigation.....	49
IV.1 Introduction.....	49
IV.2 Numerical Model.....	49
IV.3 Numerical Procedure	51
IV.4 Results for Tangential Film Cooling Injection.....	53
IV.5 Comparison with Experimental Results.....	64
V. Conclusions	66
References.....	67
Appendix A: Conduction Error	68
Appendix B: Error Analysis.....	70
Appendix C: Film Effectiveness Data.....	74
Appendix D: Sample Data Reduction	95

NOMENCLATURE

h	=	local heat transfer coefficient
H	=	mainstream plenum height
k	=	thermal conductivity
Ka	=	acceleration parameter $(\nu/U^2)(\partial U/\partial x)$
m	=	air mass flow rate
M	=	mass-velocity ratio $(\rho U)/(\rho U)_s$
q	=	heat flux
Re_x	=	Reynolds number $(U x / \nu)$
s	=	injection slot height
t	=	injection slot lip thickness
T	=	temperature
x	=	distance downstream from slot
U	=	velocity
W	=	mainstream plenum width
w	=	injection slot width
α	=	injection angle
η	=	film effectiveness $(T_g - T_{aw})/(T_g - T_s)$
ν	=	kinematic viscosity
ρ	=	density

Subscripts

aw	=	adiabatic wall value
f	=	film
s	=	property value at injection slot conditions
g	=	property value at mainstream air conditions

LIST OF FIGURES

Figure 1-1: Typical turbine blade internal and external cooling features	10
Figure 1-2: Slot configurations for air-to-air film cooling	15
Figure 2-1: Schematic diagram of experimental apparatus	19
Figure 2-2: Detailed drawing of test rig (not to scale).....	21
Figure 2-3a: Cross-sectional view of section for tangential film cooling injection and non- accelerating mainstream flow.....	23
Figure 2-3b: Cross-sectional view of section for angled film-cooling injection ($\alpha=5.0,8.5,11.5,15.0$) with non-accelerating mainstream flow.....	24
Figure 2-3c: Cross-sectional view of section for angled film-cooling injection ($\alpha=8.5$) with accelerating mainstream flow.....	25
Figure 2-4: Nozzle profile for 8.5 degree injection angle and accelerating mainstream flow.....	26
Figure 2-5: Test plate instrumentation	28
Figure 2-6: Weighted average of film effectiveness across slot width	31
Figure 3-1: Film effectiveness (η) vs. blowing ratio (M) for 0 deg. injection angle	35
Figure 3-2: Film effectiveness (η) vs. blowing ratio (M) for 5.0 deg. injection angle.....	35
Figure 3-3: Film effectiveness (η) vs. blowing ratio (M) for 8.5 deg. injection angle.....	36
Figure 3-4: Film effectiveness (η) vs. blowing ratio (M) for 11.5 deg. injection angle	36
Figure 3-5: Film effectiveness (η) vs. blowing ratio (M) for 15.0 deg. injection angle	37
Figure 3-6: Mixing due to flow instability.....	38
Figure 3-7: Film effectiveness (η) vs. blowing ratio (M) for 8.5 deg. injection angle with accelerating mainstream flow.....	39
Figure 3-8: Land film effectiveness (η) vs. blowing ratio (M) for 8.5 deg. injection angle with accelerating mainstream flow.....	39
Figure 3-9: Film effectiveness (η) vs. (x/Ms) for 0 deg. injection angle	41
Figure 3-10: Film effectiveness (η) vs. (x/Ms) for 5.0 deg. injection angle	41
Figure 3-11: Film effectiveness (η) vs. (x/Ms) for 8.5 deg. injection angle	42
Figure 3-12: Film effectiveness (η) vs. (x/Ms) for 11.5 deg. injection angle.....	42
Figure 3-13: Film effectiveness (η) vs. (x/Ms) for 15.0 deg. injection angle.....	43
Figure 3-14: Film effectiveness (η) vs. (x/Ms) for 8.5 deg. injection angle with accelerating mainstream flow	43
Figure 3-15: Film effectiveness (η) vs. (x/Ms) for 8.5 deg. injection angle. Accelerating vs. non-accelerating mainstream flow	44

Figure 3-16: Film effectiveness (η) vs. (x/Ms) for varying injection angles ($\alpha=5.0,8.5,11.5,15.0$).....	46
Figure 3-17: Comparison of experimental results with previous measurements of Seban [4]....	47
Figure 3-18: Comparison of experimental results with previous measurements of Joubert [8]...	48
Figure 4-1: Numerical model of experimental test rig for tangential film cooling injection.....	50
Figure 4-2: Finite difference grid.....	52
Figure 4-3: Velocity vector plot ($M=0.2$).....	54
Figure 4-4: Velocity vector plot ($M=0.4$).....	55
Figure 4-5: Velocity vector plot ($M=0.6$).....	56
Figure 4-6: Velocity vector plot ($M=0.8$).....	57
Figure 4-7: Velocity vector plot ($M=1.0$).....	58
Figure 4-8: Temperature profile ($M=0.2$).....	59
Figure 4-9: Temperature profile ($M=0.4$).....	60
Figure 4-10: Temperature profile ($M=0.6$).....	61
Figure 4-11: Temperature profile ($M=0.8$).....	62
Figure 4-12: Temperature profile ($M=1.0$).....	63
Figure 4-13: Numerical results (tangential injection).....	65
Figure 4-14: Experimental results (tangential injection).....	65
Figure A-1: 1-D conduction model.....	68
Figure A-2: Control volume.....	69

LIST OF TABLES

Table 2-1: Geometrical parameters and operating conditions	18
Table 2-2: Test section geometrical parameters and operating conditions	22
Table 3-1: Summary of correlations.....	45
Table 4-1: Boundary conditions fo rnumerical model.....	51
Table A-1: Condition error analysis.....	69
Table B-1: Film effectiveness uncertainty analysis.....	71
Table B-2: Mass flow rate uncertainty analysis.	71
Table B-3: Test section measurement uncertainty analysis.....	72
Table B-4: Mass-velocity uncertainty analysis.....	73

I. Introduction

I.1 The Need for Advanced Cooling Techniques in Gas Turbines

In today's advanced gas turbine engines, the limits of operating temperatures are continually pushed higher in order to meet present and future performance requirements for jet engines. In fact, typical gas turbine operating temperatures are much greater than the allowable metal temperatures of turbine airfoils. As a result of the increase in turbine inlet operating temperatures, the need for a better understanding of current cooling methods in the hope of developing more effective state-of-the-art cooling techniques applied to turbine airfoil design has become a necessity. Some of the common methods of providing thermal protection to the airfoil are based on complex applications of internal convective cooling, impingement cooling and external film cooling using slot or hole injection configurations. A typical airfoil incorporating the above mentioned cooling techniques is shown in *Figure 1-1*.

In the blade or vane cooling process, compressor bleed air is introduced into the hollow core of the blade and is channeled through complex serpentine passages. The surface of the internal passages are roughened with turbulence promoting devices located at discrete positions to increase the internal heat transfer coefficients between the blade's surface and the internal cooling air. The channeled air is then ejected out the blade via rows of holes strategically located at the leading edge and at multiple locations along the blade's convex and concave surfaces. The exiting coolant is used to convectively cool the surfaces, especially in regions of high heat fluxes, by reducing the source gas temperature next to the external surface. This external convective process is called film cooling.

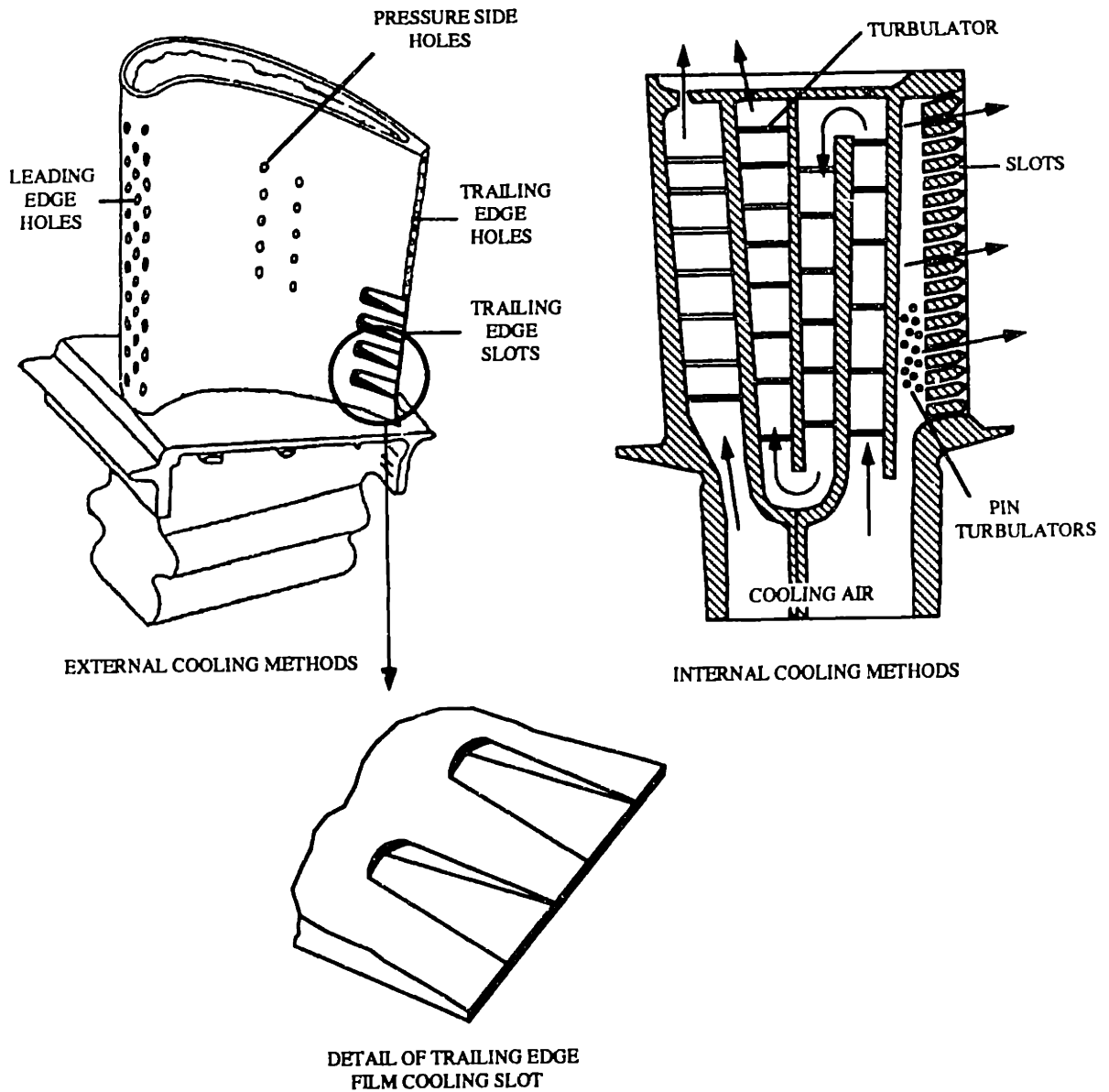


Figure 1-1: Typical turbine blade internal and external cooling features

I.2 Film Cooling Applied to Gas Turbine Airfoil Designs

Film cooling has become a widely used cooling technique as a means of protecting solid surfaces exposed to hot gaseous environments. Typically, relatively cool air is injected into the boundary layer on the surface to be protected, thereby creating an insulating layer (film) between the surface and the hot gaseous stream flowing over it. To be effective, film cooling must provide acceptable metal surface temperatures as well as a reasonably uniform temperature distribution over the blade's surface to limit thermal stresses as a result of large temperature gradients. Uniform and effective film cooling is accomplished by injecting coolant air at various locations along the blade's surface. Multiple film cooling holes are used in a showerhead configuration to cool the blade's leading edge surface. Single or multiple rows of injection holes are also located on the blade's concave and convex surfaces. The blade's trailing edge is film cooled by ejecting air through holes or rows of slots on the concave surface near the trailing edge. This life limiting area, subject to the highest thermal loads on the blade's surface, is of primary importance. Improvements in the predictive capability of the cooling requirements have significant payoffs in terms of enhanced turbine life, development cost, and turbine engine performance.

I.3 Previous Work

Much research has been devoted to the topic of film cooling and there exists a considerable amount of experimental data for air-to-air film cooling for different slot geometries and various primary and secondary flow fields. A comprehensible survey of film cooling was performed by Goldstein [1] and the information presented in the following paragraphs draws heavily from this reference with an emphasis placed on experimental results obtained for

adiabatic film effectiveness for two-dimensional slots configurations which could be applied to predict airfoil pressure side trailing edge film cooling.

Convective heat transfer associated with film cooling is determined by using a film heat transfer coefficient h_f and an adiabatic wall or film temperature T_{aw} as described by Goldstein [1]:

$$q_f = h_f(T_w - T_{aw}) \quad (1)$$

where T_w is the local wall temperature. Since the adiabatic wall temperature is not only a function of the slot injection geometry and the primary and secondary flow fields but also the temperatures of the two gas streams, it is convenient to define a dimensionless adiabatic wall temperature η , called film cooling effectiveness, in term of T_{aw} . For low speed constant property flow the film cooling effectiveness is given by:

$$\eta = \frac{T_g - T_{aw}}{T_g - T_s} \quad (2)$$

where T_g is the mainstream gas temperature and T_s is the secondary or cooling injection gas temperature. Thus, the film cooling effectiveness η varies from unity at the point of injection where $T_{aw} = T_s$ to zero far downstream from the slot where the adiabatic wall temperature approaches the mainstream gas temperature due to the mixing between the injected fluid and the mainstream. Both h_f and η must be known and both depend at least on the slot injection geometry, the coolant-to-mainstream mass-velocity ratio (M), and the distance (x) measured downstream from the injection slot. Then, for any given mainstream and coolant temperatures and a prescribed wall heat flux, the wall temperature distribution can be obtained using Eq. 1.

Most film cooling studies have primarily focused on the experimental determination of the adiabatic wall temperature distribution. Wieghardt [2] was the first to experimentally investigate film cooling for applications in de-icing of airplane wings. In Wieghardt's investigation, heated air was injected into a cold mainstream through a slot angled at approximately 30° relative to the mainstream wall. *Figure 1-2* presents Wieghardt's slot

configuration along with other investigated slot geometries. The resulting film effectiveness data was correlated according to the following relationship:

$$\text{for } x/Ms > 100 \quad \eta = 21.8 (x/Ms)^{-0.8} \quad (3)$$

where (M) is the mass-velocity ratio defined below by Eq. 4 and (x/s) is the downstream distance non-dimensionalized with respect to the slot height (s).

$$M = \frac{(\rho U)_s}{(\rho U)_g} \quad (4)$$

Hartnett, et al. [3], used the same slot geometry as Wieghardt's but performed film-cooling instead of film-heating measurements and reported a similar correlation but with a lower numerical constant:

$$\text{for } x/Ms > 60 \quad \eta = 16.9 (x/Ms)^{-0.8} \quad (5)$$

Seban, et al. [4], conducted an experimental study on film cooling by injecting the secondary air flow both normally and tangentially to the main flow with a slightly different slot configuration than Wieghardt. For tangential injection with a small slot lip thickness (t), the following results were obtained:

$$\text{for } x/Ms < 40 \quad \eta = 0.16 Re_s^{1/3} (x/Ms)^{-0.25} \quad (6)$$

$$\text{for } x/Ms > 40 \quad \eta = 0.83 Re_s^{1/3} (x/Ms)^{-0.7} \quad (7)$$

where Re_s is the Reynolds number based on the slot height (s).

Seban [5] also studied film cooling effectiveness downstream of a stepdown slot with tangential injection and correlated his data at low blowing rates with the following relation:

$$\text{for } M < 1 \quad \eta = 25 M^{0.4} (x/Ms)^{-0.8} \quad (8)$$

Chin, et al. [6], using a slot configuration similar to [4] have obtained values of the dimensionless adiabatic wall temperature for various injection rates. The correlation achieved for these data gives higher results than the data of Seban and Wieghardt:

$$\text{for } U_s/U_g < 1 \quad \eta = 1 \quad A < 15$$

$$\begin{aligned}\eta &= 1.5 A^{-0.15} & 15 \leq A \leq 72 \\ \eta &= 12.7 A^{-0.65} & A > 72\end{aligned}$$

$$\text{with } A = (\rho_s/\rho_g)^{-0.5} Re_s^{-0.3} Re_L^{0.19} (x/Ms) \quad (9)$$

$$\begin{aligned}\text{for } 1 < U_s/U_g < 2 & \quad \eta = 1 & \quad B < 10 \\ & \quad \eta = 1.41 B^{-0.15} & \quad 10 \leq B \leq 60 \\ & \quad \eta = 3.93 B^{-0.40} & \quad B > 60\end{aligned}$$

$$\text{with } B = (\rho_s/\rho_g)^{-1.5} Re_s^{-0.3} Re_L^{0.19} (x/s) \quad (10)$$

where Re_L is the Reynolds number based on the hydrodynamic starting length (L).

Papell and Trout [7] reported film cooling effectiveness for tangential injection at large temperature differences between the free stream and the injected air. The slot configuration was similar to that of Seban. Several different correlations were proposed for the effectiveness for various ranges of mass injection:

$$\begin{aligned}\text{for } \eta \leq 0.73, M \leq 2.0 \text{ and } x/s > 14 & \quad \eta = 12.6 M (x/s)^{-0.72} (T_s/T_g)^{0.5} \\ & \quad x/s < 14 \quad \eta = 1.86 M^{0.44} (x/s)^{-0.36} \\ \text{for } \eta > 0.73, M \leq 4.0 \text{ and } x/s > 18.6 & \quad \eta = 1.15 M^{0.18} (x/s)^{-0.11} \\ & \quad x/s < 18.6 \quad \eta = 0.83 M^{0.18}\end{aligned}$$

Samuel and Joubert [8] measured effectiveness downstream of a tangential injection slot similar to Seban et al. [4]. The data was correlated as follows:

$$\begin{aligned}\text{for } M < 1 & \quad M^{-1.75} x/s < 18 & \quad \eta = 1 \\ & \quad 18 < M^{-1.75} x/s < 600 & \quad \eta = 4.2 (M^{-1.75} x/s)^{-0.5} \quad (11)\end{aligned}$$

$$\begin{aligned}\text{for } M > 1 & \quad M^{0.375} x/s < 25 & \quad \eta = 1 \\ & \quad 25 < M^{0.375} x/s < 400 & \quad \eta = 3.0 (M^{0.375} x/s)^{-0.35} \quad (12)\end{aligned}$$

Papell [9] also investigated the effects of injection angle on film cooling effectiveness and made measurements with angles of 45, 80 and 90° relative to the direction of the free-stream. The measurements were carried out with large temperature differences and with Mach numbers

mainly greater than 0.5. Sivasegaram and Whitelaw [10] measured film cooling effectiveness for a similar slot configuration as in [9] with injection angles 30, 60 and 90° relative to the direction of the free-stream. Both these investigations indicated a significant decrease in film effectiveness as the injection angle increases.

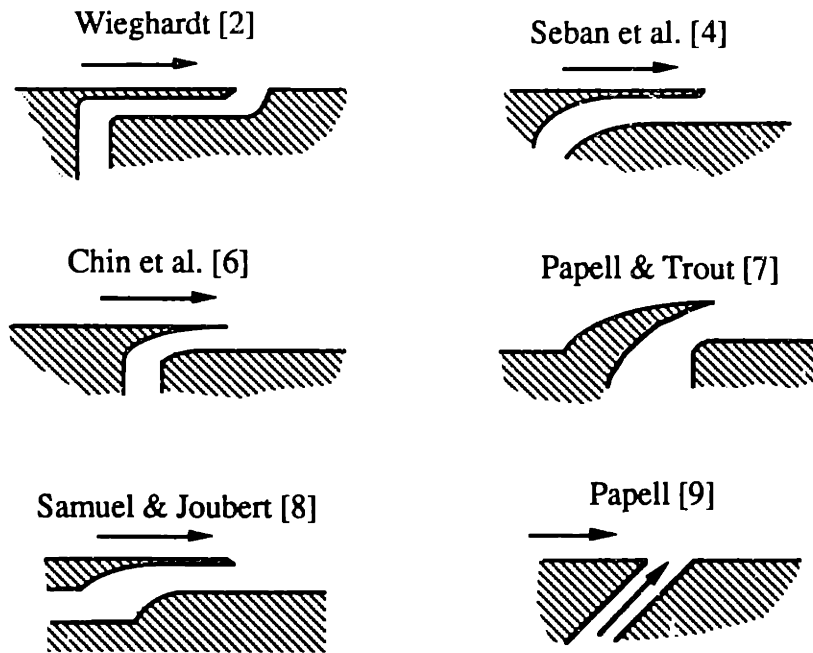


Figure 1-2: Slot configurations for air-to-air film cooling

I.4 Objectives of the Investigation

As discussed in the previous paragraph, most of the experimental studies on film cooling were investigations with tangential secondary air injection and with a single injection slot geometry. Typical turbine airfoils have a small trailing edge thickness for aerodynamic reasons and do not allow for tangential injection but instead the secondary film cooling air is injected at a discrete angle relative to the mainstream flow. Furthermore, for reasons of mechanical integrity, turbine airfoils have multi-slot configurations at the trailing edge with a

slot lip thickness representing in some cases an appreciable proportion of the slot height. Therefore, the film cooling correlations obtained from the previously mentioned investigations cannot be directly applied to airfoil designs. Most correlations can be applied at large distances downstream from the slot breakout location where the flow has reached a fully developed turbulent boundary layer velocity profile. However, for applications to turbine airfoils, the region of interest is just downstream of the slot breakout where a fully developed profile cannot be assumed because of the complex hydrodynamic flow structure. Therefore, there exists a need to quantitatively understand the geometric parameters pertinent to turbine airfoils which influence the effectiveness of film cooling.

The emphasis in this investigation is to study the effects of injection angles on film cooling effectiveness. Results are reported for five injection angles ($\alpha = 0^\circ, 5.0^\circ, 8.5^\circ, 11.5^\circ$ and 15.0°) spanning the typical jet engine operating range. The effect of accelerating mainstream flow on film cooling effectiveness is also investigated. These results will provide a further understanding and better utilization of airfoil trailing edge slot injection film cooling and will also generate a new data base for design engineers.

To check the predictability of film effectiveness a numerical study is performed using a commercially available finite difference program, FLUENT, developed by Creare Inc. (1985) [14]. A two-dimensional model of the experimental test rig for the case with tangentially injected secondary coolant into a non-accelerating mainstream flow is generated and the flow field as well as the temperature profiles are solved and effectiveness values are calculated and compared with the experimental results.

II. Experimental Program

II.1 Introduction

A 10X wooden scale model of a typical pressure side trailing edge slot configuration is designed and manufactured to study the effects of slot injection angles on film cooling effectiveness for accelerating and non-accelerating mainstream flows. Sizing of the model and determination of experimental operating conditions are based on values obtained for typical turbine airfoils. A comparison between experimental testing values and typical jet engine blade conditions is shown in *Table 1-1*. Since the objective of the investigation is to single out the effects of slot injection angle on film effectiveness, the experimental test rig does not account for rounded slots with tapered lands which is a more realistic model of a typical trailing edge film cooled geometry.

Details of the test apparatus will be discussed in this section as well as the test procedures and methods of data reduction. An error analysis is also included in this section.

II.2 Test Apparatus

Figure 2-1 shows a schematic diagram of the experimental apparatus. The apparatus consists of a main air supply, a secondary air supply, a test rig with a multi-slot test section and associated measuring instruments. A compressor station supplies the main and secondary air to the test rig. The compressed mainstream air is filtered, dried and directed through a air heater where its temperature is accurately set to desired levels. The air is then directed through a thin-plate metering orifice and into the test rig's mainstream plenum chamber.

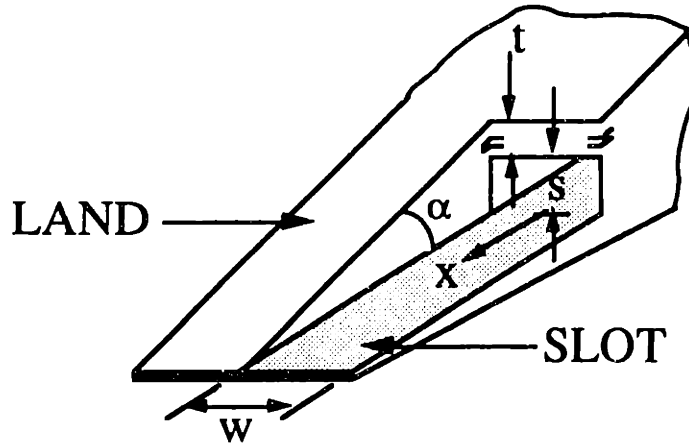


Table 2-1: Geometrical parameters and operating conditions

Typical turbine blade/vane (at slot breakout location)

α deg.	t/s	w/s	x_{max}/s	M	T_g/T_s	$Ka_{x=0}$ $\times 10^{-6}$
5.0 - 15.0	0.5 - 1.25	5.00	10 - 20.0	0.5 - 1.3	1.2 - 2.2	0.6 - 10.0

Experimental test rig (at slot breakout location)

α deg.	t/s	w/s	x_{max}/s	M	T_g/T_s	$Ka_{x=0}$ $\times 10^{-6}$
5.0 - 15.0	1.0	3.1 - 7.1	6.8 - 20.1	0.2 - 1.4	1.2 - 1.4	5.7 - 7.5

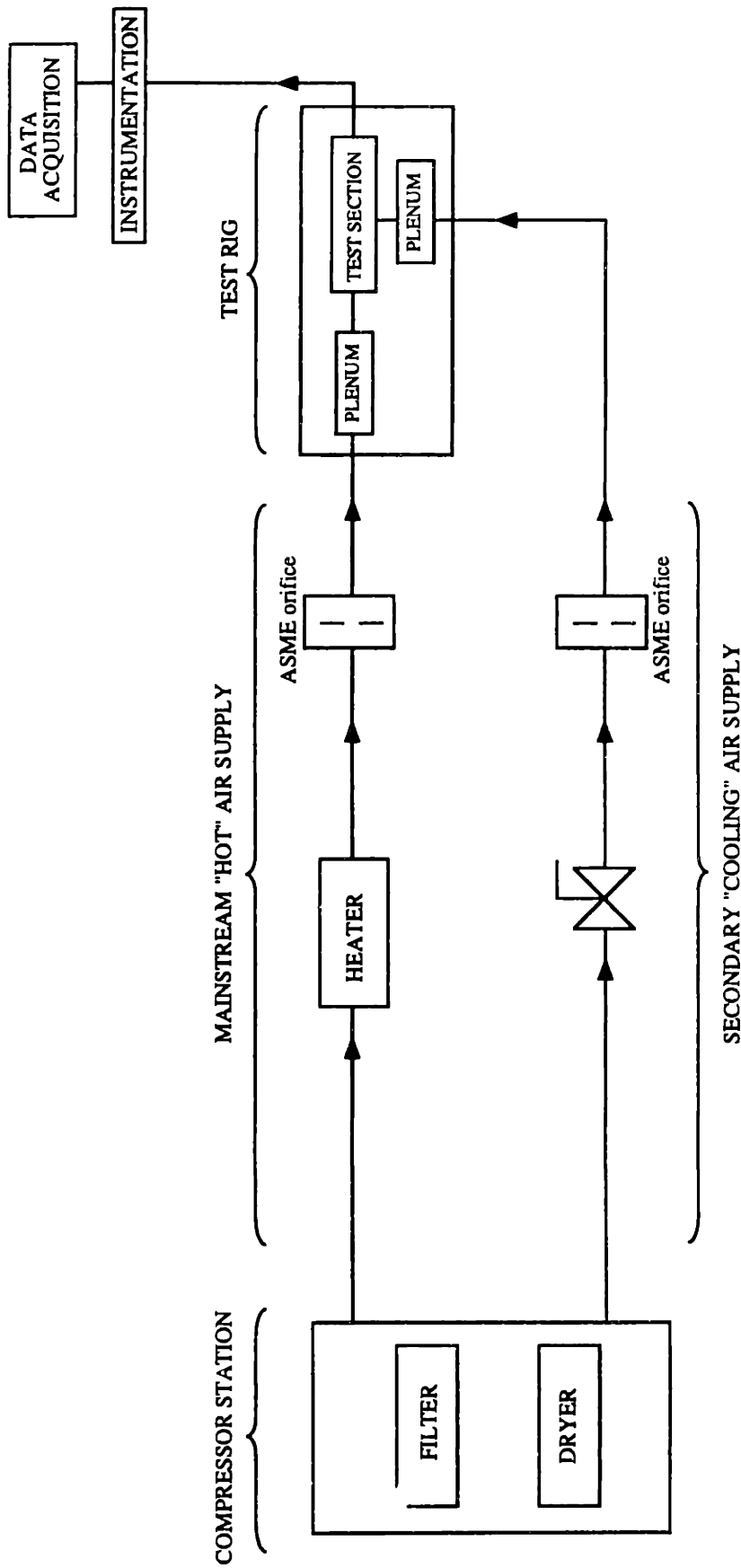


Figure 2-1: Schematic diagram of experimental apparatus

Similarly, the secondary or film-cooling air after being filtered and dried is routed through pressure and flow control valves, a thin-plate metering orifice and into the test rig's secondary plenum chamber.

The test rig used throughout the experimental investigation was manufactured out of maple wood and is shown in *Figure 2-2*. The filtered heated mainstream air is fed into the test rig's mainstream plenum via a 4 in. nominal diameter stainless steel pipe. The mainstream plenum consists of a diffuser section 3 ft. long with inlet dimensions 3 x 3 in. which diffuses to a straightening section 3 ft. long with inlet dimensions 11.65 x 3 in. The change in area of the diffuser section is a smooth transition in order to avoid flow separation and to obtain a uniform and parallel flow distribution prior to entering the test section. The secondary air passes through a plenum which also consists of a diffuser section inlet 1.5 ft. long followed by a straightening section 1 ft. long. The secondary or film cooling air is then channeled through nine parallel slots where further downstream of the slots it is injected into the mainstream flow.

Six different test section configurations were used for the experimental investigation. Originally, one test section was manufactured which corresponded to tangential injection of the secondary film cooling air into the mainstream. This configuration had been used previously to study the effects of the ratio of slot lip thickness-to-slot height on the adiabatic film effectiveness. The same test section is used in this study as a baseline case for tangentially injected secondary air.

The test section is designed as a separate module which in effect links the mainstream plenum to the secondary air supply plenum so that the coolant is injected into the mainstream via a multi-slot injection geometry. A cross sectional view along the length of the test section corresponding to this configuration is shown in *Figure 2-3a*. The entire test section was manufactured from maple, except for the slot lip plate which was made from fiberglass sheet. Wood was used as the material for the test section as well as for almost the entire test rig because of its low thermal conductivity and extremely good machineability. The slot lip plate, which separates the film-cooling air from the mainstream air prior to the slot breakout location,

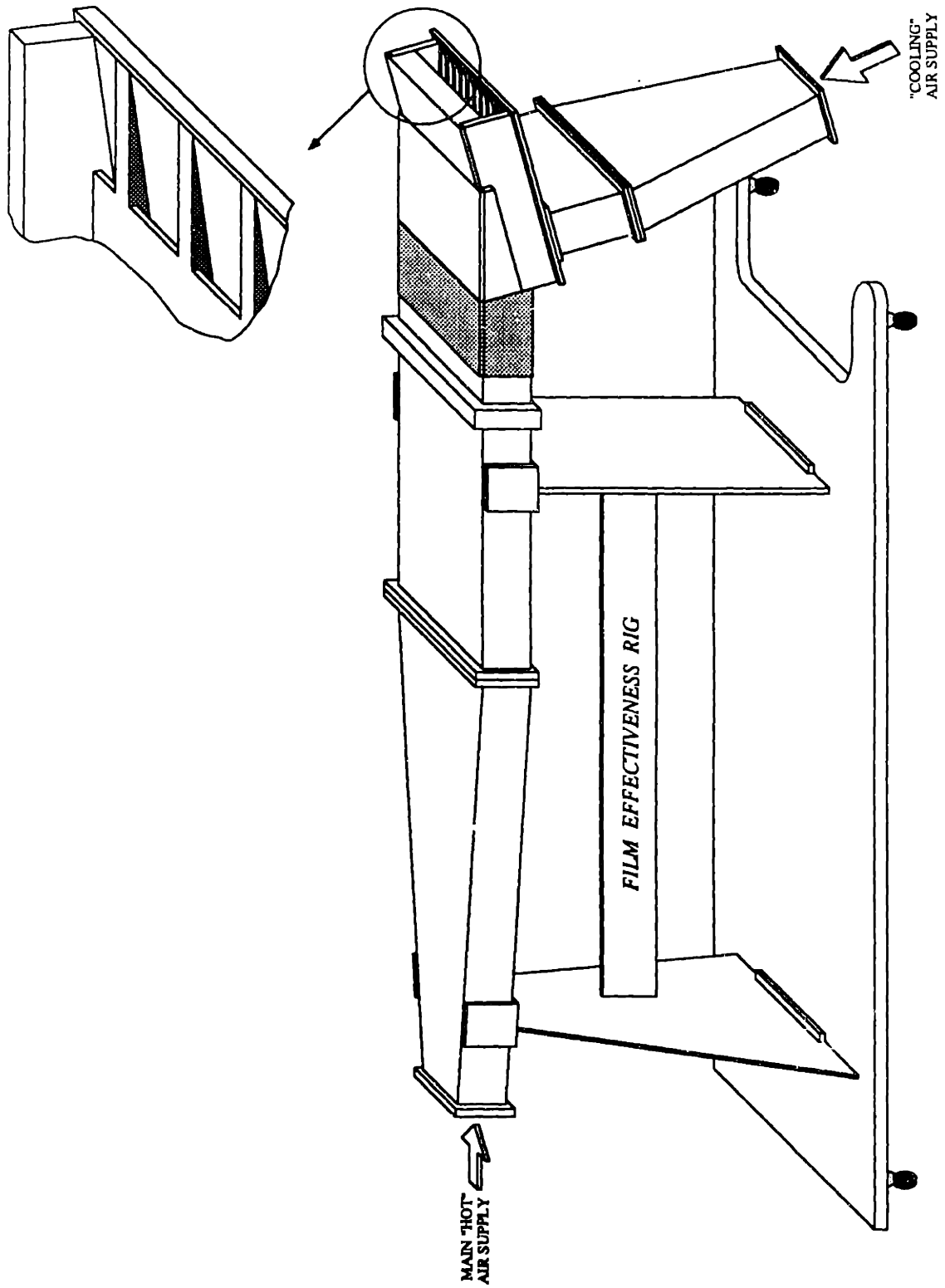


Figure 2-2: Detailed drawing of test rig (not to scale)

rests on eight wooden lands. Eight grooves were made into the 1 in. thick test plate to allow easy installation and removal of the lands and, thereby, testing of a range of geometric combinations. For the tangential injection configuration the slot height (s) is 0.25 in. and the slot lip thickness (t) is 0.25 in. Styrofoam insulation 2 in. thick is placed on the top and side walls of the test section and a 2 in. thick layer of urethane foam was sprayed under the test plate to minimize heat losses to the surroundings.

To perform angled film cooling injection tests, four new lip plates, four sets of lands, and four adapter sections were manufactured corresponding to the four angles of injection ($\alpha = 5.0^\circ, 8.5^\circ, 11.5^\circ, 15.0^\circ$). These new parts were made out of birch. A cross sectional view of a typical test section corresponding to this configuration is shown in *Figure 2-3b*. In order to maintain the lip thickness-to-slot height ratio (t/s) constant and equal to 1 for each tested configuration, the slot height varied as a function of the injection angle (α). *Table 2-2* summarizes the different values for test section geometrical parameters and operating conditions corresponding to each configuration.

For the test performed with an accelerating mainstream flow, the 8.5° slot injection angle configuration was used and a converging nozzle made from birch was placed at the exit of the test section (*Figure 2-3c*) in order to obtain a variation of the free stream velocity. The exact profile and dimensions of the converging nozzle are shown in *Figure 2-4*.

Table 2-2: Test section geometrical parameters and operating conditions

α deg	t in.	H in.	t/s	w/s	x_{max}/s	M	T_g/T_s	$K_{a,\alpha=0}$ $\times 10^{-6}$
0.0	0.250	2.93	1.0	5.00	16.00	0.2 - 1.4	1.24 - 1.31	0.0
5.0	0.175	2.98	1.0	7.14	22.86	0.2 - 1.4	1.22 - 1.26	0.0
8.5	0.299	2.90	1.0	4.18	13.38	0.2 - 1.4	1.25 - 1.30	0.0
11.5	0.407	2.90	1.0	3.07	9.83	0.2 - 1.4	1.24 - 1.29	0.0
15.0	0.536	2.93	1.0	2.33	7.46	0.2 - 1.4	1.28 - 1.33	0.0
8.5	0.299	2.29	1.0	4.18	13.38	0.2 - 1.4	1.32 - 1.37	5.7 - 7.5

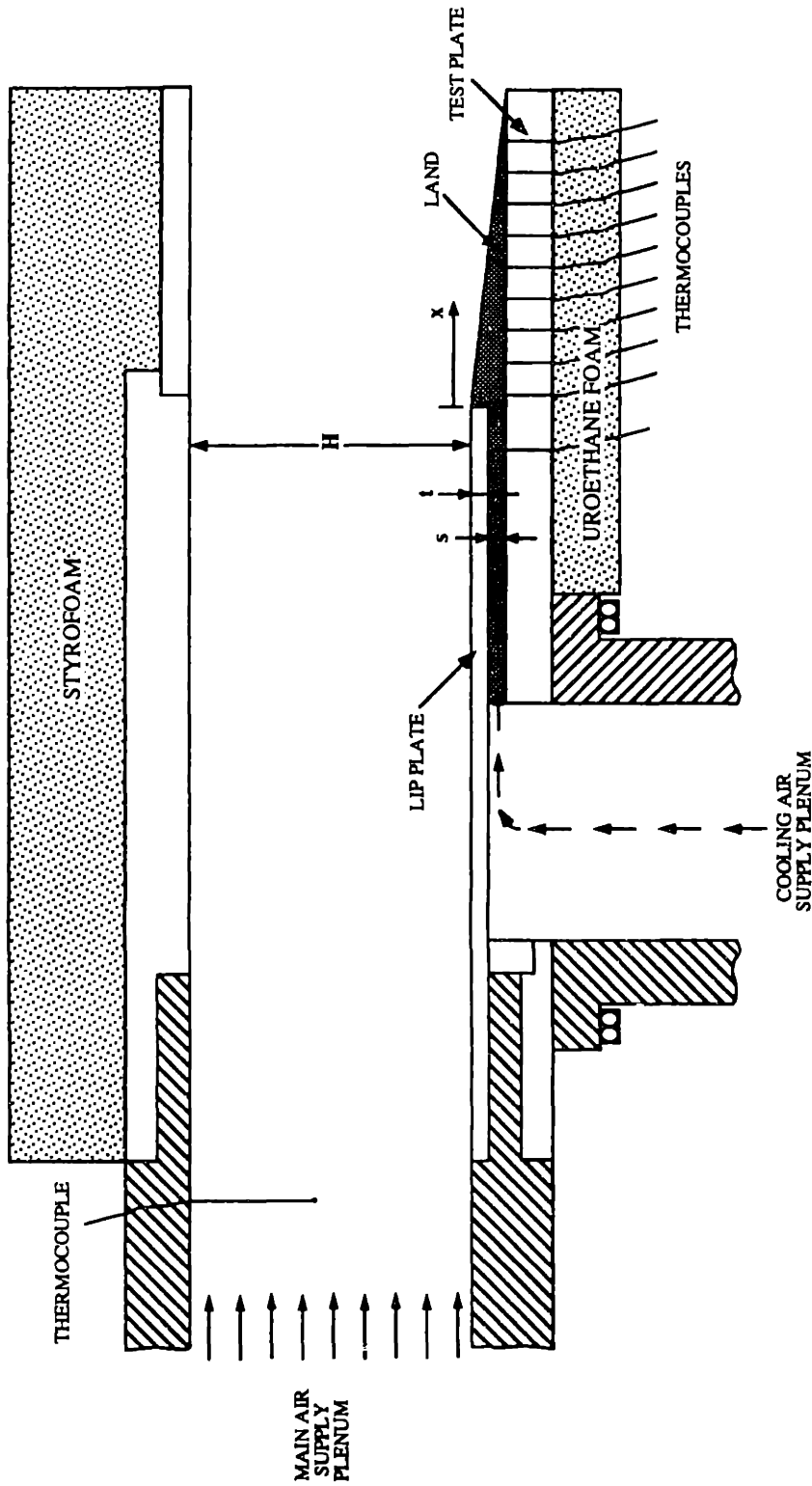


Figure 2-3a: Cross-sectional view of test section for tangential film cooling injection and non-accelerating mainstream flow

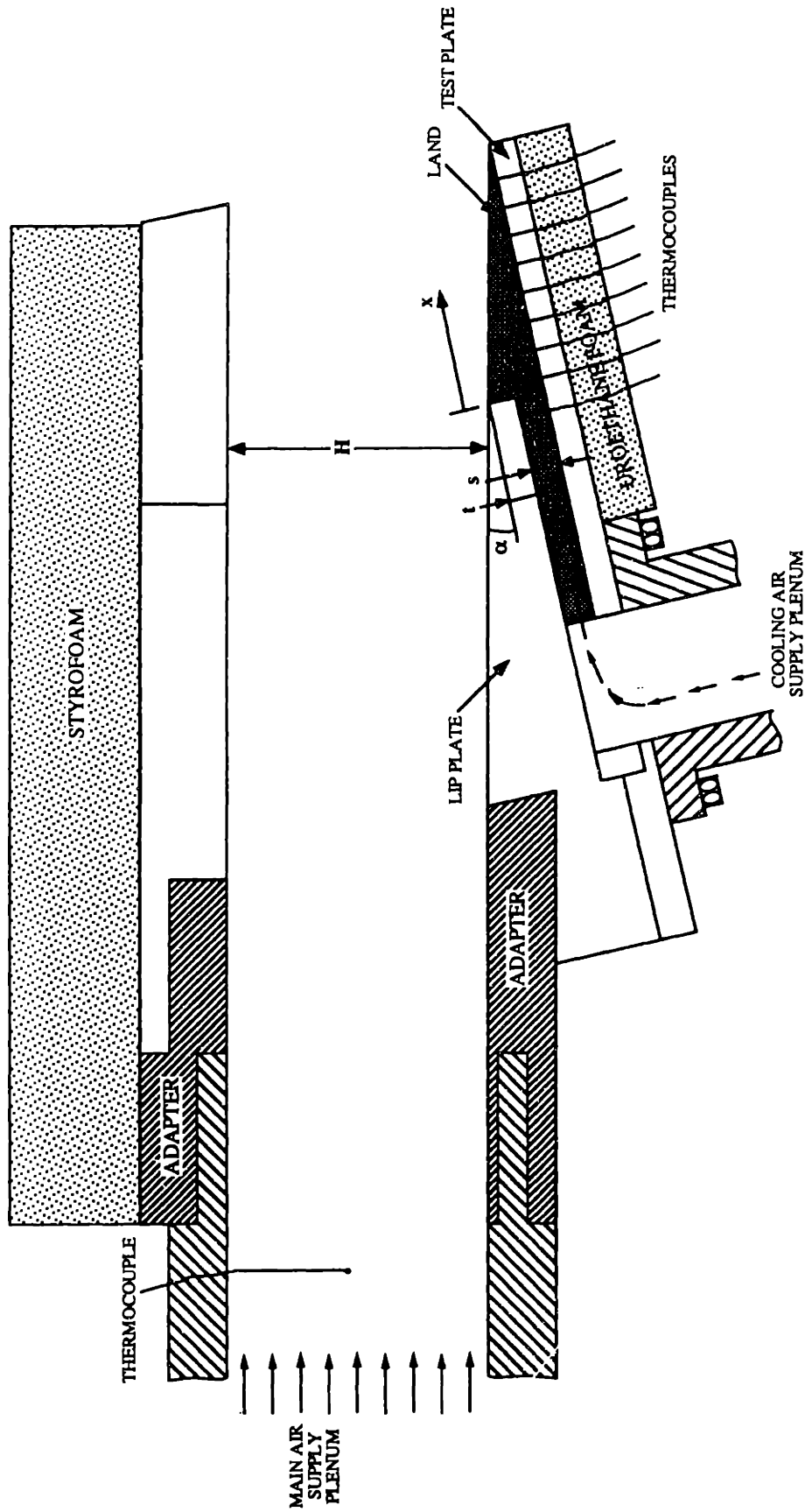


Figure 2-3b: Cross sectional view of test section for angled film-cooling injection ($\alpha= 5.0, 8.5, 11.5, 15.0$) with non-accelerating mainstream flow

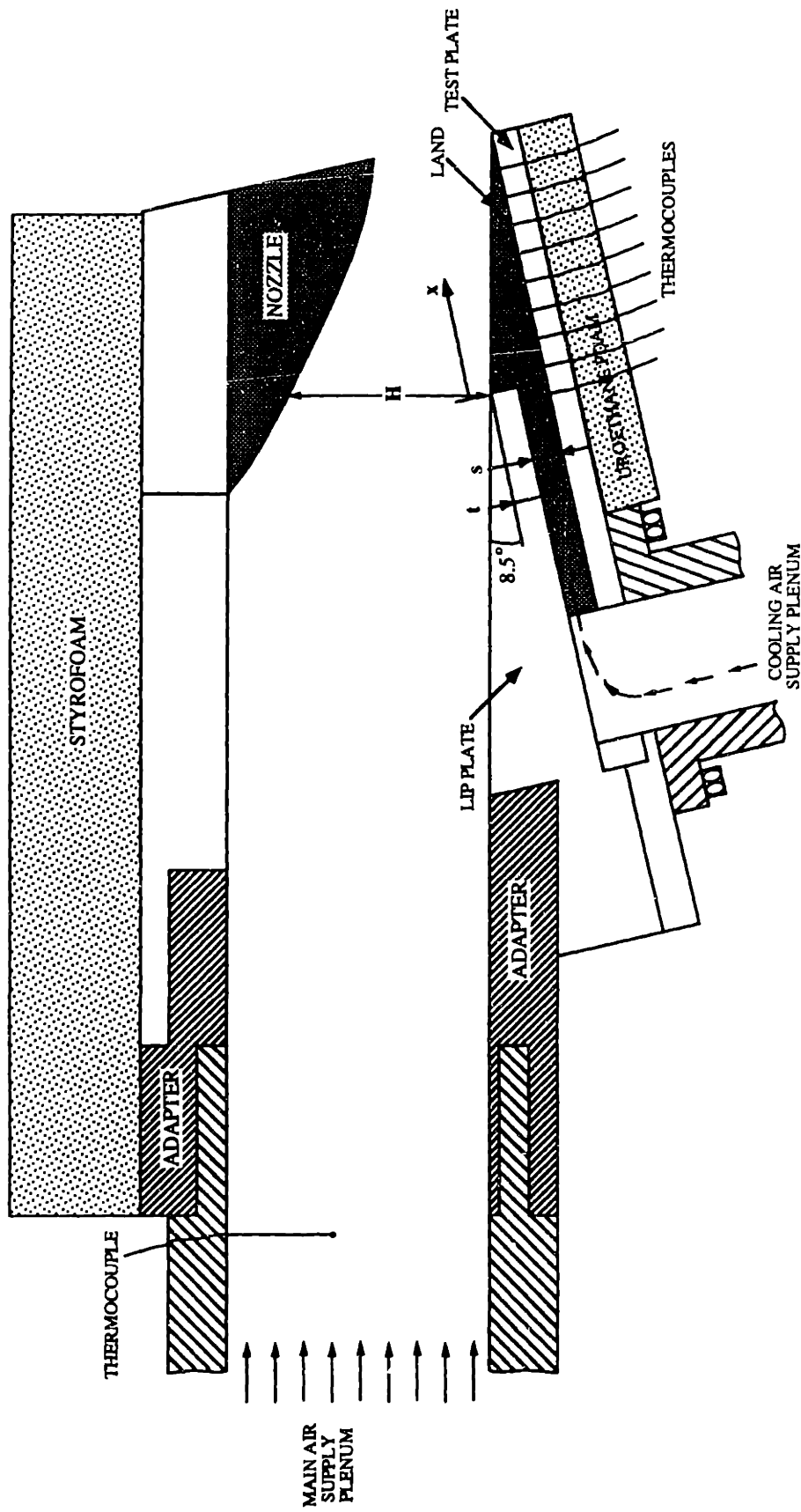


Figure 2-3c: Cross-sectional view of test section for angled film-cooling injection ($\alpha = 8.5$) with accelerating mainstream flow

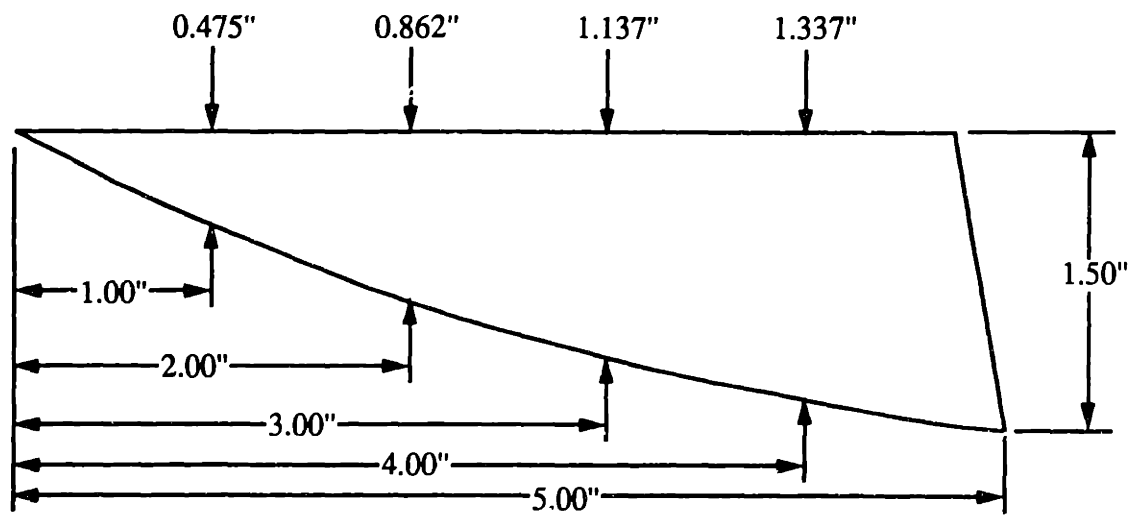


Figure 2-4: Nozzle profile for 8.5 degree injection angle and accelerating mainstream flow

Instrumentation of the test plate is identical for all tested configurations and is shown in *Figure 2-5*. Six columns of eight thermocouples placed 0.5 in. between each other with the first thermocouple placed 0.15 in. from the slot breakout. The thermocouples used are K-type Chromel-Alumel. The thermocouples were inserted into small holes drilled through the test plate such that the thermocouple bimetallic bead is flush with the surface of the test plate. The symmetry of the effectiveness distribution is investigated across the slots. The secondary film cooling temperature is measured at two different locations: at the midspan of slot #5 and slot #7 0.5 in. upstream of the slot breakout location. The mainstream air temperature is measured with three thermocouples evenly spaced across the width of the inlet section immersed into the air stream. In addition to measuring the temperature across the width of the slot, temperatures on the surface of the land located between slot #6 and slot #7 are measured for the case with the accelerating mainstream flow. Static pressure taps are also placed on the surface of the land located between slot #3 and slot #4. A total pressure probe is inserted in the mainstream to measure the total pressure upstream of the nozzle. Using Bernoulli's equation, assuming inviscid flow, average mainstream velocities are calculated based on the total and static pressure measurements. In turn the calculated velocities are used to evaluate the acceleration factor (Ka) defined as:

$$Ka = v_s \frac{dU}{U^2 dx} \quad (13)$$

where v_s is defined as the kinematic viscosity of the air evaluated at the temperature of the mainstream gas (T_s).

II.3 Test Procedure

The experimental tests are performed using General Electric's Component Test Laboratory in Building 70 in Lynn. Mainstream air was heated using a natural gas-fired burner and heat exchanger. For each run a standard procedure is employed in which all variables are

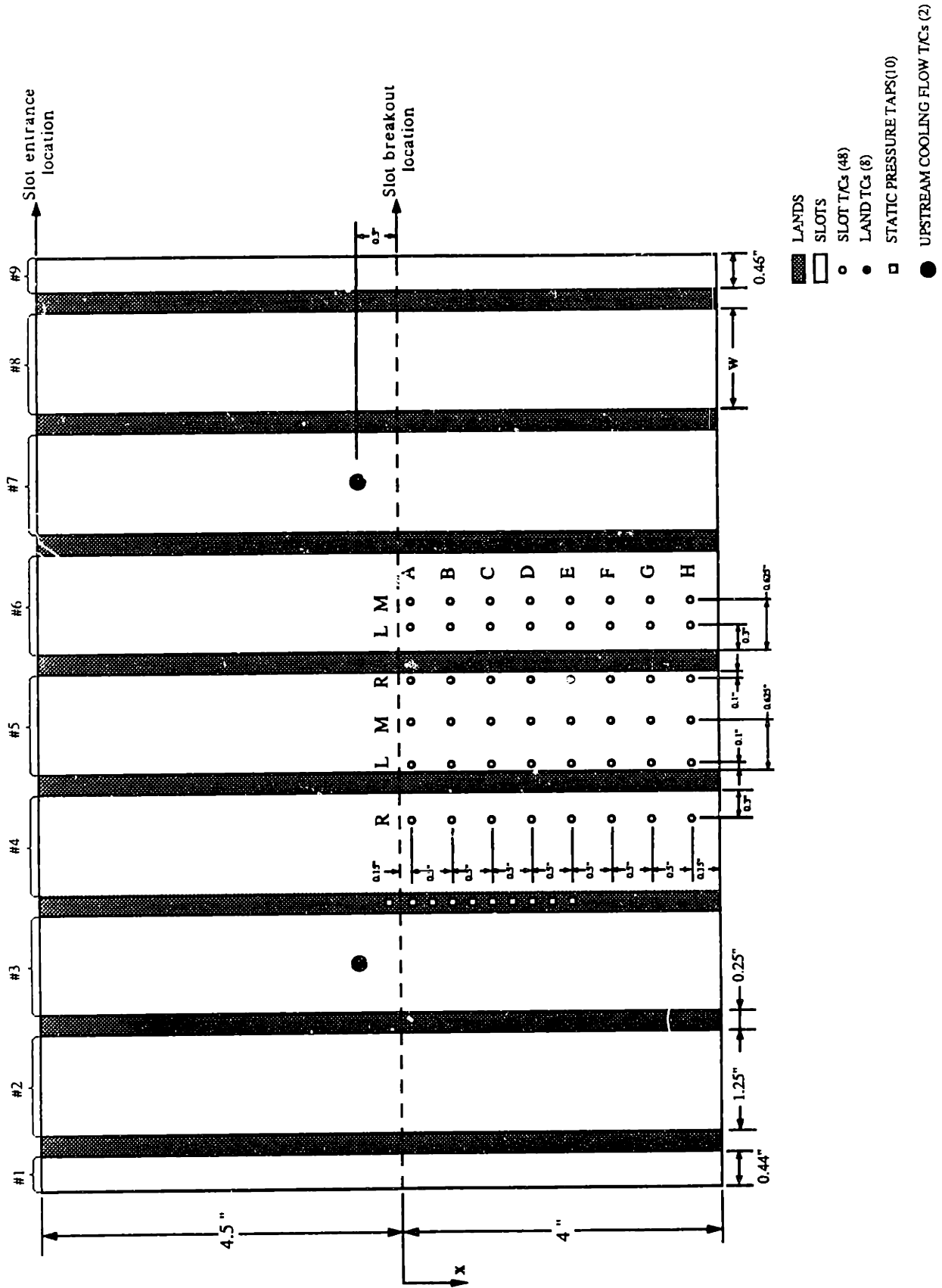


Figure 2-5: Test plate instrumentation

kept constant except for the mass-velocity ratio (M). The mainstream air temperature is set to 250 deg. F while the secondary film cooling air temperature varied depending on the outside ambient temperature and the test cell room temperature. The flow rates of the mainstream and secondary air are measured using thin-plate orifice meters in conjunction with flange taps, constructed according to the ASME Code Standards.

A typical test is performed as follows: the mainstream temperature is set to 250 deg. F and the mass flow rate at 1 lbm/sec. For the test with the converging nozzle the mainstream flow rate is set to 1.5 lbm/sec. The secondary flow rate is set such that the mass-velocity ratio is equal to approximately 0.2. At each mass-velocity ratio setting, sufficient time is allowed in order to obtain equilibrium conditions before the necessary pressures and temperatures are recorded. Equilibrium conditions are established by monitoring the transient output from a thermocouple located half way downstream of the slot breakout distance and in the middle of the slot. Once steady state is reached, thermocouple and total and static measurements are read and recorded. After sampling the data, the secondary cooling flow is increased until a satisfied mass-velocity ratio is obtained. The mass-velocity ratio varied from approximately 0.2 to 1.4. Having reached a value of 1.4 the same mass-velocity ratio settings are achieved by decreasing the secondary flow rate. This procedure is performed to investigate any hysteresis effect related to the test rig.

II.4 Data Reduction

Thermocouple and total and static pressure measurements output are read and recorded using a Motorola 6800 high speed digital data acquisition system directly connected to a Honeywell H6000. In this manner data is acquired and reduced immediately.

When the system is operated and equilibrium conditions are established, the wall temperature measured by the surface thermocouples is taken as equal to the adiabatic wall temperature T_{aw} . Then the film effectiveness is evaluated directly from the experimental results

according to Eq. 2 described in the previous section. Because some heat is lost through the test plate due to radiation from the surface and transverse as well as axial conduction, an error is incurred in performing film effectiveness calculations based on the measured wall temperature instead of the idealized adiabatic wall temperature. The largest contributions to the heat lost to the environment come from the transverse conduction. From the definition of η , it can be seen that small errors arising from conduction through the test section plate and insulating urethane foam can cause significant relative errors in η for small values of η . The conduction error is proportional to the difference between the surface temperature and the ambient temperature. These conduction errors are small for the results presented in this study in comparison with the uncertainty of temperature-recording instruments and the slight timewise variation of T_g and T_s . Accordingly, for these results, the test plate surface temperatures were taken as the adiabatic wall temperatures, with a maximum estimated error of 2 percent. A detailed calculation of the conduction error is given in Appendix A.

The reported effectiveness values are based on a weighted average of the film effectiveness calculated according to Eq. 2 based on measured surface temperatures. The effectiveness was reduced in three steps as follows:

- (1) average effectiveness for increasing and decreasing values of blowing ratio:

$$\eta = \frac{\eta_{up} + \eta_{down}}{2}$$

- (2) average effectiveness for symmetric columns of thermocouples (i.e. columns 4R and 6L):

$$\eta = \frac{\eta_{4R} + \eta_{6L}}{2}$$

- (3) average effectiveness across width of slot at a given downstream distance from breakout:

$$\bar{\eta} = [0.1 \eta_{5L,5R} + 0.2 \frac{\eta_{5L,5R} + \eta_{4R,6L}}{2} + 0.325 \frac{\eta_{4R,6L} + \eta_{5M,6M}}{2}] / 0.625$$

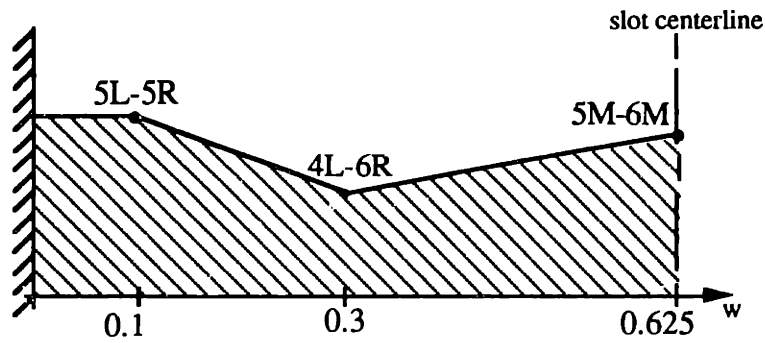


Figure 2-6: Weighted average of film effectiveness across slot width

A sample data reduction for the adiabatic wall temperature measurements for 8.5 degree injection angle is given in Appendix D.

II.5 Error Analysis

There is always a certain degree of experimental uncertainty resulting from the inaccuracy of the measuring devices. A brief discussion of the uncertainty of measurements and their effects on the experimental results is described in this section. Detailed calculations of these uncertainties are given in Appendix B.

II.5.1 Temperature Measurements

Temperature measurements using K-type (Alumel-Chromel) thermocouples are accurate to within $\pm 1.0^\circ \text{F}$ [11]. Since the film effectiveness (η) defined by Eq. 2 is inversely proportional to $(T_g - T_s)$ and proportional to $(T_g - T_{aw})$, it is important to maintain the temperature difference between the gas and the adiabatic wall temperature sufficiently large such that the thermocouple accuracy does not strongly affect the calculated film effectiveness. From reference 1, the maximum uncertainty for the film effectiveness is $\pm 4\%$.

II.5.2 Mass Flow Rate Measurements

The air mass flow rates measured using ASME sharp edged orifices in conjunction with flange taps can be calculated as follows [12]:

$$m = 0.86275 \frac{C Y d^2 F_a}{\sqrt{1-\beta^4}} \sqrt{\frac{P_1 (\Delta P)}{T_1}} \quad (14)$$

where	m = mass flow rate	(lbm / sec)
	Y = expansion factor	(dimensionless)
	C = discharge coefficient	(dimensionless)
	d = orifice diameter	(in.)
	D = pipe diameter	(in.)
	β = diameter ratio (d/D)	(dimensionless)
	F_a = area thermal expansion factor	(dimensionless)
	P_1 = pressure upstream of orifice	(psia)
	P_2 = pressure downstream of orifice	(psia)
	$\Delta P = P_1 - P_2$ = pressure drop across orifice	(psia)
	T_1 = temperature upstream of orifice	(°R)

From Eq. 14, the maximum uncertainty interval according to reference 13 was found to be equal to $\pm 2.4\%$.

II.5.3 Accuracy of Test Section Geometries

From the definition of the mass velocity ratio (M) blowing ratio, the accuracy of M depends on the accuracy of the total slot area A_s and the mainstream area A_g . From reference 1, the maximum uncertainty interval of the slot area A_s and for the mainstream area A_g is $\pm 5.6\%$ and $\pm 0.4\%$ respectively.

II.5.4 Accuracy of Mass Velocity Ratio

To specify the secondary film cooling air injected into the mainstream flow, the mass-velocity ratio or blowing ratio (M) defined in Eq. 4 can also be expressed in terms of the secondary and mainstream flow rates as follows:

$$M = \frac{(\rho U)_s}{(\rho U)_g} = \frac{(m/A)_s}{(m/A)_g} \quad (5)$$

From the accuracy of the flow rates and the test section geometries described in the previous paragraph, the uncertainty interval for the mass-velocity ratio is equal to $\pm 6.5\%$.

III. Experimental Results

III.1 Introduction

Results for the adiabatic wall temperature are presented in terms of the average film effectiveness (η) and are plotted against mass-velocity ratio (M) for various dimensionless distances (x/s) from the slot breakout location. An attempt is made to correlate the experimental data on a purely empirical basis where the average film effectiveness is presented in terms of the non-dimensional parameter (x/Ms). A comparison of film effectiveness data with previous investigator's results for tangentially injected secondary flow is also discussed.

Adiabatic wall temperature data as well as film effectiveness data for each run and for each test configuration are presented in tabular form in Appendix C.

III.2 Effect of Injection Angle on Film Effectiveness

III.2.1 Non-Accelerating Mainstream Flow

Figures 3-1 through 3-5 show the effect of varying the secondary cooling air injection angle (α) on the film effectiveness for the case when the mainstream flow is uniform and non-accelerating. In each figure, the average film effectiveness (η) is plotted against the mass-velocity ratio (M) for various slot heights downstream of the injection slot breakout location. A salient feature of the representation of the data for all figures is the dependence of η on both the value of M and the value of (x/s). For distances close to the slot breakout, η exhibits a strong dependence on M and (x/s). As the distance from the slot increases, film effectiveness decreases since more mixing occurs between the injected coolant and the hot mainstream. For increasing blowing ratios, the film effectiveness increases and tends towards unity but becomes

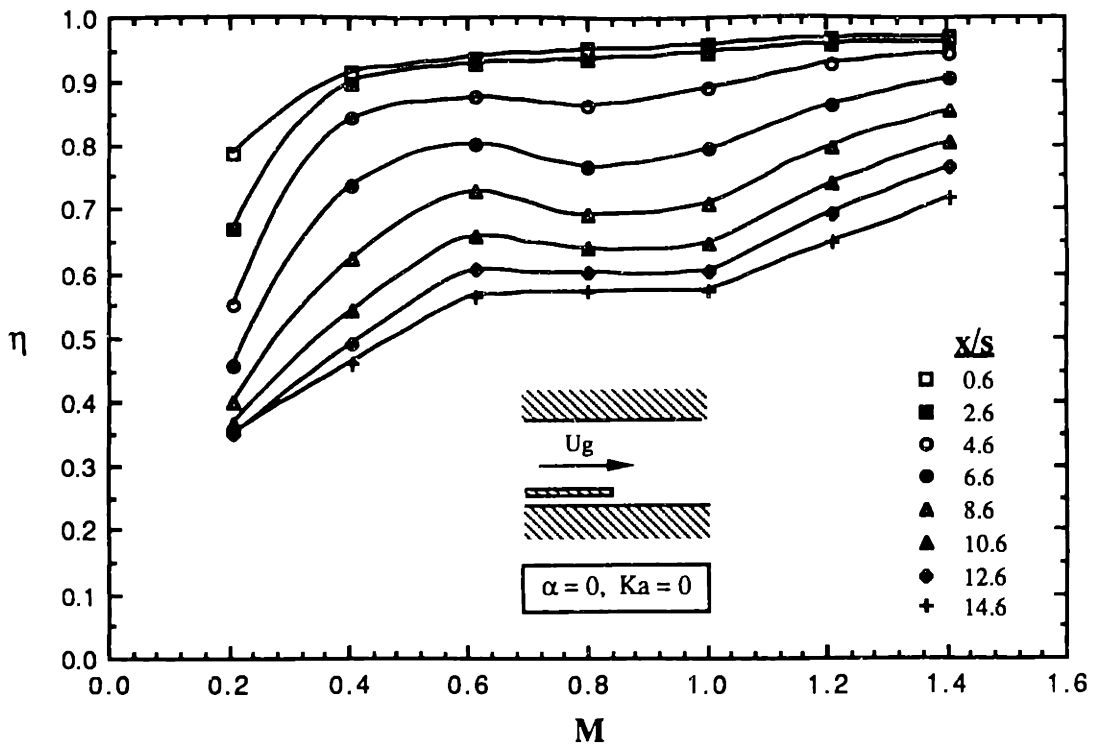


Figure 3-1: Film effectiveness (η) vs. blowing ratio (M) for 0° injection angle

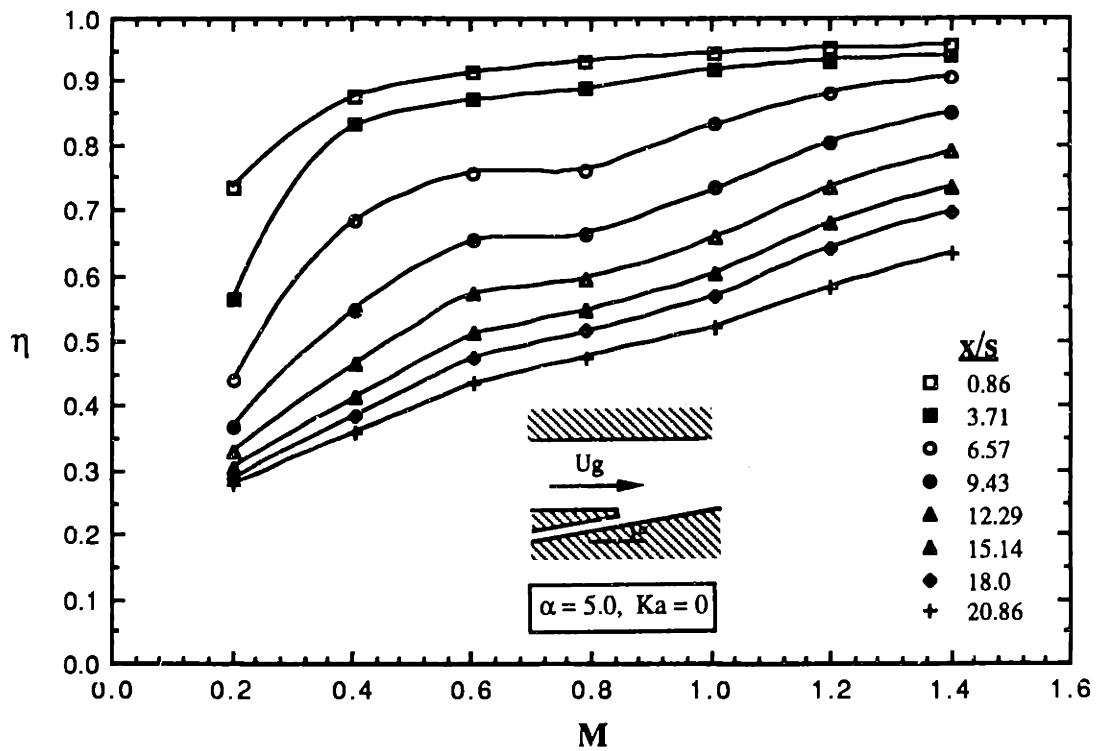


Figure 3-2: Film effectiveness (η) vs. blowing ratio (M) for 5.0° injection angle

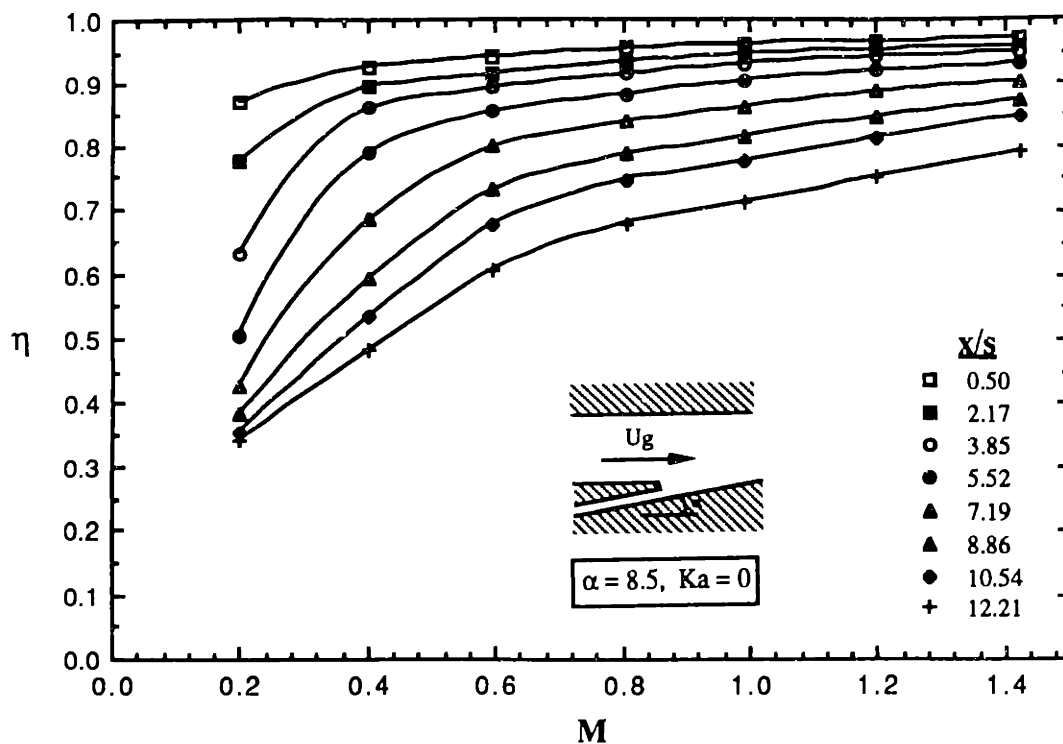


Figure 3-3: Film effectiveness (η) vs. blowing ratio (M) for 8.5 deg. injection angle

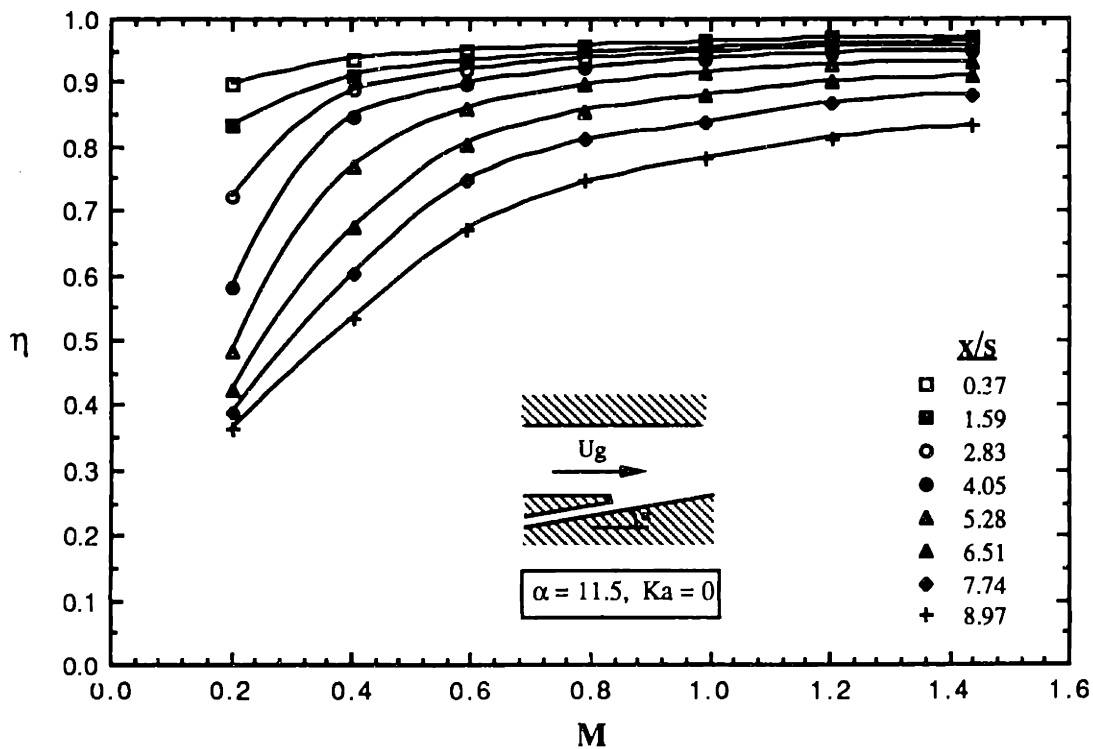


Figure 3-4: Film effectiveness (η) vs. blowing ratio (M) for 11.5 deg. injection angle

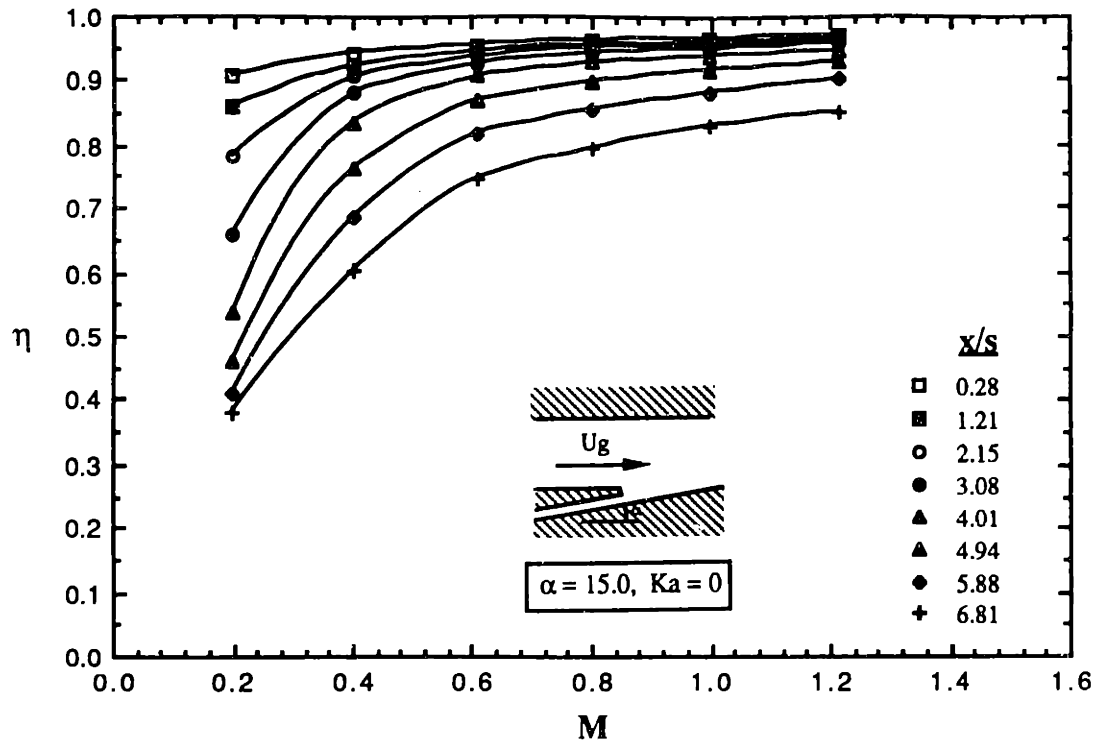


Figure 3-5: Film effectiveness (η) vs. blowing ratio (M) for 15.0 deg. injection angle

less a function of (x/s) especially for higher injection angles as can be seen from the collapsing of the effectiveness values.

For the case when the secondary flow is tangentially injected into the mainstream flow (Figure 3-1), the curve η versus M is divided into three regions. In the first region the average film effectiveness increases as the blowing ratio M increases from a value of 0.2 to 0.6. The second region is characterized by a leveling off of film effectiveness for M ratios between approximately 0.6 and 1.0 and for (x/s) ratios between 4.6 and 10.6, η drops to a local minimum. The third region is similar to the first one where an increase in M results in an increase in effectiveness value. A similar trend is observed for the case when the injection angle is equal to 5 degrees with the existence of a local maximum effectiveness also occurring at a blowing ratio equal to $M=0.6$ although, for downstream locations greater than approximately 16 slot heights, the transition plateau is not present. For injection angles greater than 5 degrees film effectiveness curves vary monotonically as a function of M and thus, a leveling off or dip

in film effectiveness is not observed. It must be noted that because of the increase in slot height (s) with increasing injection angles greater than 5 degrees the range of (x/s) values corresponding to thermocouple wall locations decreases with increasing angles and the dip in film effectiveness might occur for greater values of (x/s) which were not investigated. Nevertheless, there clearly exists a dip in film effectiveness for which its magnitude and location depends at least on the blowing ratio and the slot geometry. Qualitatively speaking, the dip in film effectiveness may result from an instability in mixing between the injected coolant and mainstream flow. For low blowing ratios, mixing occurs uniformly over the slot length. For M ratios between 0.6 and 1.0 a flow instability develops and causes more mixing between the coolant and the mainstream thereby decreasing film effectiveness values. As the blowing ratio is increased the instability still exists but the film effectiveness must increase in value since a larger mass of coolant is injected into the mainstream. A pictorial sketch of this mixing mechanism for varying M ratios is shown in *Figure 3-6*.

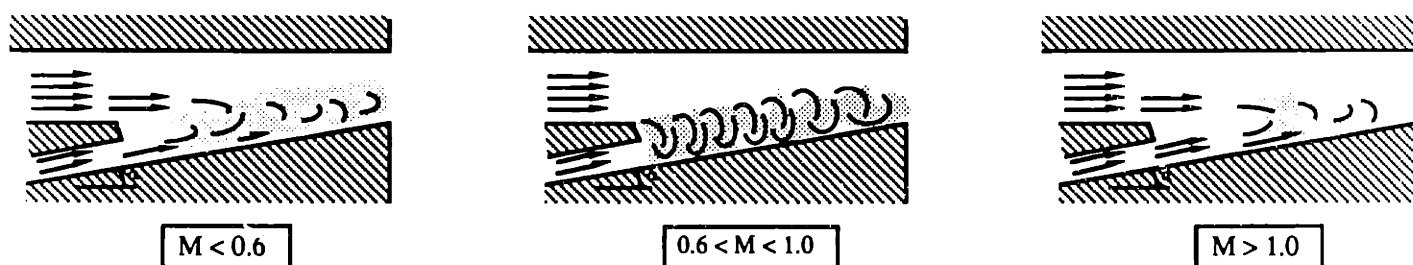


Figure 3-6: Mixing due to flow instability

III.2.2 Accelerating Mainstream Flow

Film effectiveness values obtained for the case when the converging nozzle is present in the mainstream are presented in *Figure 3-7*. A similar trend as for the tangentially injected flow

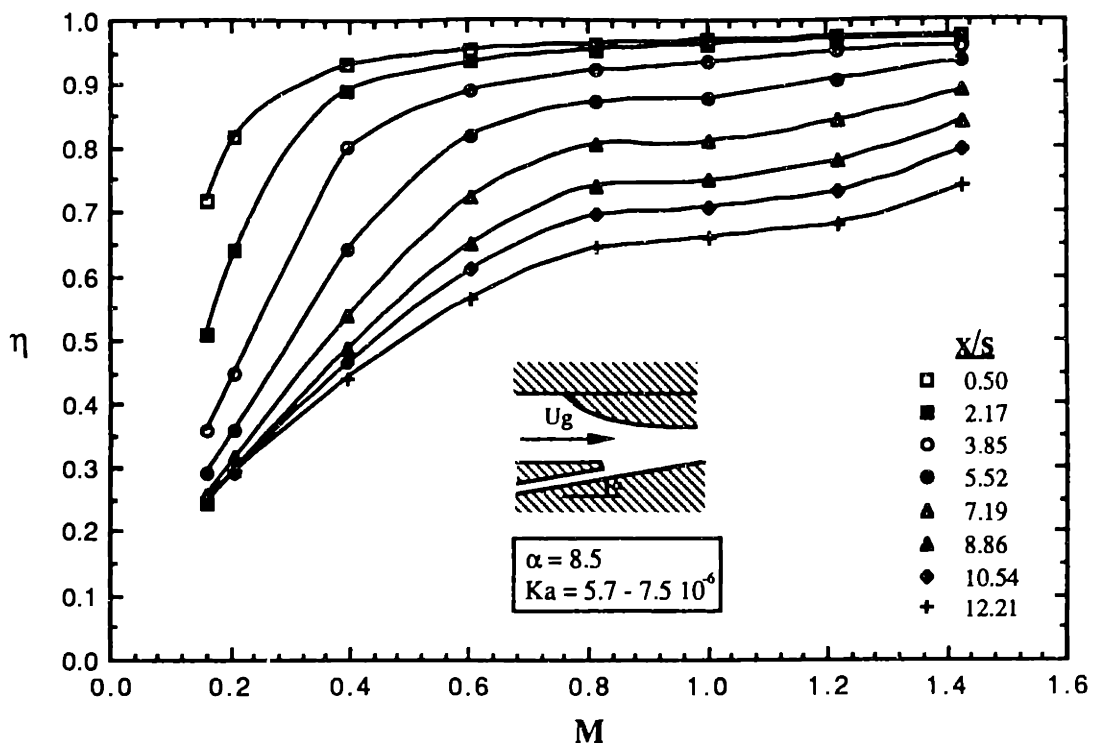


Figure 3-7: Film effectiveness (η) vs. blowing ratio (M) for 8.5 degree injection angle with accelerating mainstream flow

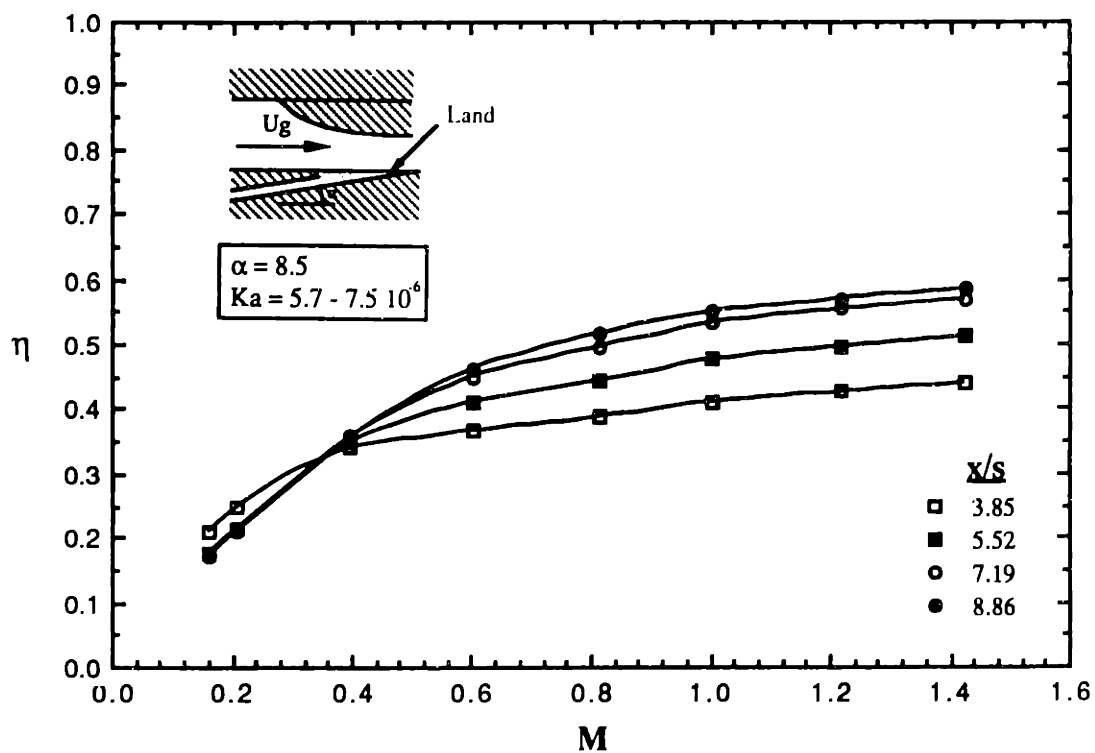


Figure 3-8: Land film effectiveness (η) vs. blowing ratio (M) for 8.5 degree injection angle with accelerating mainstream flow

is observed where film effectiveness values level off for blowing ratios between 0.8 and 1.0 for downstream slot heights greater than 5.

Average film effectiveness values for temperature measurements made on the land surfaces are presented in *Figure 3-8*. For low blowing ratios the land effectiveness value is close to zero and as the downstream distance from the slot increases mixing becomes more important thus, creating a complex three dimensional hydrodynamic structure which causes some amount of the injected coolant to diffuse over the surface of the land. Hence, the increase in land effectiveness for increasing (x/s) .

III.3 Correlation of Film Effectiveness Data

To compare film effectiveness results for various downstream slot heights (x/s) , each for different injection angles, the film cooling effectiveness is correlated in terms of the parameter (x/Ms) which is also another form of a dimensionless distance from the slot breakout. This type of correlation is very convenient for a heat transfer engineer who has a particular mass flow of secondary air available and a specific injection slot height and who wishes to choose an effectiveness value as a function of the distance downstream from the slot breakout. The resulting graphs are shown in *Figures 3-9* through *3-14* where average film effectiveness is represented logarithmically as a function of (x/Ms) . Typical of all the figures is an initial constant value of the effectiveness close to unity followed by a transition to an approximate power-law dependence on the non-dimensional distance (x/Ms) . Beyond the point of transition which is independent of the downstream distance (x/s) , the results are roughly linear and so indicate a power-law relation. The constant and the exponent of the power law relation were evaluated by performing a least-squares fit to the data for a range of (x/Ms) values. Reasonable correlations are obtained for the different injection angles except for

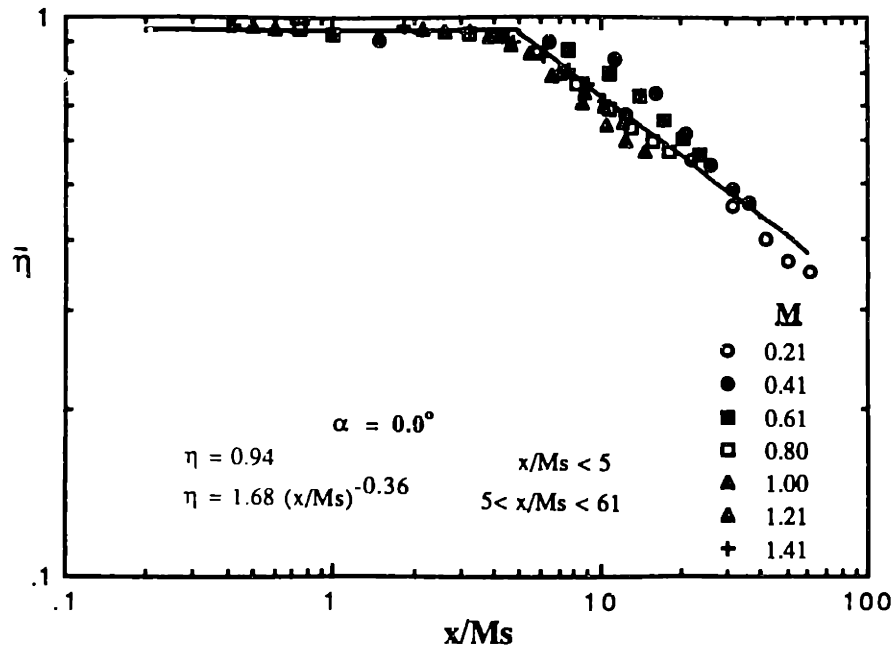


Figure 3-9: Film effectiveness (η) vs. (x/Ms) for 0 deg. injection angle

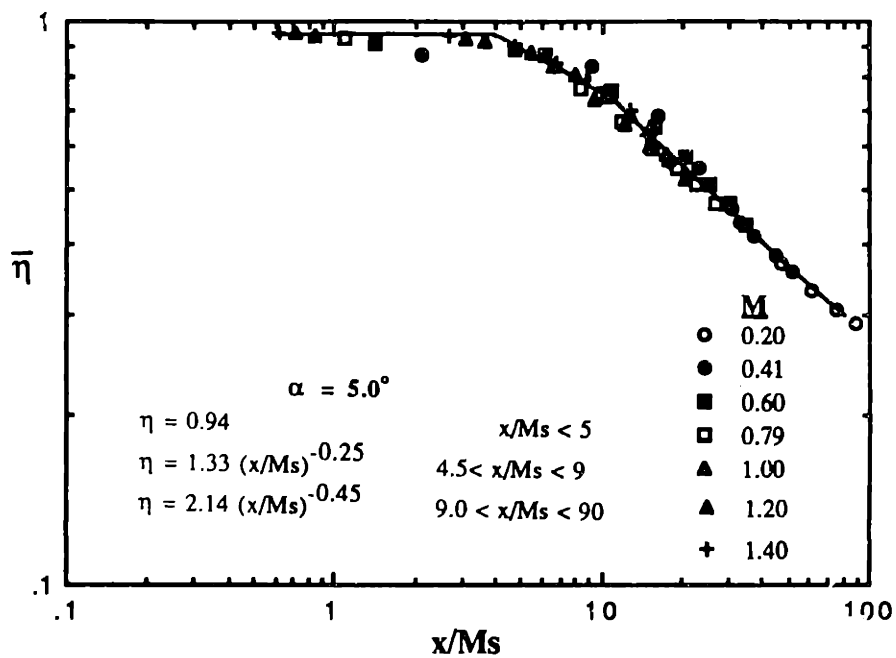


Figure 3-10: Film effectiveness (η) vs. (x/Ms) for 5.0 deg. injection angle

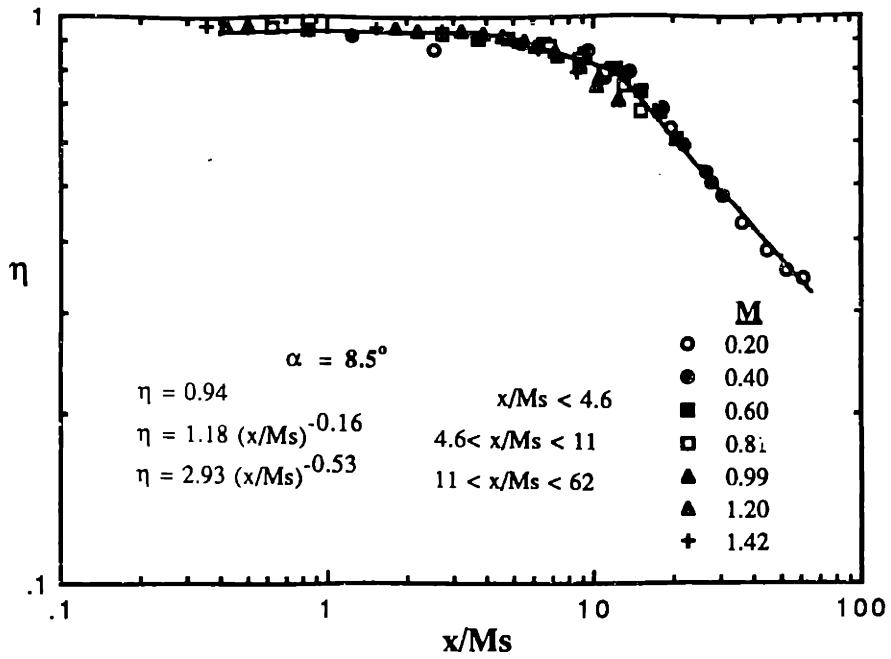


Figure 3-11: Film effectiveness (η) vs. (x/Ms) for 8.5 deg. injection angle

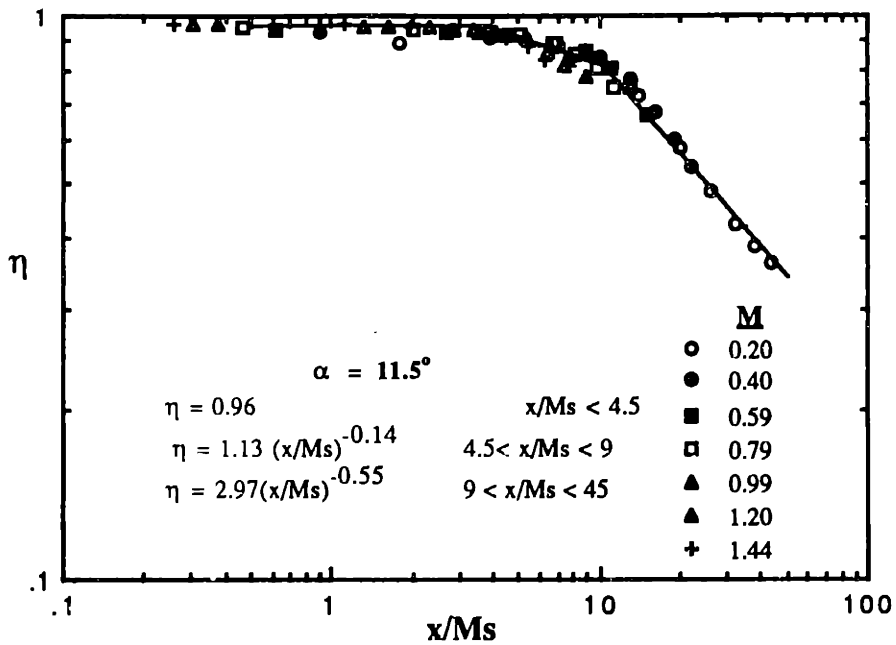


Figure 3-12: Film effectiveness (η) vs. (x/Ms) for 11.5 deg. injection angle

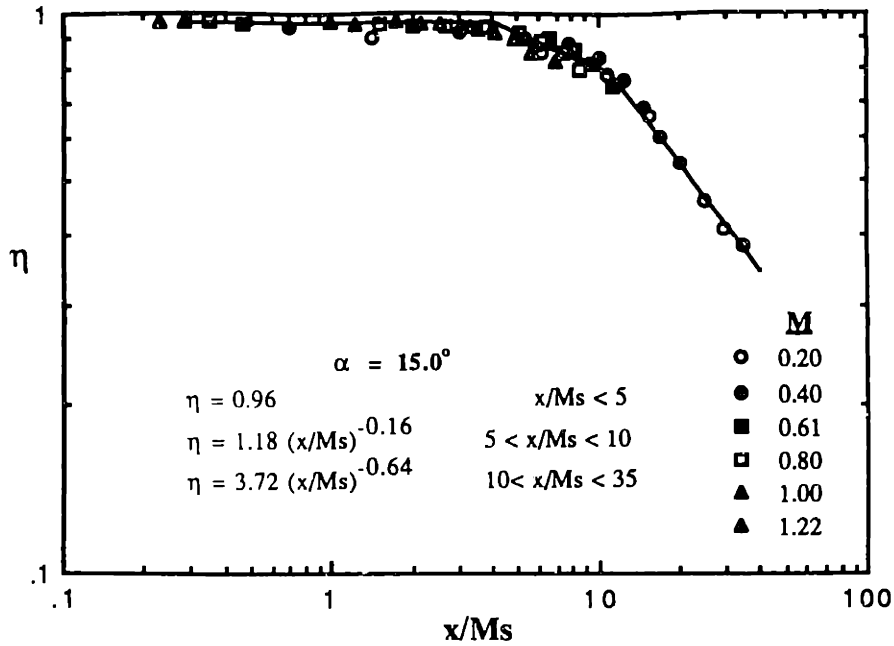


Figure 3-13: Film effectiveness (η) vs. (x/Ms) for 15.0 deg. injection angle

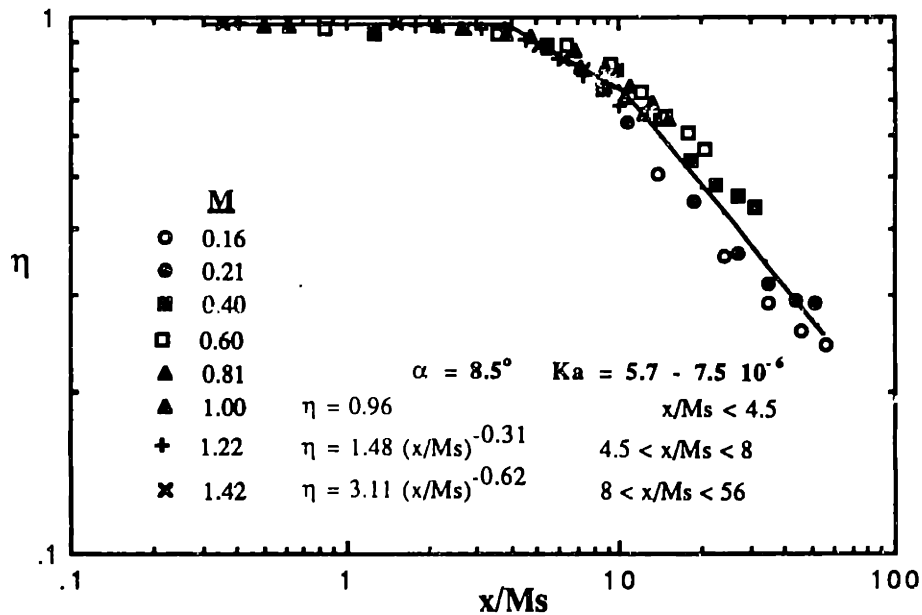


Figure 3-14: Film effectiveness (η) vs. (x/Ms) for 8.5 deg. injection angle with accelerating mainstream flow

the tangential injection case and the case for which the mainstream is accelerated. The correlation parameter (x/Ms) does not collapse the data for the tangential injection configuration because of the non-monotonic behavior of the film effectiveness η as a function of the blowing ratio (M) as was discussed in the previous paragraphs.

A comparison is made between film effectiveness values obtained for 8.5 degree injection into an accelerating and non-accelerating mainstream for which the results are shown in *Figure 3-15*. The presence of the converging nozzle alters the free-stream velocity and the large acceleration in the mixing region produced by the variable free-stream velocity clearly lowers effectiveness values. For an x/Ms value equal to 20 the film effectiveness decreases by approximately 20% when the nozzle is added in the mainstream.

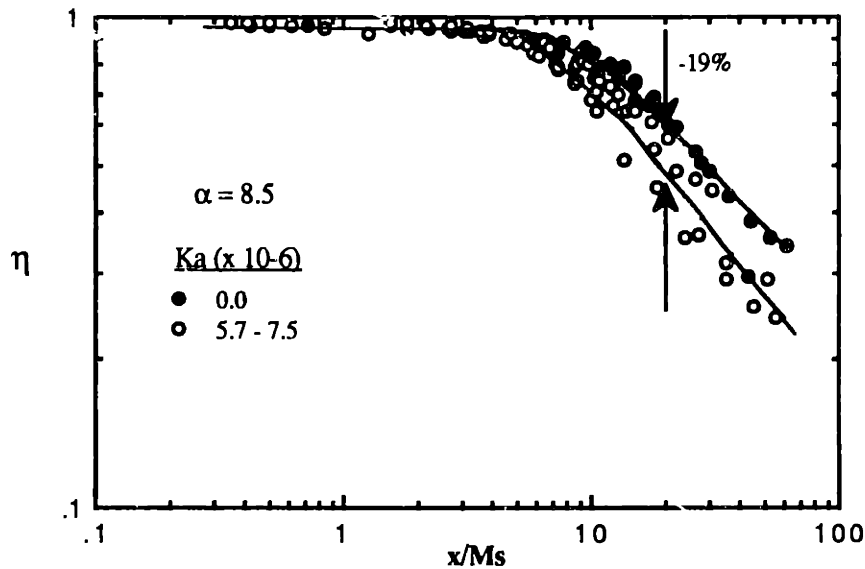


Figure 3-15: Film effectiveness (η) vs. (x/Ms) for 8.5 deg. injection angle. Accelerating vs. non-accelerating mainstream flow

III.4 Summary of Correlations

Table 3-1 summarizes the results obtained from the previous discussed correlations. The value of R corresponds to the correlation coefficient for the linear least-squares fit on a log-

log scale. Based on these correlations, a plot of the average film effectiveness as a function of (x/Ms) is presented for different injection angles. The resulting graph is shown in *Figure 3-16* and an optimal injection angle equal to 8.5 degrees is observed. Since tangential injection is never achieved in practice for turbine airfoil designs, results for this configuration are omitted in this graph.

Table 3-1: Summary of correlations

α	$Ka_{\alpha=0}$	x/Ms	$\eta = a (x/Ms)^b$		R^2
			a	b	
0.0	0	5-61	1.68438	-0.36340	0.90
		0.4 - 5	0.94	0	
5.0	0	9 - 90	2.13998	-0.45040	0.98
		4.5 - 9	1.3285	-0.24534	0.90
		0.6-4.5	0.94	0	
8.5	0	11 - 62	2.9273	-0.5252	0.98
		4.6 - 11	1.17846	-0.15771	0.71
		0.4 - 4.6	0.94	0	
11.5	0	9 - 45	2.9711	-0.55183	0.97
		4.5 - 9	1.1339	-0.13880	0.52
		0.2 - 4.5	0.96	0	
15.0	0	10 - 35	3.71575	-0.6449	0.99
		5 - 10	1.183469	-0.16377	0.60
		0.2 - 5	0.96	0	
8.5	5.7 - 7.5	8 - 56	3.10914	-0.6226	0.92
		4.5 - 8	1.482043	-0.30808	0.81
		0.35 - 4.5	0.96	0	

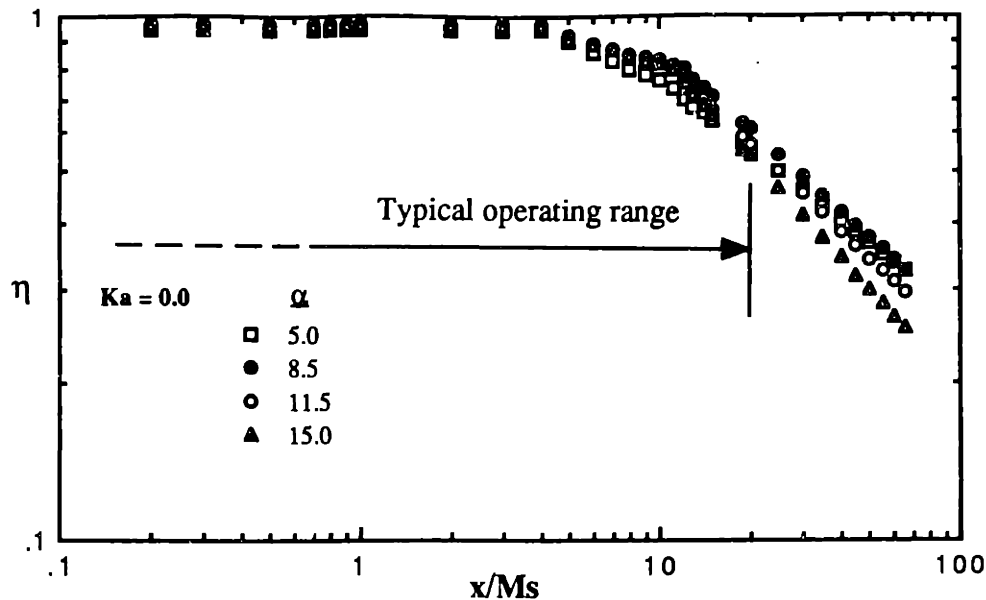


Figure 3-16: Film effectiveness (η) vs. (x/Ms) for varying injection angles. ($\alpha = 5.0^\circ, 8.5^\circ, 11.5^\circ, 15.0^\circ$)

III.5 Comparisons with Previous Work

Experimental results obtained for the tangentially injected flow configuration are compared to results obtained by Seban et al. [4]. Since the method of correlation was similar to the one used in this study, the experimental results are plotted in *Figure 3-17* according to the correlating parameter (x/Ms) and compared to the correlating equation of Seban described previously (Eq. 6 and 7). The experimental results obtained in this study are lower than those obtained by [4] although the power law dependence of η on x/Ms is comparable. The discrepancy in film effectiveness magnitude can be explained by the difference in slot geometry. Seban et al. used an infinitely small slot lip thickness which gives higher effectiveness values particularly for downstream locations close to the slot breakout.

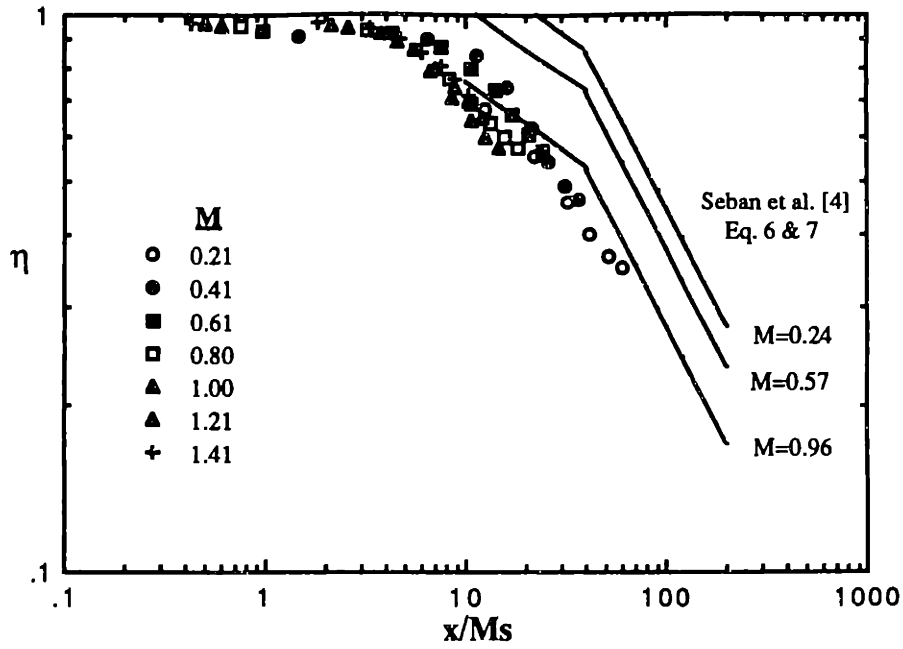


Figure 3-17: Comparison of experimental results with previous correlations of Seban et al. [4].

As a further comparison, results are compared with those of Joubert and Samuel [8]. Reasonably good agreement is found with the authors' correlating curve for low M ratios, bearing in mind that Joubert's curve pertains to greater downstream distances than the present results.

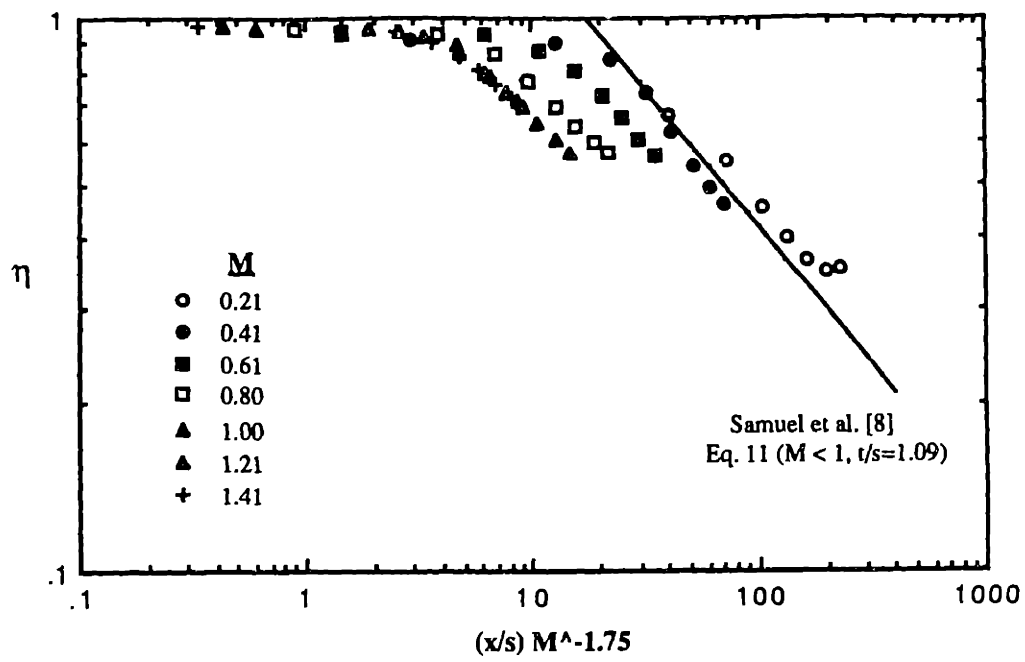


Figure 3-18: Comparison of experimental results with previous correlations of Samuel and Joubert [8].

IV. Numerical Investigation

IV.1 Introduction

An experimental investigation gives the most reliable source of information about a physical process and often small scale models are constructed to predict the physics behind the phenomena under investigation. However, small scale models do not always simulate all the features of the full-scale equipment. On the other hand, building full-scale tests are extremely expensive and often impossible. With the advent of large digital computers, a theoretical prediction of the physical process based on a mathematical model has become a more attractive alternative. In particular, a very attractive advantage is the low cost associated with using a theoretical prediction based on a computational numerical method. A computational prediction can also be performed with remarkable speed and the solution can provide extremely detailed and complete information about various variables pertinent to the physical process (such as velocity, pressure, temperature, turbulence intensity, etc.).

With the availability of commercial Computational Fluid Dynamics (CFD) codes, a numerical model is used to predict the film cooling effectiveness for a two-dimensional slot geometry identical to the one used in the experimental investigation. Numerical results are compared with experimental results. The CFD code used for this study is FLUENT developed by Create Inc. (1985).

IV.2 Numerical Model

The experimental geometry of the test rig used for the case with tangential film cooling injection in a non-accelerating mainstream flow is modelled as a two-dimensional flow field. *Figure 4-1* shows the numerical model used in this study. The dimensions and boundary

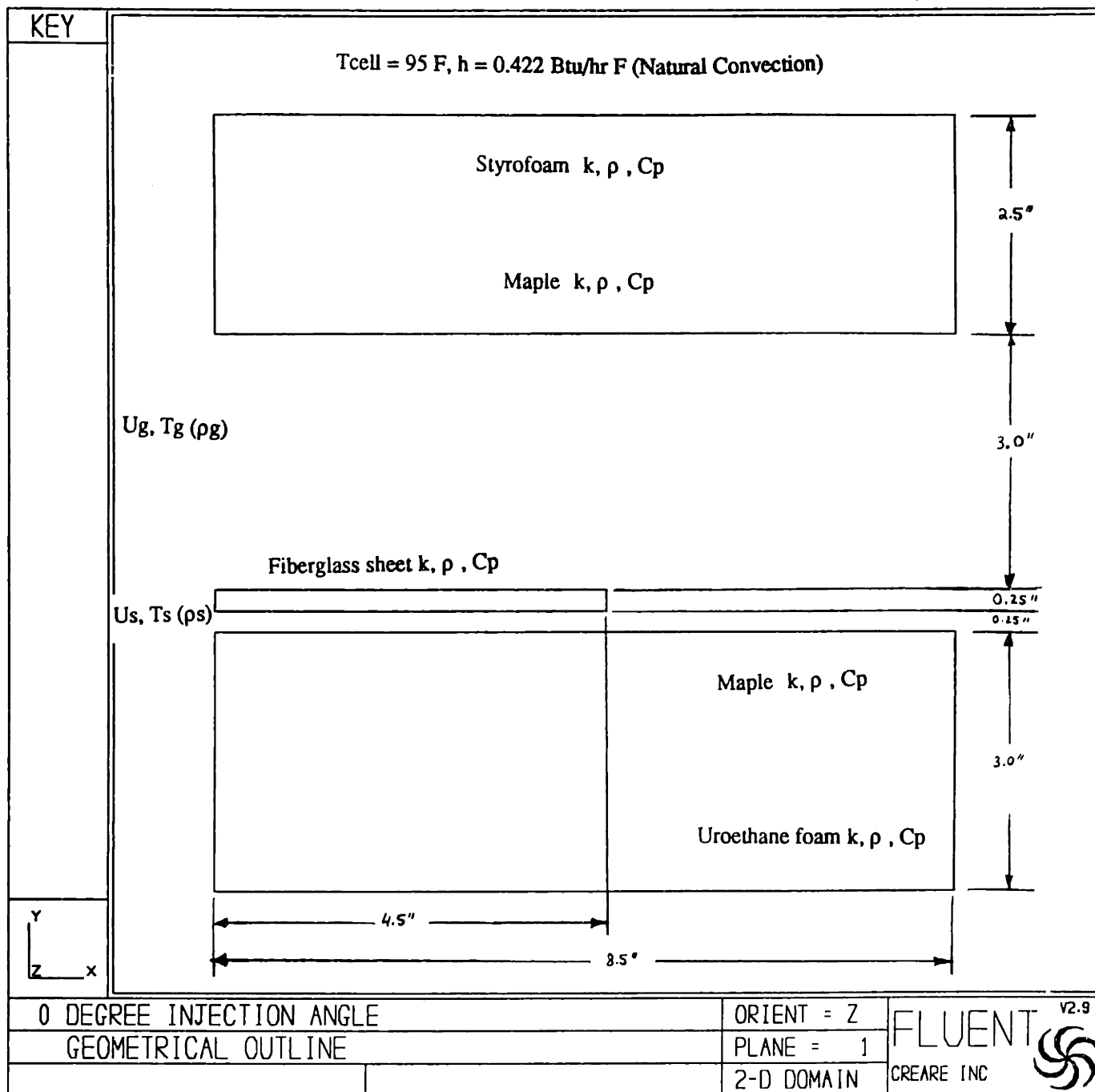


Figure 4-1: Numerical Model of experimental test rig for tangential film cooling injection

conditions of the computational domain are based on actual test rig dimensions and operating conditions such that an accurate model of the experiment is obtained. The main air flow inlet velocity is set at 74.44 ft/s and the temperature at 250 deg. F. The inlet velocities of the secondary cooling air flow are given in *Table 4-1* as well as the corresponding blowing ratios (M). The secondary air flow inlet temperature is set at 100 deg. F. Since air is used for both the main and secondary flows, the ideal gas law is applied to determine the density at any point in the fluid domain. The turbulence intensity for both flows is set to 8%. A two-dimensional finite difference grid for the fluid and solid domain, shown in *Figure 4-2*, is generated and is unchanged for all the simulations. A finer mesh for the grid is used for regions just downstream of the injection slot in order to obtain more accurate results in this hydrodynamically complex region.

Table 4-1: Boundary conditions for numerical model

U_g	U_s	M	T_g	T_s	
1	74.44	11.74	0.2	250	100
1	74.44	23.48	0.4	250	100
1	74.44	35.22	0.6	250	100
1	74.44	46.97	0.8	250	100
1	74.44	58.71	1.0	250	100

IV.3 Numerical Procedure

The numerical procedure is based on the solution of a finite-difference representation of the time-averaged, three dimensional form of the Navier-Stokes equations. The turbulence model for the predictions is based on Prandtl's mixing length model. Most of the pre-processing work involved generating the finite difference grid and defining the thermal and fluid boundary conditions. Then, for each simulation, only the inlet slot velocity specified as a

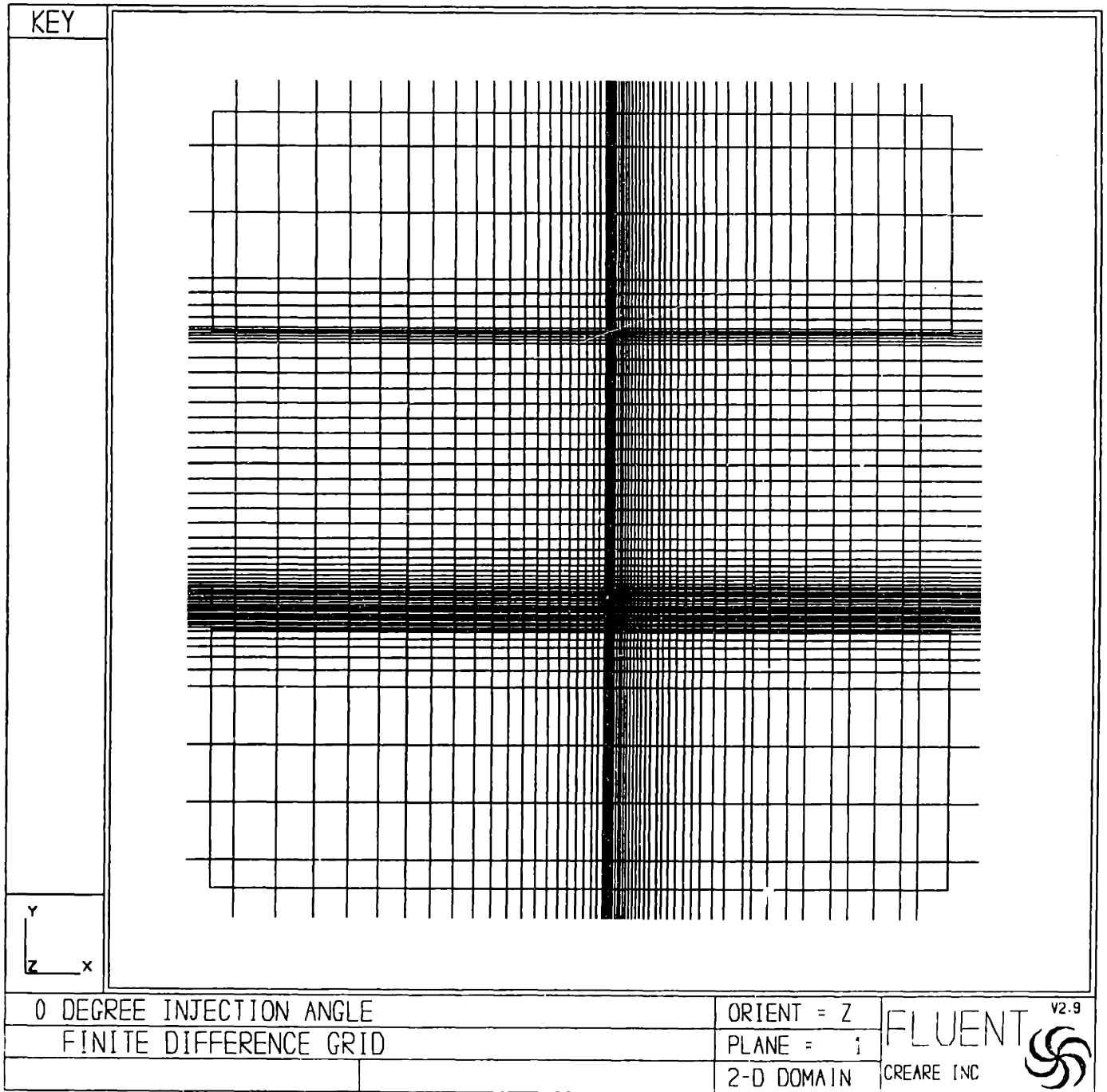


Figure 4-2: Finite difference grid

fluid boundary condition is set which in effect is the same as setting the blowing ratio (M). Numerical simulations were performed on a VAX 8820.

IV.3 Results for Tangential Film Cooling Injection

Velocity vector plots for various blowing ratios (M) are shown in *Figures 4-3* through *4-8*, and indicate the magnitude of the resultant velocity at each point in the flow field. The vectors are scaled in length according to the magnitude of the velocity. For low blowing ratios a recirculation zone is established just downstream of the slot breakout location and a stagnation point is observed approximately 2 slot heights downstream where the velocity is practically zero. As the blowing ratio increases the stagnation point disappears and the flow region downstream of the slot is similar to that of a wake flow behind a bluff body. Temperature profiles are shown in *Figures 4-8* through *4-12*. Note that the dashed line refers to the datum location. The distance between the dashed datum line and the solid profile line indicates the magnitude of the temperature. Because the temperatures are reported in degrees Rankine, it is difficult to distinguish differences in the shape of the profiles for increasing blowing ratios. For each node, defined by the intersection of two grid lines, a temperature is calculated and the data is readily available in an output data file. By selecting nodes on the surface of the slot, adiabatic film effectiveness values (η) are determined from Eq. 2 based on the temperature corresponding to the respective node.

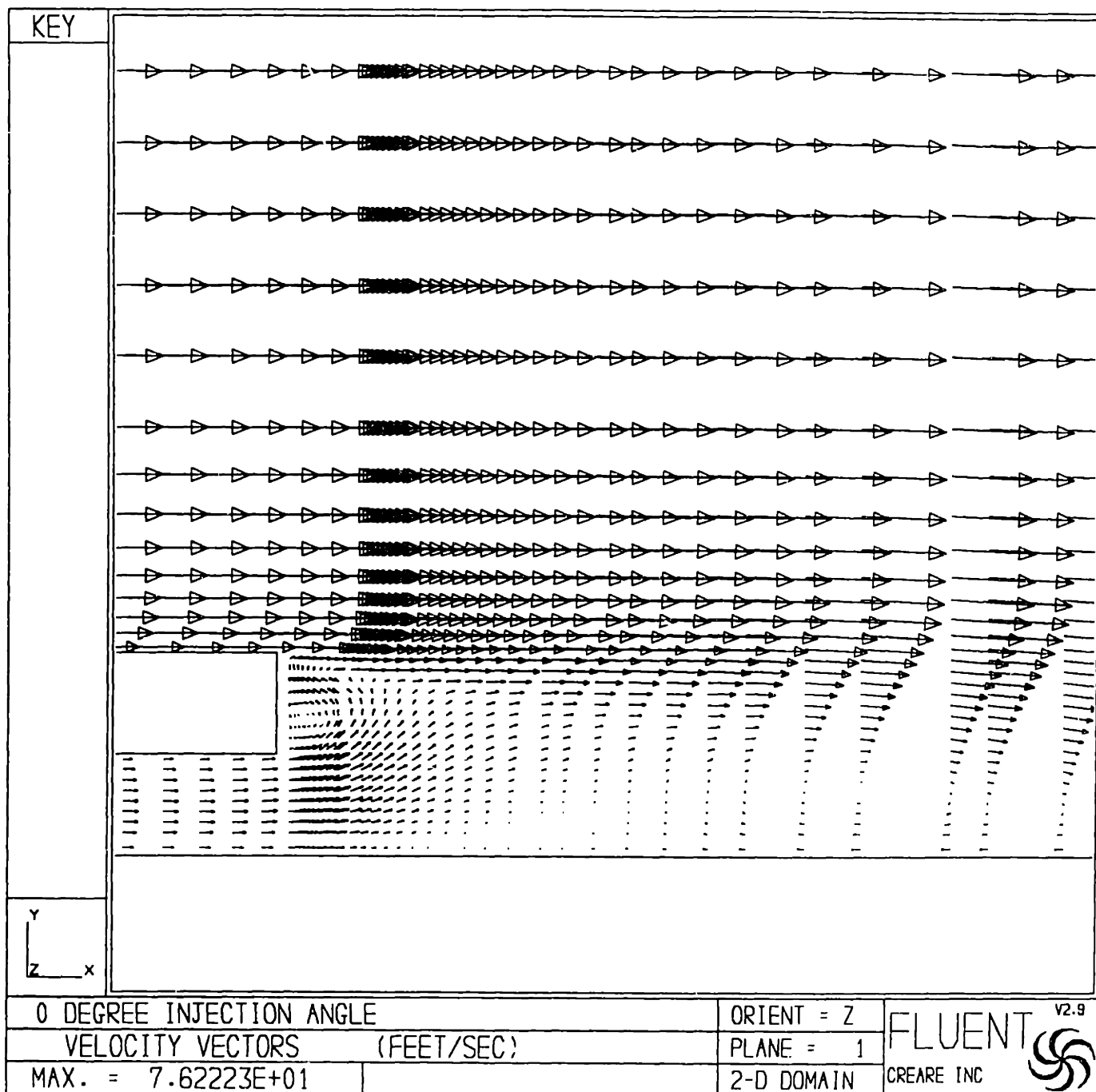


Figure 4-3: Velocity vector plot (M=0.2)

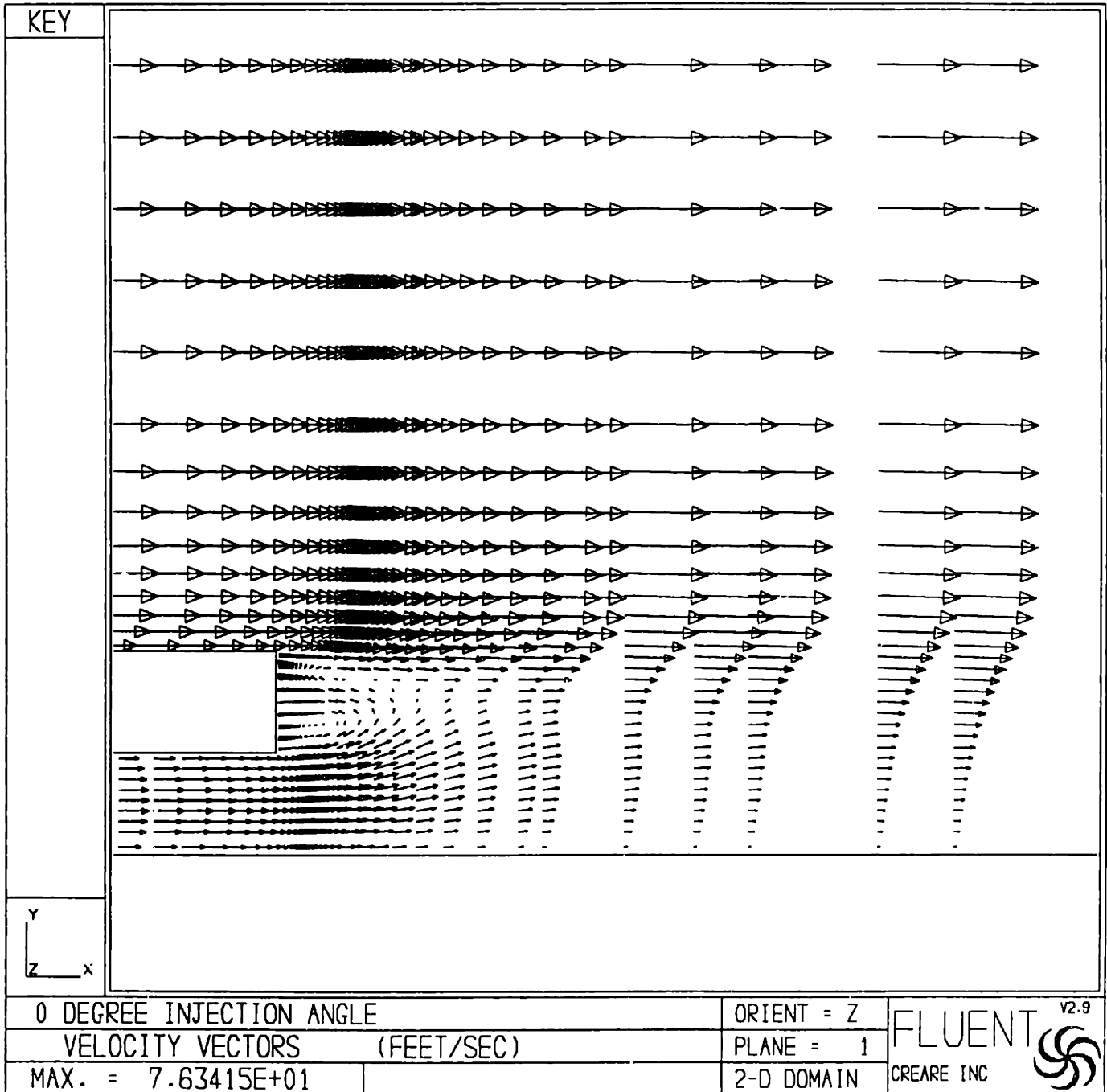


Figure 4-4: Velocity vector plot (M=0.4)

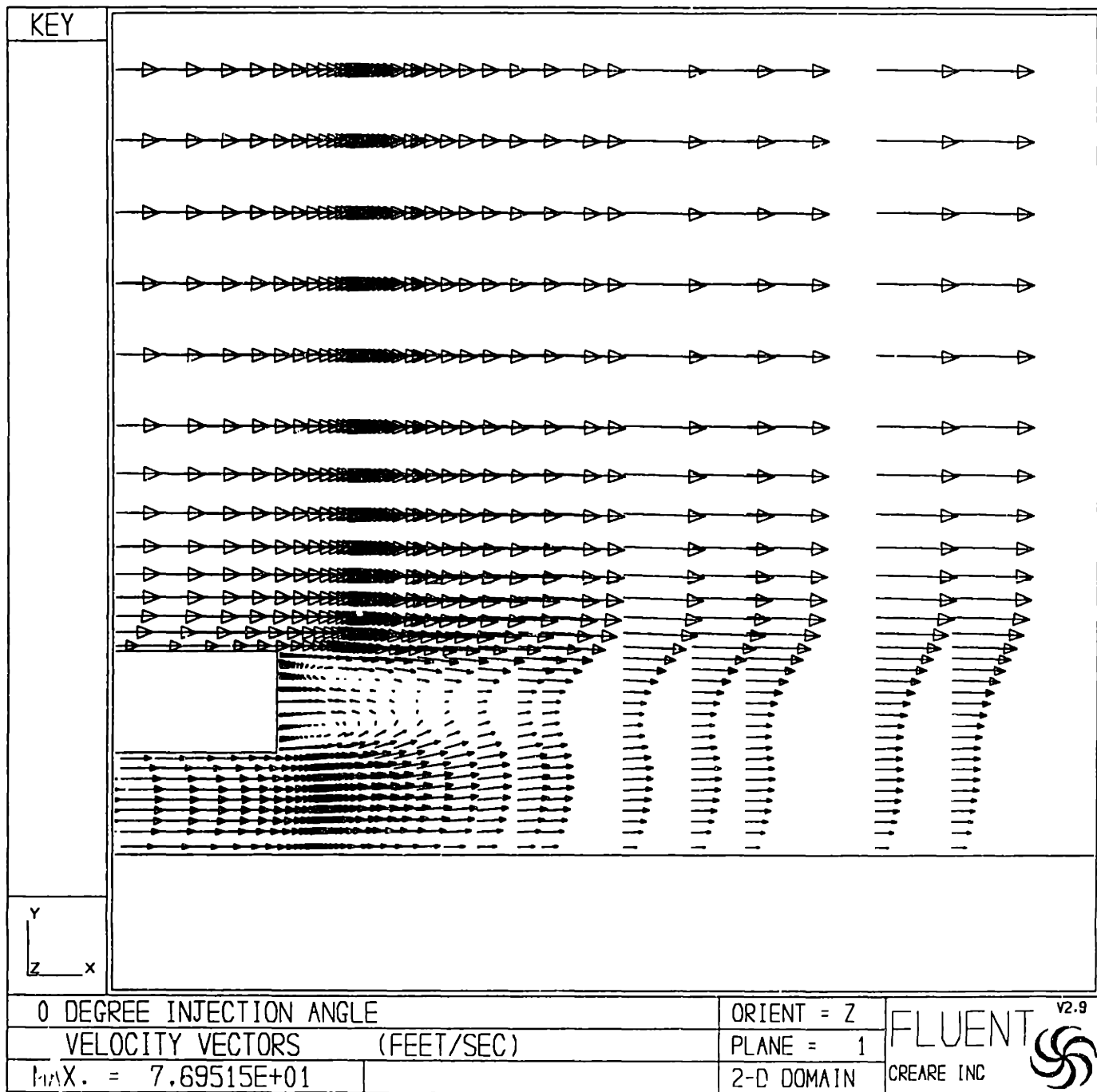


Figure 4-5: Velocity vector plot (M=0.6)

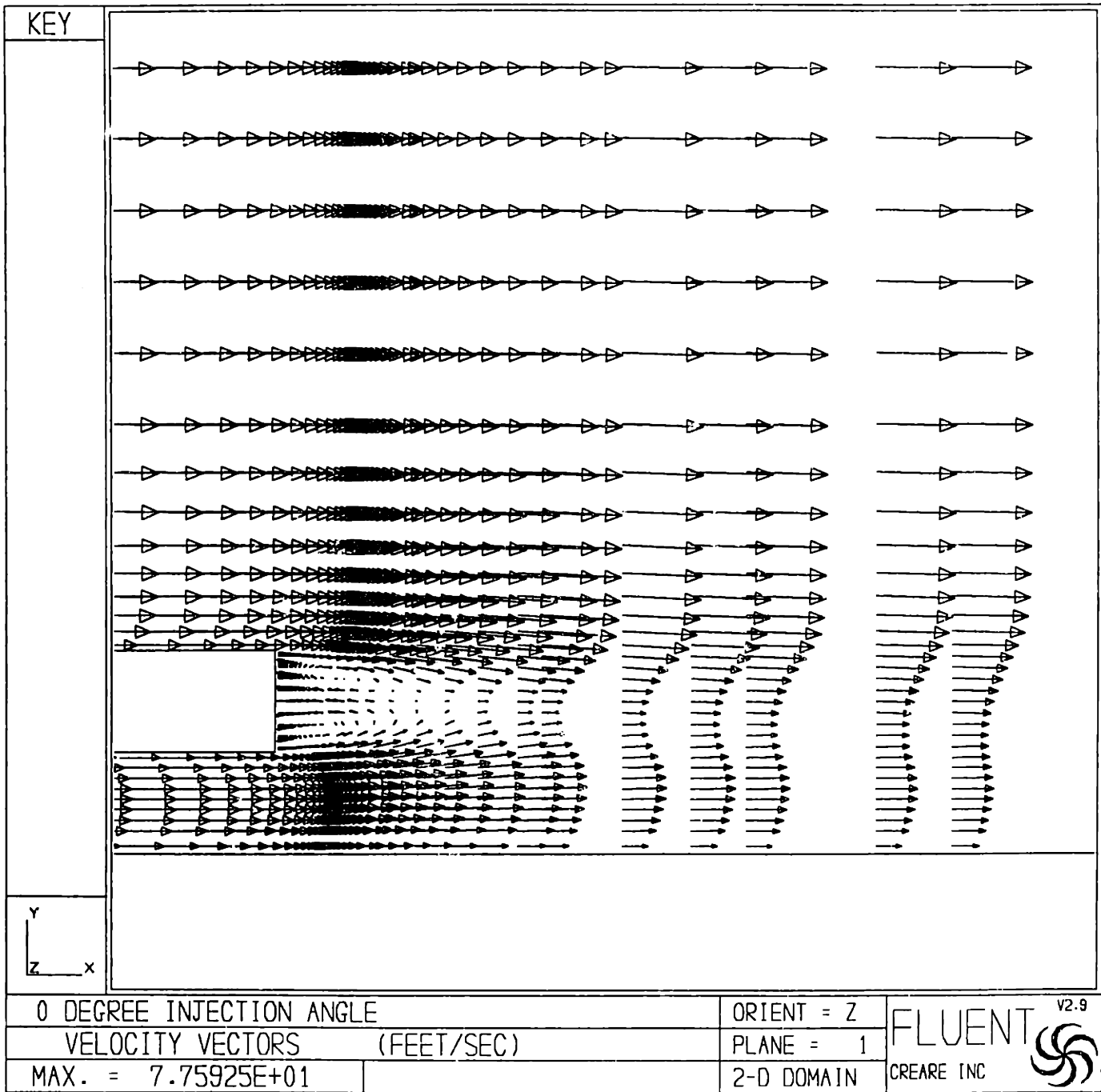


Figure 4-6: Velocity vector plot (M=0.8)

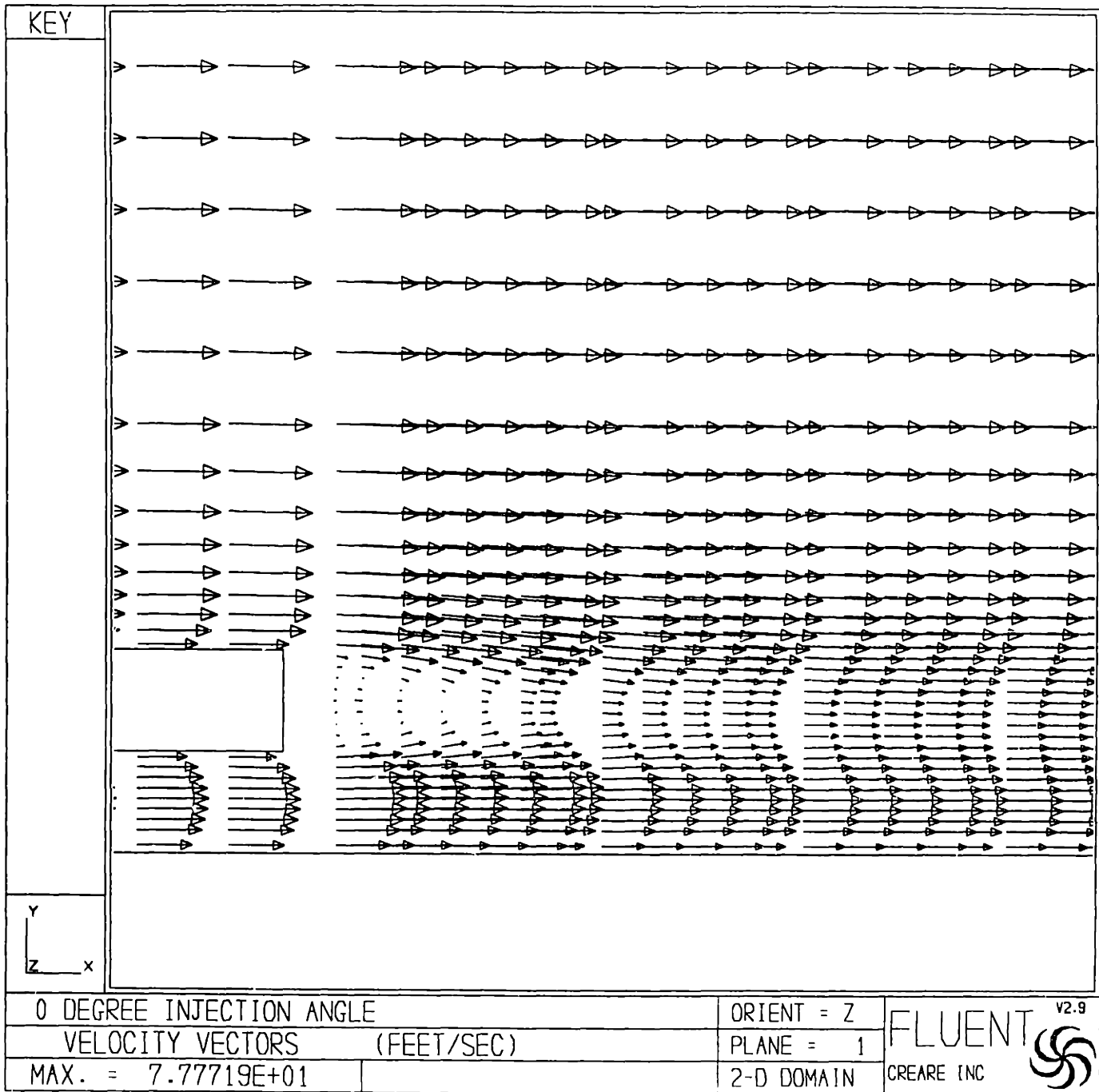


Figure 4-7: Velocity vector plot (M=1.0)

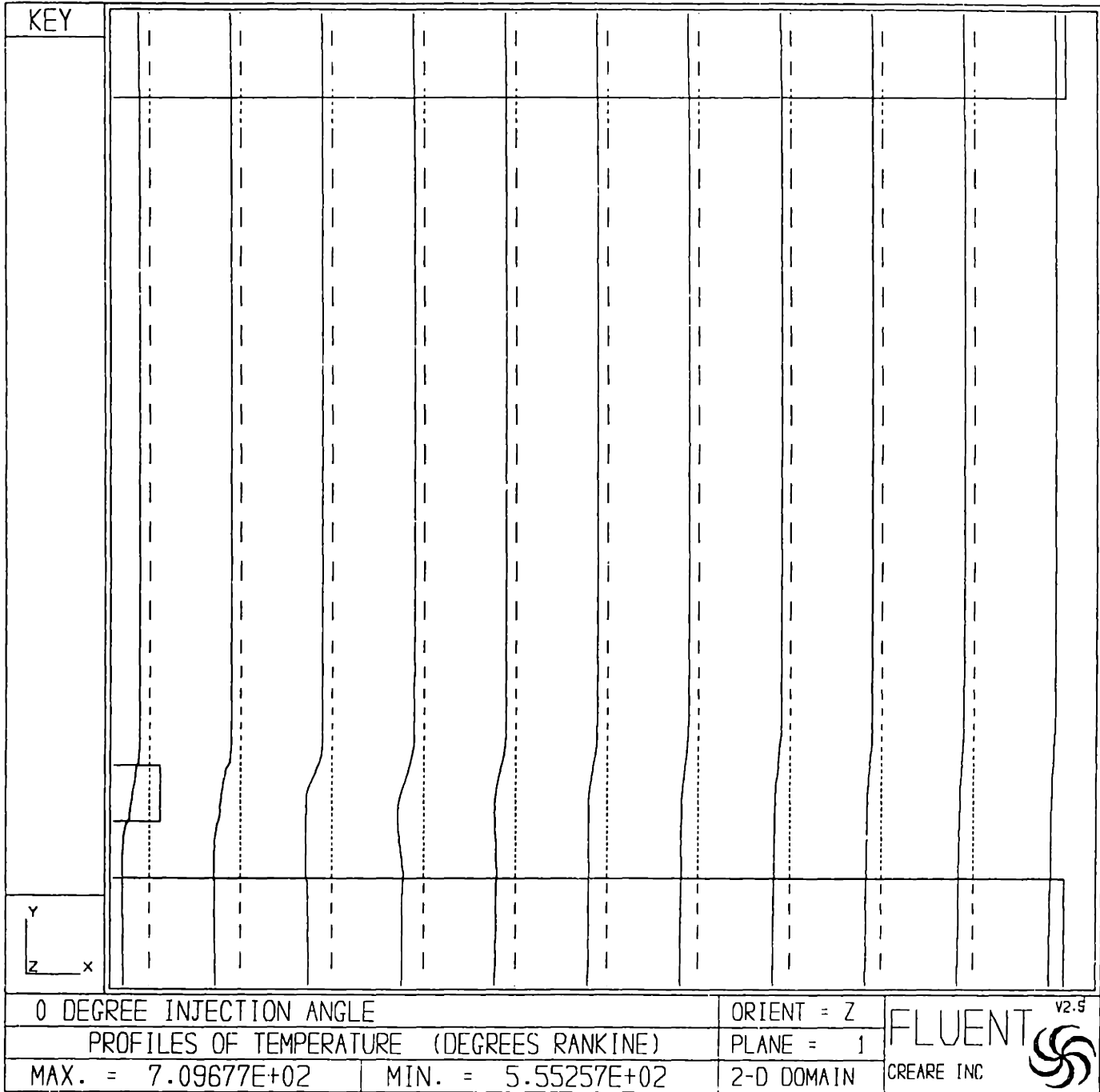


Figure 4-8: Temperature profile (M=0.2)

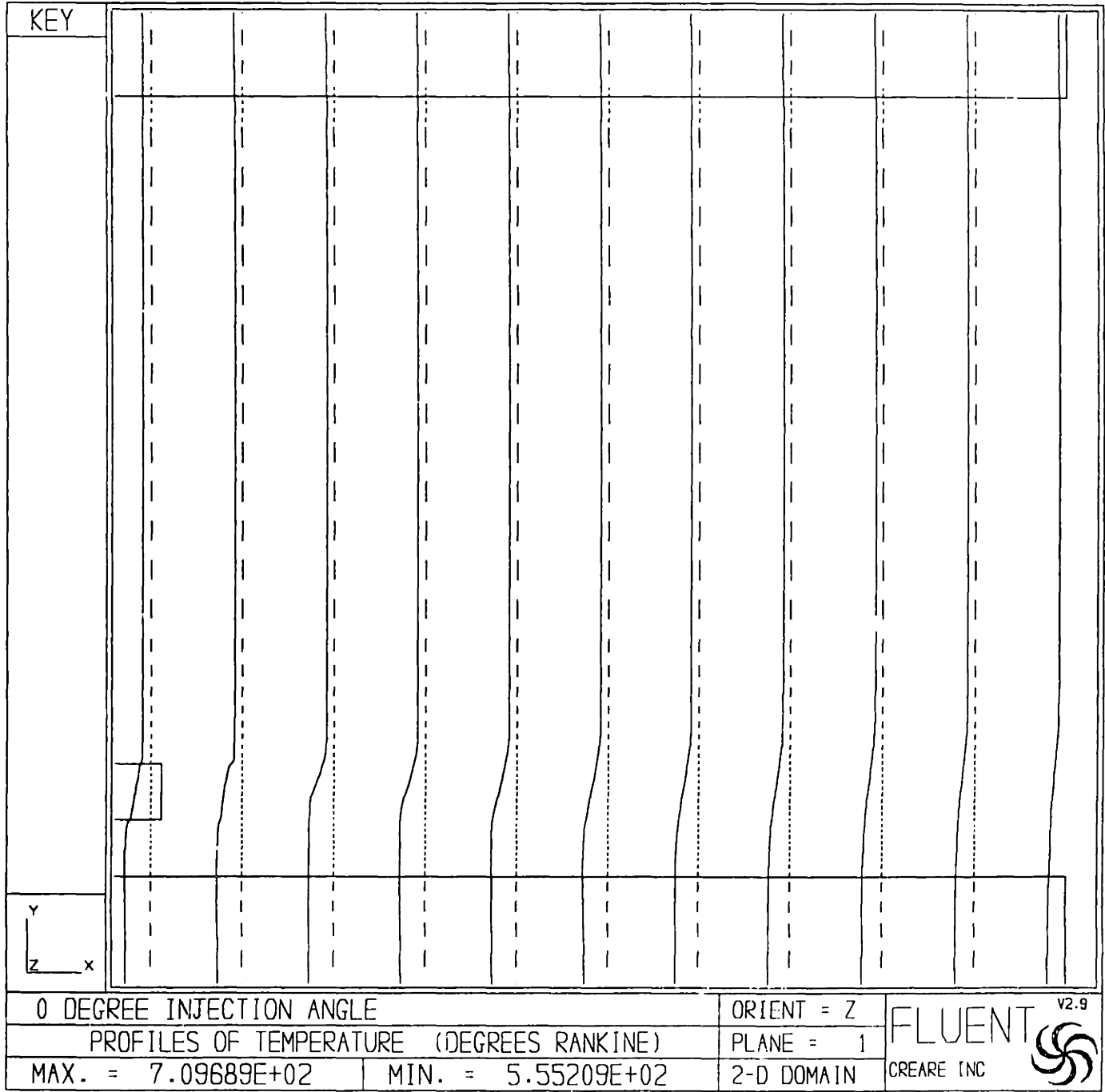


Figure 4-9: Temperature profile (M=0.4)



Figure 4-10: Temperature profile (M=0.6)



Figure 4-11: Temperature profile (M=0.8)



Figure 4-12: Temperature profile (M=1.0)

IV.4 Comparison with Experimental Results

Results from the computational simulations are shown in *Figure 4-13* where once film effectiveness (η) is plotted against blowing ratio (M). The experimental results for the same slot injection geometry are shown in *Figure 4-14*. As can be seen, the numerically computed effectiveness increases much more rapidly as a function of blowing ratio, when compared to the experimental results. This trend is confirmed by the velocity vector plots shown in the previous section since for M ratios greater than 6 the flow basically corresponds to that of a free jet boundary with very little mixing between the coolant and the mainstream hot gas. The model developed to predict the film effectiveness for tangentially injected coolant is somewhat crude and therefore, close agreement with experimental results is not expected. The results obtained with Fluent are not completely discouraging. Parametric calculations need to be performed to study the effect of turbulence intensity, upstream starting length of the mainstream boundary layer, grid size, etc.

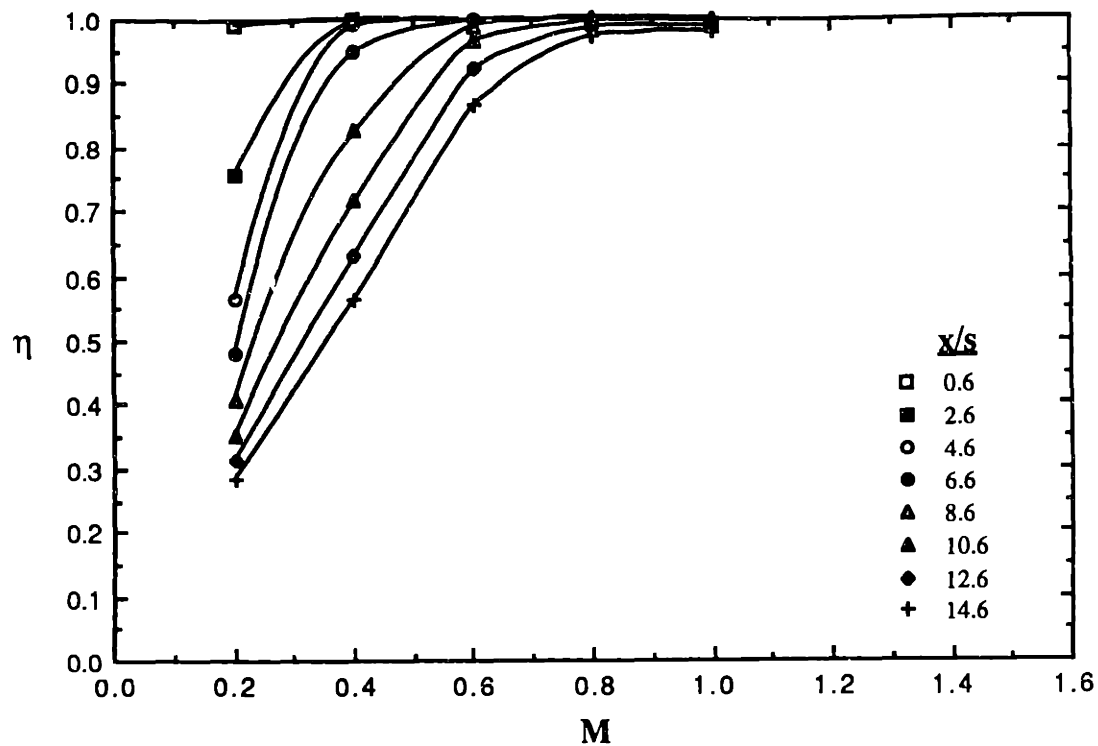


Figure 4-13: Numerical results (tangential injection)

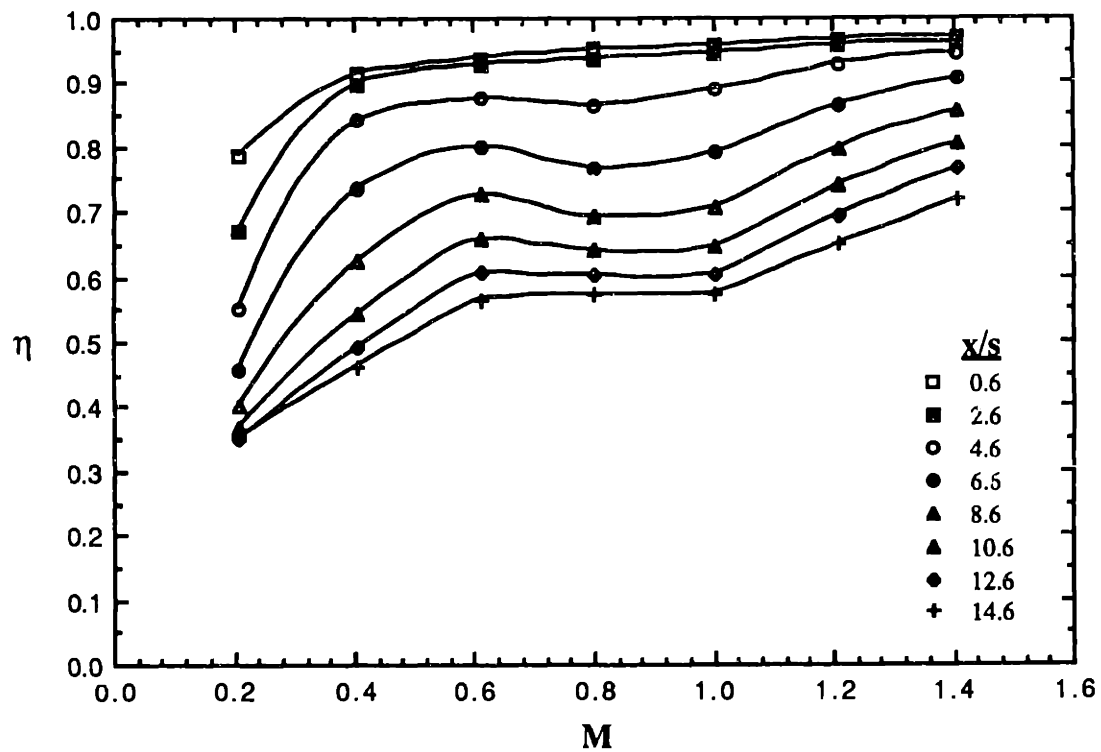


Figure 4-14: Experimental results (tangential injection)

V. Conclusions

Experimental results have been presented for adiabatic wall temperatures downstream of a multi-slot configuration through which air was injected into a mainstream for various injection angles. Because of the complex hydrodynamic behavior in the region immediately downstream of the slot, a purely empirical correlation of the results was performed.

Film effectiveness measurements showed a strong dependence on the blowing ratio, particularly at low values, and on the downstream distance from the slot. Correlations based on a parameter combining both these effects were relatively successful. An optimum injection angle was observed at 8.5° .

Although limited results were obtained for film effectiveness in the presence of strong acceleration factors, a reduction in film effectiveness was observed for typical gas turbine airfoil accelerations factors. An adjustment is needed for correlations based on (x/Ms) parameter to account for this drop in value.

The results of the numerical analysis performed with the commercially available CFD code, FLUENT, compared relatively well with experimental results for low blowing ratios but were much higher in value for increasing blowing ratios. A more refined turbulence model is needed to accurately describe in terms of film effectiveness the mixing region downstream of the injection slot.

References

1. R.J. Goldstein, "Film Cooling", *Advances in Heat Transfer*, pp. 321-379, 1971.
2. K. Wiegardt, "Hot-Air Discharge for De-Icing", AAF Trans. No F-TS-919-RE, December, 1946.
3. J. P. Hartnett, R. C. Birkebak and E. R. G. Eckert, "Velocity Distributions, Temperature Distributions, Effectiveness and Heat Transfer for Air injected Through a Tangential Slot Into a Turbulent Boundary Layer", *Journal of Heat Transfer*, August 1961.
4. R. A. Seban, H. W. Chan and S. Scesa, "Heat Transfer to a Turbulent Boundary Layer Downstream of an Injection Slot", Paper No. 57-A-36 ASME Annual Meeting, 1957.
5. R. A. Seban, "Heat Transfer and Effectiveness for a Turbulent Boundary Layer with Tangential Fluid Injection", *Journal of Heat Transfer*, November 1960.
6. J. H. Chin, S. C. Skirvin, L. E. Hayes, and A. H. Silver, "Adiabatic Wall Temperature Downstream of a Single Injection Slot", ASME Paper No. 58-A-104.
7. S. S. Papell and A. M. Trout, "Experimental Investigation of Air Film-Cooling Applied to an Adiabatic Wall by Means of an Axially Discharging Slot", NASA TN-D-9, 1959.
8. A. E. Samuel and P. N. Joubert, "Film Cooling of an Adiabatic Flat Plate in Zero Pressure Gradient in the Presence of a Hot Mainstream and Cold Tangential Secondary Injection", ASME Paper No. 64-WA/HT-48, 1964.
9. S. S. Papell, "Effect on Gaseous Film Cooling Injection Through Angled Slots and Normal Holes", NASA TN-D-299, 1960.
10. S. Sivasegaram and J. H. Whitelaw, "Film Cooling Slots: the Importance of Lip Thickness and Injection Angle", *Journal of Mechanical Engineering Science*, Vol 11 No. 1, 1969.
11. Temperature Measurement Handbook and Encyclopedia, Omega Engineering Inc., 1985.
12. ASME Interim Supplement 19.5 on Instruments and Apparatus, Sixth Edition 1971.
13. S.J. Kline and F.A. McClintock, "Describing Uncertainties in Single-Sample Experiments", *Mechanical Engineering*, Vol. 75, pp. 3-8, 1953.
14. Creare Inc., Etna Road. P. O. Box 71 Hanover, NH 03755.

Appendix A: Conduction Error

The measured test plate surface temperature T_w is in fact slightly lower than the idealized adiabatic wall temperature $T_{w,ad}$ because of the conduction across the test plate and urethane insulation. In this appendix an upper bound estimate using a simple control volume approach and a 1-D conduction model is performed to evaluate the percent decrease in adiabatic wall temperature due to the heat flux across the test plate. Radiation losses and axial conduction across the grain of the maple test plate contribute significantly less to the overall heat losses to the environment and are neglected in this calculation.

A 1-D conduction model of the test plate is shown in *Figure A-1*.

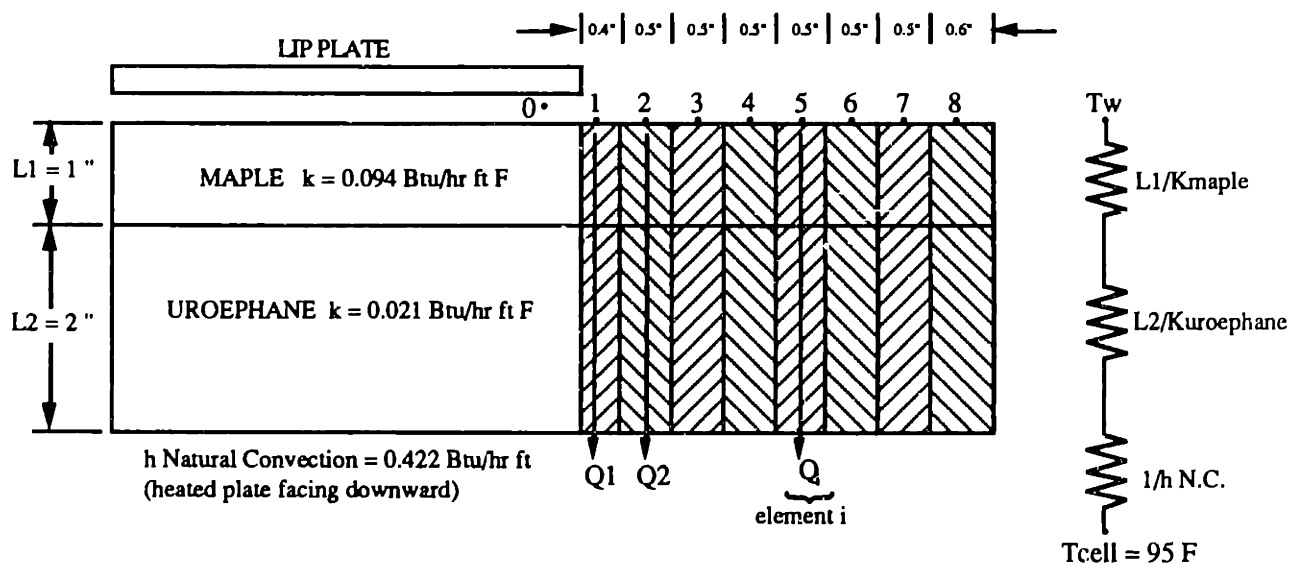


Figure A-1: 1-D conduction model

From the measured surface temperature at thermocouple locations 1 through 8 the heat flux q_i across the test plate for element i is given by:

$$q_i = \frac{T_{cell} - T_{wi}}{1/h_{N.C.} + L_1/K_{maple} + L_2/K_{uroephane}}$$

Substituting numerical values the following equation is obtained:

$$q_i = 0.08934 (95 - T_{\text{wall}}) \quad [\text{Btu/hr ft}^2]$$

Knowing the heat flux across the test plate, the decrease in adiabatic wall temperature can be estimated by performing an energy balance on a control volume as shown in *Figure A-2*.

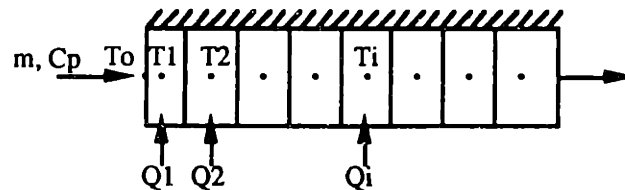


Figure A-2: Control volume

Energy balance:
$$\Delta T_i = T_i - T_o = \sum \frac{A_i q_i}{m C_p}$$

Results for the increase in temperature are presented in tabular form in *Table A-1* and indicated a maximum increase in temperature less than 2 percent.

Table A-1: Conduction error analysis

T/C #	1	2	3	4	5	6	7	8
T_w	139.3	155.5	172.5	186	193.95	198.64	201.1	200.7
q	3.976	5.405	6.924	8.130	8.84	9.259	9.479	9.443
ΔT	0.119	0.321	0.580	0.884	1.215	1.562	1.916	2.269

Appendix B: Error Analysis

According to reference 13, given a result R to be a linear function of n independent variables (v_1, v_2, \dots, v_n) described by the uncertainty intervals (u_1, u_2, \dots, u_n) then the uncertainty interval u_R for the result, based on the same odds as the intervals for each of the variables, is given by:

$$u_R = \left[\left(\frac{\partial R}{\partial v_1} u_1 \right)^2 + \left(\frac{\partial R}{\partial v_2} u_2 \right)^2 + \dots + \left(\frac{\partial R}{\partial v_n} u_n \right)^2 \right]^{1/2} \quad (B1)$$

For product functions of the form $f = v_1^{n_1} v_2^{n_2} \dots v_n^{n_n}$ the uncertainty interval is conveniently found by logarithmic differentiation:

$$\ln(f) = n_1 \ln(v_1) + n_2 \ln(v_2) + \dots + n_n \ln(v_n)$$

$$\frac{df}{f} = n_1 \frac{dv_1}{v_1} + n_2 \frac{dv_2}{v_2} + \dots + n_n \frac{dv_n}{v_n}$$

Thus, the relative uncertainty is given by:

$$u_R/R = \left[\left(n_1 \frac{u_1}{v_1} \right)^2 + \left(n_2 \frac{u_2}{v_2} \right)^2 + \dots + \left(n_n \frac{u_n}{v_n} \right)^2 \right]^{1/2} \quad (B2)$$

Film Effectiveness Uncertainty

From Eq. B1 and Eq. 2, the film effectiveness uncertainty (u_η) is equal to:

$$u_\eta = \left[\left(\frac{T_g - T_{aw}}{(T_g - T_s)^2} u_{T_s} \right)^2 + \left(\frac{1}{T_g - T_s} u_{T_{aw}} \right)^2 + \left(\frac{T_{aw} - T_s}{(T_g - T_s)^2} u_{T_g} \right)^2 \right]^{1/2}$$

and the relative uncertainty is equal to:

$$u_\eta/\eta = \left[\left(\frac{u_{T_s}}{T_g - T_s} \right)^2 + \left(\frac{u_{T_{aw}}}{T_g - T_{aw}} \right)^2 + \left(\frac{(T_{aw} - T_s) u_{T_g}}{(T_g - T_s)(T_g - T_{aw})} \right)^2 \right]^{1/2}$$

The maximum relative uncertainty occurs for minimum values of $(T_g - T_s)$ and $(T_g - T_{aw})$ or equivalently for maximum values of T_s and T_{aw} (i.e. low M ratio and high x/s ratio). *Table B-1* summarizes the uncertainty results for the different experimental tests.

Table B-1: Film effectiveness uncertainty analysis

$$u_{T_s} = u_{T_{aw}} = u_{T_g} = \pm 1.0 \text{ deg. F}$$

α deg	$Ka_{x=0}$ $\times 10^{-6}$	T_{max} ° F	T_g ° F	$T_{aw,max}$ ° F	$(u_\eta/\eta)_{max}$ %
0.0	0.0	113.9	251.	204.4	2.7
5.0	0.0	123.2	252	217.9	3.7
8.5	0.0	103.9	250	203.0	2.7
11.5	0.0	111.7	251	201.2	2.5
15.0	0.0	95.3	251	192.6	2.1
8.5	0.2 - 6.0	77.1	249	210.0	3.3

Mass Flow Rate Uncertainty

The equation to compute the air mass flow rate is given by Eq. 14 and is in the form of a product. Therefore, Eq. B2 may be used to determine the mass flow rate uncertainty u_m for which the results are conveniently summarized in *Table B-2*.

Table B-2: Mass flow rate uncertainty analysis

Component	v_i	u_i 20:1	u_i/v_i %	n_i	$(n_i u_i/v_i)^2$ (%) ²
C	0.6169	0.005	0.811	1	0.658
Y	0.9983	0.001	0.100	1	0.01
d	0.644	0.001	0.155	2	0.096
F_s	1.0005	0.0005	0.05	1	0.0025
P_1	14.720	0.0088	0.06	0.5	0.009
T_1	97.7	1.0	1.02	-0.5	0.26
ΔP	0.3	0.0125	4.167	0.5	4.34
β	0.4	0.001	0.25	-2	0.25

$$u_m / m = \sqrt{\sum (n_i u_i/v_i)^2} = 2.37 \%$$

Test Section Measurement Uncertainties

From the definition of the blowing ratio given by Eq. 4, the accuracy of measurements of the mainstream plenum area A_g and the slot area A_s will determine the accuracy of the calculated blowing ratio. The mainstream plenum area is equal to:

$$A_g = H W$$

where W is the total width of the plenum and h the height of the plenum as given in *Table 1*.

The slot area is given by:

$$A_s = s (w_1 + 7w + w_2)$$

where s is the lip thickness, w is the slot width, and w_1 and w_2 are the widths of the first and last slot of the test plate having lengths 0.44 and 0.46 in. respectively (see *Figure 2-5*). *Table B-3* summarizes the uncertainty analysis performed on both areas.

Table B-3: Test section measurement uncertainty analysis

Component	v_i	u_i 20:1	u_i/v_i %	n_i	$(n_i u_i/v_i)^2$ (%) ²
A_g					
H	2.90	0.01	0.34483	1	0.11891
W	11.65	0.01	0.08584	1	0.00737
$u_{A_g} / A_g = 0.355\%$					
Component	v_i	u_i 20:1	u_i/v_i %	n_i	$(n_i u_i/v_i)^2$ (%) ²
A_s					
s	0.18	0.01	5.55556	1	30.8642
w+7w ₂ +w ₁ lw	9.65	0.01	0.10363	7	0.52619
w+7w ₂ +w ₁ lw ₁	9.65	0.01	0.10363	1	0.01074
w+7w ₂ +w ₁ lw ₂	9.65	0.01	0.10363	1	0.01074
$u_{A_s} / A_s = 5.604\%$					

Mass-Velocity Ratio Uncertainty

The mass-velocity ratio is calculated according to Eq. 4. From the results of the uncertainty analysis performed for the mass flow rates and test section measurements, the uncertainty interval for the mass velocity ratio may be calculated and the results are shown in *Table B-4*.

Table B-4: Mass-velocity uncertainty analysis

Component	v_i	u_i 20:1	u_i/v_i %	n_i	$(n_i u_i/v_i)^2$ (%) ²
m_g	—	—	2.37	1	5.617
m_s	—	—	2.37	1	5.617
A_g	—	—	0.355	1	0.126
A_s	—	—	5.604	1	31.405

$$u_M / M = 6.54 \%$$

Appendix C: Film Effectiveness Data

FILM EFFECTIVENESS TEST
ANGLED INJECTION WITH NON-ACCELERATING FLOW

INJECTION ANGLE = 0.0 DEG. NUMBER OF SLOTS = 9 SLOT WIDTH = 1.25 (IN.)
SLOT HEIGHT = 0.25 (IN.) LIP THICKNESS = 0.25 (IN.)
HOT SIDE AREA = 34.1350 (SQ. IN) COLD SIDE AREA = 2.4100 (SQ. IN.)

T/C LOCATIONS

T/C#	X/S	4R	5L	5M	5R	6L	6M
1	0.600	X	X	X	X	X	X
2	2.600	X	X	X	X	X	X
3	4.600	X	X	X	X	X	X
4	6.600	X	X	X	X	X	X
5	8.600	X	X	X	X	X	X
6	10.600	X	X	X	X	X	X
7	12.600	X	X	X	X	X	X
8	14.600	X	X	X	X	X	X

Notes: D(X1,X2) = 100*(X2-X1)/X1
Note: Ef = (Igas - Tavg) / (Igas - Telot)

FILM EFFECTIVENESS DATA

SPANWISE AVERAGED EFFECTIVENESS DATA

***** Columns 4R-5L, 5L-5R, 5M-6L *****

T/C#	Mavg	Tavg	Efavg	X/S	X/MS
1	0.209	139.340	0.787	0.600	2.875
2	0.209	155.482	0.673	2.600	12.458
3	0.209	172.454	0.553	4.600	22.041
4	0.209	185.009	0.457	6.600	31.624
5	0.209	193.950	0.401	8.600	41.207
6	0.209	198.638	0.368	10.600	50.791
7	0.209	201.072	0.351	12.600	60.374
8	0.209	200.696	0.353	14.600	69.957

T/C#	Mavg	Tavg	Efavg	X/S	X/MS
1	0.406	112.432	0.913	0.600	1.478
2	0.406	114.472	0.899	2.600	6.403
3	0.406	123.436	0.840	4.600	11.329
4	0.406	139.539	0.734	6.600	16.254
5	0.406	155.116	0.624	8.600	21.180
6	0.406	168.480	0.543	10.600	26.105
7	0.406	176.264	0.491	12.600	31.031
8	0.406	180.458	0.463	14.600	35.956

T/C#	Mavg	Tavg	Efavg	X/S	X/MS
1	0.612	103.025	0.938	0.600	0.981
2	0.612	104.452	0.929	2.600	4.251
3	0.612	113.013	0.875	4.600	7.521
4	0.612	124.604	0.801	6.600	10.791
5	0.612	136.255	0.727	8.600	14.061
6	0.612	146.782	0.660	10.600	17.332
7	0.612	155.232	0.607	12.600	20.602
8	0.612	161.684	0.566	14.600	23.872

T/C#	Mavg	Tavg	Efavg	X/S	X/MS
1	0.802	98.021	0.951	0.600	0.748
2	0.802	100.170	0.937	2.600	3.243
3	0.802	111.832	0.865	4.600	5.737
4	0.802	127.627	0.766	6.600	8.231
5	0.802	139.514	0.692	8.600	10.725
6	0.802	147.923	0.640	10.600	13.219
7	0.802	154.213	0.601	12.600	15.714
8	0.802	158.598	0.573	14.600	18.208

T/C#	Mavg	Tavg	Efavg	X/S	X/MS
1	1.003	93.590	0.958	0.600	0.598
2	1.003	95.596	0.946	2.600	2.593
3	1.003	105.013	0.889	4.600	4.587
4	1.003	121.121	0.790	6.600	6.582
5	1.003	134.845	0.707	8.600	8.576
6	1.003	144.968	0.645	10.600	10.571
7	1.003	151.796	0.603	12.600	12.565
8	1.003	156.937	0.572	14.600	14.560

T/C#	Mavg	Tavg	Efavg	X/S	X/MS
1	1.209	90.736	0.967	0.600	0.496
2	1.209	92.258	0.958	2.600	2.150
3	1.209	97.227	0.928	4.600	3.804
4	1.209	107.825	0.863	6.600	5.459
5	1.209	118.843	0.797	8.600	7.113
6	1.209	128.513	0.738	10.600	8.767
7	1.209	136.010	0.693	12.600	10.421
8	1.209	143.465	0.648	14.600	12.075

T/C#	Mavg	Tavg	Efavg	X/S	X/MS
1	1.409	89.038	0.970	0.600	0.426
2	1.409	90.235	0.963	2.600	1.845
3	1.409	92.944	0.946	4.600	3.265
4	1.409	99.777	0.905	6.600	4.685
5	1.409	108.220	0.855	8.600	6.104
6	1.409	116.470	0.805	10.600	7.524
7	1.409	123.473	0.763	12.600	8.943
8	1.409	131.340	0.716	14.600	10.363

FILM EFFECTIVENESS TEST
ANGLED INJECTION WITH NON-ACCELERATING FLOW

INJECTION ANGLE - 11.5 DEG NUMBER OF SLOTS - 9 SLOT WIDTH - 1.25 (IN.)
SLOT HEIGHT - 0.407 (IN.) LIP THICKNESS - 0.407 (IN.)
HOT SIDE AREA - 33.7850 (SQ. IN) COLD SIDE AREA - 3.9240 (SQ. IN.)

T/C LOCATIONS

T/C#	X/S	4R	5L	5M	5R	6L	6M
1	0.369	X	X	X	X	X	X
2	1.597	X	X	X	X	X	X
3	2.826	X	X	X	X	X	X
4	4.054	X	X	X	X	X	X
5	5.283	X	X	X	X	X	X
6	6.511	X	X	X	X	X	X
7	7.740	X	X	X	X	X	X
8	8.968	X	X	X	X	X	X

Note: D(X1,X2) - 100*(X2-X1)/X1
Note: EF = (Tgas - Tavg)/(Tgas - Tslot)

FILM EFFECTIVENESS DATA
SPANWISE AVERAGED FILM EFFECTIVENESS DATA

**** Column 4R-5L, 5L-5R, 5M-6L ****

T/C#	Mavg	Tavg	EFavg	X/S	X/M/S
1	0.203	120.216	0.898	0.369	1.812
2	0.203	129.495	0.834	1.597	7.852
3	0.203	145.619	0.723	2.826	13.892
4	0.203	166.123	0.582	4.054	19.931
5	0.203	189.251	0.485	5.283	25.971
6	0.203	189.105	0.424	6.511	32.011
7	0.203	194.573	0.387	7.740	38.051
8	0.203	197.925	0.363	8.968	44.091

T/C#	Mavg	Tavg	EFavg	X/S	X/M/S
1	0.404	110.846	0.937	0.369	0.913
2	0.404	114.729	0.911	1.597	3.956
3	0.404	118.160	0.888	2.826	6.998
4	0.404	124.256	0.848	4.054	10.041
5	0.404	135.993	0.769	5.283	13.084
6	0.404	150.155	0.674	6.511	16.126
7	0.404	160.871	0.603	7.740	19.169
8	0.404	170.964	0.535	8.968	22.212

T/C#	Mavg	Tavg	EFavg	X/S	X/M/S
1	0.591	106.094	0.950	0.369	0.624
2	0.591	108.620	0.934	1.597	2.703
3	0.591	110.881	0.919	2.826	4.783
4	0.591	114.204	0.897	4.054	6.863
5	0.591	119.849	0.860	5.283	8.942
6	0.591	128.499	0.804	6.511	11.022
7	0.591	137.157	0.747	7.740	13.101
8	0.591	148.933	0.669	8.968	15.181

T/C#	Mavg	Tavg	EFavg	X/S	X/M/S
1	0.790	103.482	0.959	0.369	0.466
2	0.790	104.239	0.947	1.597	2.021
3	0.790	105.691	0.938	2.826	3.576
4	0.790	108.000	0.923	4.054	5.130
5	0.790	112.229	0.896	5.283	6.685
6	0.790	118.406	0.856	6.511	8.239
7	0.790	125.523	0.810	7.740	9.794
8	0.790	135.409	0.746	8.968	11.348

T/C#	Mavg	Tavg	EFavg	X/S	X/M/S
1	0.991	100.122	0.964	0.369	0.372
2	0.991	101.514	0.955	1.597	1.612
3	0.991	102.567	0.948	2.826	2.851
4	0.991	104.331	0.937	4.054	4.091
5	0.991	107.851	0.915	5.283	5.331
6	0.991	113.223	0.880	6.511	6.570
7	0.991	119.892	0.838	7.740	7.810
8	0.991	128.828	0.781	8.968	9.050

T/C#	Mavg	Tavg	EFavg	X/S	X/M/S
1	1.203	98.641	0.969	0.369	0.306
2	1.203	99.826	0.961	1.597	1.327
3	1.203	100.664	0.956	2.826	2.348
4	1.203	102.141	0.946	4.054	3.369
5	1.203	104.945	0.928	5.283	4.390
6	1.203	109.230	0.901	6.511	5.411
7	1.203	114.475	0.868	7.740	6.432
8	1.203	122.966	0.814	8.968	7.453

T/C#	Mavg	Tavg	EFavg	X/S	X/M/S
1	1.437	97.458	0.971	0.369	0.256
2	1.437	98.491	0.964	1.597	1.111
3	1.437	99.279	0.959	2.826	1.966
4	1.437	100.776	0.933	4.054	2.821
5	1.437	103.459	0.933	5.283	3.676
6	1.437	107.213	0.909	6.511	4.530
7	1.437	111.475	0.882	7.740	5.385
8	1.437	119.406	0.832	8.968	6.240

MOSE	V/C	M	Time	Time	Time	Total	HR	E/Min
402	1	0.200	113.318	210.300	84.400	0.874	4.032	
403	2	0.200	113.047	210.300	84.400	0.848	13.384	
404	3	0.200	112.816	210.300	84.400	0.824	16.768	
405	4	0.200	112.585	210.300	84.400	0.800	20.160	
406	5	0.200	112.354	210.300	84.400	0.776	23.568	
407	6	0.200	112.123	210.300	84.400	0.752	26.976	
408	7	0.200	111.892	210.300	84.400	0.728	30.384	
409	8	0.200	111.661	210.300	84.400	0.704	33.792	
410	9	0.200	111.430	210.300	84.400	0.680	37.200	
411	10	0.200	111.199	210.300	84.400	0.656	40.608	
412	11	0.200	110.968	210.300	84.400	0.632	44.016	
413	12	0.200	110.737	210.300	84.400	0.608	47.424	
414	13	0.200	110.506	210.300	84.400	0.584	50.832	
415	14	0.200	110.275	210.300	84.400	0.560	54.240	
416	15	0.200	110.044	210.300	84.400	0.536	57.648	
417	16	0.200	109.813	210.300	84.400	0.512	61.056	
418	17	0.200	109.582	210.300	84.400	0.488	64.464	
419	18	0.200	109.351	210.300	84.400	0.464	67.872	
420	19	0.200	109.120	210.300	84.400	0.440	71.280	
421	20	0.200	108.889	210.300	84.400	0.416	74.688	
422	21	0.200	108.658	210.300	84.400	0.392	78.096	
423	22	0.200	108.427	210.300	84.400	0.368	81.504	
424	23	0.200	108.196	210.300	84.400	0.344	84.912	
425	24	0.200	107.965	210.300	84.400	0.320	88.320	
426	25	0.200	107.734	210.300	84.400	0.296	91.728	
427	26	0.200	107.503	210.300	84.400	0.272	95.136	
428	27	0.200	107.272	210.300	84.400	0.248	98.544	
429	28	0.200	107.041	210.300	84.400	0.224	101.952	
430	29	0.200	106.810	210.300	84.400	0.200	105.360	
431	30	0.200	106.579	210.300	84.400	0.176	108.768	
432	31	0.200	106.348	210.300	84.400	0.152	112.176	
433	32	0.200	106.117	210.300	84.400	0.128	115.584	
434	33	0.200	105.886	210.300	84.400	0.104	118.992	
435	34	0.200	105.655	210.300	84.400	0.080	122.400	
436	35	0.200	105.424	210.300	84.400	0.056	125.808	
437	36	0.200	105.193	210.300	84.400	0.032	129.216	
438	37	0.200	104.962	210.300	84.400	0.008	132.624	
439	38	0.200	104.731	210.300	84.400	0.000	136.032	
440	39	0.200	104.500	210.300	84.400	0.000	139.440	
441	40	0.200	104.269	210.300	84.400	0.000	142.848	
442	41	0.200	104.038	210.300	84.400	0.000	146.256	
443	42	0.200	103.807	210.300	84.400	0.000	149.664	
444	43	0.200	103.576	210.300	84.400	0.000	153.072	
445	44	0.200	103.345	210.300	84.400	0.000	156.480	
446	45	0.200	103.114	210.300	84.400	0.000	159.888	
447	46	0.200	102.883	210.300	84.400	0.000	163.296	
448	47	0.200	102.652	210.300	84.400	0.000	166.704	
449	48	0.200	102.421	210.300	84.400	0.000	170.112	
450	49	0.200	102.190	210.300	84.400	0.000	173.520	
451	50	0.200	101.959	210.300	84.400	0.000	176.928	
452	51	0.200	101.728	210.300	84.400	0.000	180.336	
453	52	0.200	101.497	210.300	84.400	0.000	183.744	
454	53	0.200	101.266	210.300	84.400	0.000	187.152	
455	54	0.200	101.035	210.300	84.400	0.000	190.560	
456	55	0.200	100.804	210.300	84.400	0.000	193.968	
457	56	0.200	100.573	210.300	84.400	0.000	197.376	
458	57	0.200	100.342	210.300	84.400	0.000	200.784	
459	58	0.200	100.111	210.300	84.400	0.000	204.192	
460	59	0.200	99.880	210.300	84.400	0.000	207.600	
461	60	0.200	99.649	210.300	84.400	0.000	211.008	
462	61	0.200	99.418	210.300	84.400	0.000	214.416	
463	62	0.200	99.187	210.300	84.400	0.000	217.824	
464	63	0.200	98.956	210.300	84.400	0.000	221.232	
465	64	0.200	98.725	210.300	84.400	0.000	224.640	
466	65	0.200	98.494	210.300	84.400	0.000	228.048	
467	66	0.200	98.263	210.300	84.400	0.000	231.456	
468	67	0.200	98.032	210.300	84.400	0.000	234.864	
469	68	0.200	97.801	210.300	84.400	0.000	238.272	
470	69	0.200	97.570	210.300	84.400	0.000	241.680	
471	70	0.200	97.339	210.300	84.400	0.000	245.088	
472	71	0.200	97.108	210.300	84.400	0.000	248.496	
473	72	0.200	96.877	210.300	84.400	0.000	251.904	
474	73	0.200	96.646	210.300	84.400	0.000	255.312	
475	74	0.200	96.415	210.300	84.400	0.000	258.720	
476	75	0.200	96.184	210.300	84.400	0.000	262.128	
477	76	0.200	95.953	210.300	84.400	0.000	265.536	
478	77	0.200	95.722	210.300	84.400	0.000	268.944	
479	78	0.200	95.491	210.300	84.400	0.000	272.352	
480	79	0.200	95.260	210.300	84.400	0.000	275.760	
481	80	0.200	95.029	210.300	84.400	0.000	279.168	
482	81	0.200	94.798	210.300	84.400	0.000	282.576	
483	82	0.200	94.567	210.300	84.400	0.000	285.984	
484	83	0.200	94.336	210.300	84.400	0.000	289.392	
485	84	0.200	94.105	210.300	84.400	0.000	292.800	
486	85	0.200	93.874	210.300	84.400	0.000	296.208	
487	86	0.200	93.643	210.300	84.400	0.000	299.616	
488	87	0.200	93.412	210.300	84.400	0.000	303.024	
489	88	0.200	93.181	210.300	84.400	0.000	306.432	
490	89	0.200	92.950	210.300	84.400	0.000	309.840	
491	90	0.200	92.719	210.300	84.400	0.000	313.248	
492	91	0.200	92.488	210.300	84.400	0.000	316.656	
493	92	0.200	92.257	210.300	84.400	0.000	320.064	
494	93	0.200	92.026	210.300	84.400	0.000	323.472	
495	94	0.200	91.795	210.300	84.400	0.000	326.880	
496	95	0.200	91.564	210.300	84.400	0.000	330.288	
497	96	0.200	91.333	210.300	84.400	0.000	333.696	
498	97	0.200	91.102	210.300	84.400	0.000	337.104	
499	98	0.200	90.871	210.300	84.400	0.000	340.512	
500	99	0.200	90.640	210.300	84.400	0.000	343.920	

MOSE	V/C	M	Time	Time	Time	Total	HR	E/Min
402	1	0.200	113.318	210.300	84.400	0.874	4.032	
403	2	0.200	113.047	210.300	84.400	0.848	13.384	
404	3	0.200	112.816	210.300	84.400	0.824	16.768	
405	4	0.200	112.585	210.300	84.400	0.800	20.160	
406	5	0.200	112.354	210.300	84.400	0.776	23.568	
407	6	0.200	112.123	210.300	84.400	0.752	26.976	
408	7	0.200	111.892	210.300	84.400	0.728	30.384	
409	8	0.200	111.661	210.300	84.400	0.704	33.792	
410	9	0.200	111.430	210.300	84.400	0.680	37.200	
411	10	0.200	111.199	210.300	84.400	0.656	40.608	
412	11	0.200	110.968	210.300	84.400	0.632	44.016	
413	12	0.200	110.737	210.300	84.400	0.608	47.424	
414	13	0.200	110.506	210.300	84.400	0.584	50.832	
415	14	0.200	110.275	210.300	84.400	0.560	54.240	
416	15	0.200	110.044	210.300	84.400	0.536	57.648	
417	16	0.200	109.813	210.300	84.400	0.512	61.056	
418	17	0.200	109.582	210.300	84.400	0.488	64.464	
419	18	0.200	109.351	210.300	84.400	0.464	67.872	
420	19	0.200	109.120	210.300	84.400	0.440	71.280	
421	20	0.200	108.889	210.300	84.400	0.416	74.688	
422	21	0.200	108.658	210.300	84.400	0.392	78.096	
423	22	0.200	108.427	210.300	84.400	0.368	81.504	
424	23	0.200	108.196	210.300	84.400	0.344	84.912	
425	24	0.200	107.965	210.300	84.400	0.320	88.320	
426	25	0.200	107.734	210.300	84.400	0.296	91.728	
427	26	0.200	107.503	210.300	84.400	0.272	95.136	
428	27	0.200	107.272	210.300	84.400	0.248	98.544	
429	28	0.200	107.041	210.300	84.400	0.224	101.952	
430	29	0.200	106.810	210.300	84.400	0.200	105.360	
431	30	0.200	106.579	210.300	84.400	0.176	108.768	
432	31	0.200	106.348	210.300	84.400	0.152	112.176	
433	32	0.200	106.117	210.300	84.400	0.128	115.584	
434	33	0.200	105.886	210.300	84.400	0.104	118.992	
435	34	0.200	105.655	210.300	84.400	0.080	122.400	
436	35	0.200	105.424	210.300	84.400	0.056	125.808	
437	36	0.200	105.193	210.300	84.400	0.032	129.216	
438	37	0.200	104.962	210.300	84.400	0.008	132.624	
439	38	0.200	104.731	210.300	84.400	0.000	136.032	
440	39	0.200	104.500	210.300	84.400	0.000	139.440	
441	40	0.200	104.269	210.300	84.400	0.000	142.848	
442	41	0.200	104.038	210.300	84.400	0.000	146.256	
443	42	0.200	103.807	210.300	84.400	0.000	149.66	

FILM EFFECTIVENESS TEST
ANGLED INJECTION WITH NON-ACCELERATING FLOW

INJECTION ANGLE - 15.0 DEG NUMBER OF SLOTS - 9 SLOT WIDTH - 1.25 (IN.)
SLOT HEIGHT - 0.536 (IN.) LIP THICKNESS - 0.536 (IN.)
HOT SIDE AREA - 34.1350 (SQ. IN) COLD SIDE AREA - 5.1670 (SQ. IN.)

T/C LOCATIONS

T/C#	X/S	4R	5L	5M	5R	6L	6M
1	0.280	X	X	X	X	X	X
2	1.213	X	X	X	X	X	X
3	2.146	X	X	X	X	X	X
4	3.078	X	X	X	X	X	X
5	4.011	X	X	X	X	X	X
6	4.944	X	X	X	X	X	X
7	5.877	X	X	X	X	X	X
8	6.810	X	X	X	X	X	X

Note: $D(X1, X2) = 100 * (X2 - X1) / X1$
Note: $EF = (Tg_{ave} - Taw) / (Tg_{ave} - T_{tot})$

FILM EFFECTIVENESS DATA
SPANWISE AVERAGED FILM EFFECTIVENESS DATA

***** Columns 4R-5L, 5L-5R, 5M-6L *****

T/C#	MAVG	TAVG	EFavg	X/S	X/MS
1	0.199	105.186	0.905	0.280	1.405
2	0.199	112.977	0.858	1.213	6.086
3	0.199	124.993	0.783	2.146	10.768
4	0.199	145.147	0.657	3.078	15.450
5	0.199	164.272	0.538	4.011	20.131
6	0.199	176.739	0.461	4.944	24.813
7	0.199	184.691	0.411	5.877	29.495
8	0.199	189.515	0.381	6.810	34.177

T/C#	MAVG	TAVG	EFavg	X/S	X/MS
1	0.400	93.906	0.942	0.280	0.699
2	0.400	97.263	0.922	1.213	3.030
3	0.400	100.290	0.904	2.146	5.361
4	0.400	104.329	0.879	3.078	7.692
5	0.400	111.877	0.834	4.011	10.023
6	0.400	124.425	0.759	4.944	12.354
7	0.400	136.969	0.683	5.877	14.685
8	0.400	150.509	0.602	6.810	17.016

T/C#	MAVG	TAVG	EFavg	X/S	X/MS
1	0.606	88.159	0.955	0.280	0.462
2	0.606	90.004	0.944	1.213	2.000
3	0.606	91.464	0.935	2.146	3.538
4	0.606	93.343	0.924	3.078	5.077
5	0.606	96.891	0.904	4.011	6.615
6	0.606	103.192	0.867	4.944	8.154
7	0.606	111.775	0.816	5.877	9.692
8	0.606	124.145	0.744	6.810	11.231

T/C#	MAVG	TAVG	EFavg	X/S	X/MS
1	0.799	84.575	0.963	0.280	0.350
2	0.799	85.919	0.955	1.213	1.518
3	0.799	86.888	0.950	2.146	2.686
4	0.799	88.201	0.942	3.078	3.854
5	0.799	91.002	0.926	4.011	5.022
6	0.799	95.982	0.897	4.944	6.190
7	0.799	103.495	0.854	5.877	7.358
8	0.799	113.552	0.795	6.810	8.527

T/C#	MAVG	TAVG	EFavg	X/S	X/MS
1	0.997	81.996	0.967	0.280	0.281
2	0.997	83.096	0.961	1.213	1.217
3	0.997	83.621	0.956	2.146	2.153
4	0.997	84.892	0.950	3.078	3.089
5	0.997	87.097	0.938	4.011	4.024
6	0.997	90.919	0.916	4.944	4.960
7	0.997	96.915	0.881	5.877	5.896
8	0.997	106.056	0.829	6.810	6.832

T/C#	MAVG	TAVG	EFavg	X/S	X/MS
1	1.215	80.315	0.971	0.280	0.230
2	1.215	81.181	0.966	1.213	0.998
3	1.215	81.753	0.963	2.146	1.766
4	1.215	82.770	0.957	3.078	2.534
5	1.215	84.828	0.945	4.011	3.301
6	1.215	88.107	0.927	4.944	4.069
7	1.215	92.772	0.900	5.877	4.837
8	1.215	101.218	0.852	6.810	5.605

FILM IDENTIFICATION SYSTEM
 IDENTIFICATION NUMBER = 9.1.3.000 (FILM NUMBER) (REEL NUMBER) (TAPE NUMBER) (TAPE POSITION)
 REEL NUMBER = 01 (FILM NUMBER) (REEL NUMBER) (TAPE NUMBER) (TAPE POSITION)
 TAPE POSITION = 01 (FILM NUMBER) (REEL NUMBER) (TAPE NUMBER) (TAPE POSITION)

F/LC LOCATIONS

V/C#	F/C#	48	3M	3S	4L	4M	4W	LAND
1	0.100	X	X	X	X	X	X	X
2	0.100	X	X	X	X	X	X	X
3	0.100	X	X	X	X	X	X	X
4	0.100	X	X	X	X	X	X	X
5	0.100	X	X	X	X	X	X	X
6	0.100	X	X	X	X	X	X	X
7	0.100	X	X	X	X	X	X	X
8	0.100	X	X	X	X	X	X	X

Data: D(1,1) = 100*(12-11)/71
 Data: W = (Type - 700)/(1900 - 700)

FILM IDENTIFICATION DATA

Column 48

NO#	V/C#	M	Time	Frame	Start	End	Rate	Time
439	1	0.139	121.783	248.400	72.800	0.732	3.189	
440	1	0.139	121.783	248.400	72.800	0.732	3.189	
441	1	0.139	121.783	248.400	72.800	0.732	3.189	
442	1	0.139	121.783	248.400	72.800	0.732	3.189	
443	1	0.139	121.783	248.400	72.800	0.732	3.189	
444	1	0.139	121.783	248.400	72.800	0.732	3.189	
445	1	0.139	121.783	248.400	72.800	0.732	3.189	
446	1	0.139	121.783	248.400	72.800	0.732	3.189	
447	1	0.139	121.783	248.400	72.800	0.732	3.189	
448	1	0.139	121.783	248.400	72.800	0.732	3.189	
449	1	0.139	121.783	248.400	72.800	0.732	3.189	

NO#	V/C#	M	Time	Frame	Start	End	Rate	Time
441	1	0.404	170.708	248.400	61.700	0.430	1.261	
442	1	0.404	170.708	248.400	61.700	0.430	1.261	
443	1	0.404	170.708	248.400	61.700	0.430	1.261	
444	1	0.404	170.708	248.400	61.700	0.430	1.261	
445	1	0.404	170.708	248.400	61.700	0.430	1.261	
446	1	0.404	170.708	248.400	61.700	0.430	1.261	
447	1	0.404	170.708	248.400	61.700	0.430	1.261	
448	1	0.404	170.708	248.400	61.700	0.430	1.261	
449	1	0.404	170.708	248.400	61.700	0.430	1.261	
450	1	0.404	170.708	248.400	61.700	0.430	1.261	

NO#	V/C#	M	Time	Frame	Start	End	Rate	Time
441	1	0.603	47.916	248.400	74.400	0.633	1.608	
442	1	0.603	47.916	248.400	74.400	0.633	1.608	
443	1	0.603	47.916	248.400	74.400	0.633	1.608	
444	1	0.603	47.916	248.400	74.400	0.633	1.608	
445	1	0.603	47.916	248.400	74.400	0.633	1.608	
446	1	0.603	47.916	248.400	74.400	0.633	1.608	
447	1	0.603	47.916	248.400	74.400	0.633	1.608	
448	1	0.603	47.916	248.400	74.400	0.633	1.608	
449	1	0.603	47.916	248.400	74.400	0.633	1.608	
450	1	0.603	47.916	248.400	74.400	0.633	1.608	

NO#	V/C#	M	Time	Frame	Start	End	Rate	Time
441	1	0.830	67.878	248.400	78.400	0.864	2.183	
442	1	0.830	67.878	248.400	78.400	0.864	2.183	
443	1	0.830	67.878	248.400	78.400	0.864	2.183	
444	1	0.830	67.878	248.400	78.400	0.864	2.183	
445	1	0.830	67.878	248.400	78.400	0.864	2.183	
446	1	0.830	67.878	248.400	78.400	0.864	2.183	
447	1	0.830	67.878	248.400	78.400	0.864	2.183	
448	1	0.830	67.878	248.400	78.400	0.864	2.183	
449	1	0.830	67.878	248.400	78.400	0.864	2.183	
450	1	0.830	67.878	248.400	78.400	0.864	2.183	

NO#	V/C#	M	Time	Frame	Start	End	Rate	Time
441	1	1.005	87.916	248.400	80.100	0.936	2.488	
442	1	1.005	87.916	248.400	80.100	0.936	2.488	
443	1	1.005	87.916	248.400	80.100	0.936	2.488	
444	1	1.005	87.916	248.400	80.100	0.936	2.488	
445	1	1.005	87.916	248.400	80.100	0.936	2.488	
446	1	1.005	87.916	248.400	80.100	0.936	2.488	
447	1	1.005	87.916	248.400	80.100	0.936	2.488	
448	1	1.005	87.916	248.400	80.100	0.936	2.488	
449	1	1.005	87.916	248.400	80.100	0.936	2.488	
450	1	1.005	87.916	248.400	80.100	0.936	2.488	

NO#	V/C#	M	Time	Frame	Start	End	Rate	Time
441	1	1.218	117.810	248.400	82.400	0.975	2.641	
442	1	1.218	117.810	248.400	82.400	0.975	2.641	
443	1	1.218	117.810	248.400	82.400	0.975	2.641	
444	1	1.218	117.810	248.400	82.400	0.975	2.641	
445	1	1.218	117.810	248.400	82.400	0.975	2.641	
446	1	1.218	117.810	248.400	82.400	0.975	2.641	
447	1	1.218	117.810	248.400	82.400	0.975	2.641	
448	1	1.218	117.810	248.400	82.400	0.975	2.641	
449	1	1.218	117.810	248.400	82.400	0.975	2.641	
450	1	1.218	117.810	248.400	82.400	0.975	2.641	

NO#	V/C#	M	Time	Frame	Start	End	Rate	Time
441	1	1.432	147.810	248.400	84.400	0.985	2.705	
442	1	1.432	147.810	248.400	84.400	0.985	2.705	
443	1	1.432	147.810	248.400	84.400	0.985	2.705	
444	1	1.432	147.810	248.400	84.400	0.985	2.705	
445	1	1.432	147.810	248.400	84.400	0.985	2.705	
446	1	1.432	147.810	248.400	84.400	0.985	2.705	
447	1	1.432	147.810	248.400	84.400	0.985	2.705	
448	1	1.432	147.810	248.400	84.400	0.985	2.705	
449	1	1.432	147.810	248.400	84.400	0.985	2.705	
450	1	1.432	147.810	248.400	84.400	0.985	2.705	

NO#	V/C#	M	Time	Frame	Start	End	Rate	Time
441	1	1.645	177.810	248.400	86.400	0.985	2.705	
442	1	1.645	177.810	248.400	86.400	0.985	2.705	
443	1	1.645	177.810	248.400	86.400	0.985	2.705	
444	1	1.645	177.810	248.400	86.400	0.985	2.705	
445	1	1.645	177.810	248.400	86.400	0.985	2.705	
446	1	1.645	177.810	248.400	86.400	0.985	2.705	
447	1	1.645	177.810	248.400	86.400	0.985	2.705	
448	1	1.645	177.810	248.400	86.400	0.985	2.705	
449	1	1.645	177.810	248.400	86.400	0.985	2.705	
450	1	1.645	177.810	248.400	86.400	0.985	2.705	

NO#	V/C#	M	Time	Frame	Start	End	Rate	Time
441	1	1.858	207.810	248.400	88.400	0.985	2.705	
442	1	1.858	207.810	248.400	88.400	0.985	2.705	
443	1	1.858	207.810	248.400	88.400	0.985	2.705	
444	1	1.858	207.810	248.400	88.400	0.985	2.705	
445	1	1.858	207.810	248.400	88.400	0.985	2.705	
446	1	1.858	207.810	248.400	88.400	0.985	2.705	
447	1	1.858	207.810	248.400	88.400	0.985	2.705	
448	1	1.858	207.810	248.400	88.400	0.985	2.705	
449	1	1.858	207.810	248.400	88.400	0.985	2.705	
450	1	1.858	207.810	248.400	88.400	0.985	2.705	

NO#	V/C#	M	Time	Frame	Start	End	Rate	Time
441	1	2.071	237.810	248.400	90.400	0.985	2.705	
442	1	2.071	237.810	248.400	90.400	0.985	2.705	
443	1	2.071	237.810	248.400	90.400	0.985	2.705	
444	1	2.071	237.810	248.400	90.400	0.985	2.705	
445	1	2.071	237.810	248.400	90.400	0.985	2.705	
446	1	2.071	237.810	248.400	90.400	0.985	2.705	
447	1	2.071	237.810	248.400	90.400	0.985	2.705	
448	1	2.071	237.810	248.400	90.400	0.985	2.705	
449	1	2.071	237.810	248.400	90.400	0.985	2.705	
450	1	2.071	237.810	248.400	90.400	0.985	2.705	

NO#	V/C#	M	Time	Frame	Start	End	Rate	Time
449	1	1.00						

Model	V/C	M	Yr	Tot	Pr	ER	V/M
446	1	0.432	150,215	248,400	66,400	0.312	1.328
446	2	0.432	150,215	248,400	66,400	0.440	2.792
446	3	0.432	150,215	248,400	66,400	0.440	3.354
446	4	0.432	150,215	248,400	66,400	0.440	3.916
446	5	0.432	150,215	248,400	66,400	0.440	4.478
446	6	0.432	150,215	248,400	66,400	0.440	5.040
446	7	0.432	150,215	248,400	66,400	0.440	5.602
446	8	0.432	150,215	248,400	66,400	0.440	6.164
447	1	0.432	150,215	248,400	66,400	0.312	1.328
447	2	0.432	150,215	248,400	66,400	0.440	2.792
447	3	0.432	150,215	248,400	66,400	0.440	3.354
447	4	0.432	150,215	248,400	66,400	0.440	3.916
447	5	0.432	150,215	248,400	66,400	0.440	4.478
447	6	0.432	150,215	248,400	66,400	0.440	5.040
447	7	0.432	150,215	248,400	66,400	0.440	5.602
447	8	0.432	150,215	248,400	66,400	0.440	6.164

Model	V/C	M	Yr	Tot	Pr	ER	V/M
448	1	0.432	150,215	248,400	66,400	0.312	1.328
448	2	0.432	150,215	248,400	66,400	0.440	2.792
448	3	0.432	150,215	248,400	66,400	0.440	3.354
448	4	0.432	150,215	248,400	66,400	0.440	3.916
448	5	0.432	150,215	248,400	66,400	0.440	4.478
448	6	0.432	150,215	248,400	66,400	0.440	5.040
448	7	0.432	150,215	248,400	66,400	0.440	5.602
448	8	0.432	150,215	248,400	66,400	0.440	6.164

Model	V/C	M	Yr	Tot	Pr	ER	V/M
449	1	0.432	150,215	248,400	66,400	0.312	1.328
449	2	0.432	150,215	248,400	66,400	0.440	2.792
449	3	0.432	150,215	248,400	66,400	0.440	3.354
449	4	0.432	150,215	248,400	66,400	0.440	3.916
449	5	0.432	150,215	248,400	66,400	0.440	4.478
449	6	0.432	150,215	248,400	66,400	0.440	5.040
449	7	0.432	150,215	248,400	66,400	0.440	5.602
449	8	0.432	150,215	248,400	66,400	0.440	6.164

Model	V/C	M	Yr	Tot	Pr	ER	V/M
450	1	0.432	150,215	248,400	66,400	0.312	1.328
450	2	0.432	150,215	248,400	66,400	0.440	2.792
450	3	0.432	150,215	248,400	66,400	0.440	3.354
450	4	0.432	150,215	248,400	66,400	0.440	3.916
450	5	0.432	150,215	248,400	66,400	0.440	4.478
450	6	0.432	150,215	248,400	66,400	0.440	5.040
450	7	0.432	150,215	248,400	66,400	0.440	5.602
450	8	0.432	150,215	248,400	66,400	0.440	6.164

FILM EFFECTIVENESS TEST
ANGLED INJECTION WITH ACCELERATING FLOW

INJECTION ANGLE - 8.5 DEG NUMBER OF SLOTS - 9 SLOT WIDTH - 1.25 (IN.)
SLOT HEIGHT - 0.299 (IN.) LIP THICKNESS - 0.299 (IN.)
HOT SIDE AREA - 26.6790 (SQ. IN) COLD SIDE AREA - 2.8820 (SQ. IN.)

T/C LOCATIONS

T/C#	X/S	4R	5M	5R	6L	6M	LAND
1	0.502	X	X	X	X	X	X
2	2.174	X	X	X	X	X	X
3	3.846	X	X	X	X	X	X
4	5.518	X	X	X	X	X	X
5	7.191	X	X	X	X	X	X
6	8.863	X	X	X	X	X	X
7	10.535	X	X	X	X	X	X
8	12.207	X	X	X	X	X	X

Note: D(X1,X2) = 100*(X2-X1)/X1
Note: EF = (Tgas - Taw)/(Tgas - Tslot)

FILM EFFECTIVENESS DATA
SPANWISE AVERAGED FILM EFFECTIVENESS DATA

***** Columns 4R-5L, 5R, 5M-6L *****

T/C#	MAVG	TAVG	EFAVG	X/S	X/MS
1	0.159	122.205	0.720	0.502	3.149
2	0.159	159.524	0.509	2.174	13.647
3	0.159	186.318	0.357	3.846	24.144
4	0.159	198.087	0.291	5.518	34.642
5	0.159	203.928	0.257	7.191	45.139
6	0.159	206.396	0.244	8.863	55.636
7	0.159	206.323	0.244	10.535	66.134
8	0.159	204.925	0.252	12.207	76.631

T/C#	MAVG	TAVG	EFAVG	X/S	X/MS
1	0.206	105.663	0.818	0.502	2.436
2	0.206	136.922	0.640	2.174	10.558
3	0.206	170.292	0.449	3.846	18.680
4	0.206	186.192	0.359	5.518	26.801
5	0.206	193.774	0.315	7.191	34.923
6	0.206	197.181	0.296	8.863	43.045
7	0.206	197.836	0.292	10.535	51.166
8	0.206	197.697	0.293	12.207	59.288

T/C#	MAVG	TAVG	EFAVG	X/S	X/MS
1	0.396	79.301	0.930	0.502	1.267
2	0.396	86.488	0.891	2.174	5.490
3	0.396	103.477	0.798	3.846	9.714
4	0.396	132.008	0.642	5.518	13.937
5	0.396	150.965	0.538	7.191	18.160
6	0.396	160.395	0.487	8.863	22.384
7	0.396	164.525	0.464	10.535	26.607
8	0.396	168.799	0.441	12.207	30.831

T/C#	MAVG	TAVG	EFAVG	X/S	X/MS
1	0.601	72.611	0.953	0.502	0.834
2	0.601	76.100	0.935	2.174	3.614
3	0.601	84.587	0.889	3.846	6.395
4	0.601	97.973	0.817	5.518	9.175
5	0.601	115.525	0.722	7.191	11.955
6	0.601	128.846	0.650	8.863	14.736
7	0.601	136.523	0.609	10.535	17.516
8	0.601	144.570	0.565	12.207	20.297

T/C#	MAVG	TAVG	EFAVG	X/S	X/MS
1	0.812	70.174	0.963	0.502	0.618
2	0.812	71.782	0.954	2.174	2.676
3	0.812	78.012	0.921	3.846	4.735
4	0.812	87.242	0.871	5.518	6.794
5	0.812	99.944	0.803	7.191	8.852
6	0.812	111.541	0.740	8.863	10.911
7	0.812	119.902	0.695	10.535	12.969
8	0.812	129.423	0.644	12.207	15.028

T/C#	MAVG	TAVG	EFAVG	X/S	X/MS
1	1.003	69.780	0.969	0.502	0.500
2	1.003	70.721	0.963	2.174	2.167
3	1.003	76.087	0.935	3.846	3.834
4	1.003	86.565	0.878	5.518	5.501
5	1.003	99.731	0.807	7.191	7.167
6	1.003	110.780	0.747	8.863	8.834
7	1.003	118.437	0.706	10.535	10.501
8	1.003	127.145	0.659	12.207	12.168

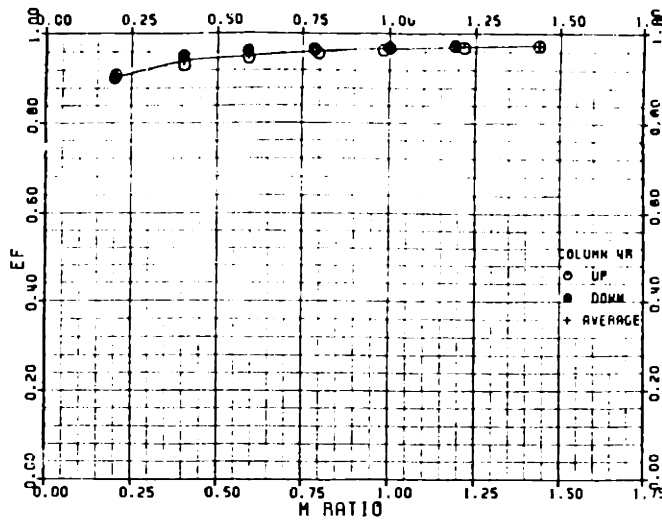
T/C#	MAVG	TAVG	EFAVG	X/S	X/MS
1	1.217	69.411	0.973	0.502	0.412
2	1.217	70.044	0.969	2.174	1.786
3	1.217	73.532	0.951	3.846	3.159
4	1.217	81.669	0.907	5.518	4.533
5	1.217	93.943	0.840	7.191	5.907
6	1.217	105.485	0.778	8.863	7.280
7	1.217	114.001	0.731	10.535	8.654
8	1.217	123.461	0.680	12.207	10.027

T/C#	MAVG	TAVG	EFAVG	X/S	X/MS
1	1.423	69.235	0.975	0.502	0.353
2	1.423	69.686	0.972	2.174	1.528
3	1.423	72.119	0.959	3.846	2.703
4	1.423	76.768	0.934	5.518	3.878
5	1.423	85.441	0.887	7.191	5.054
6	1.423	94.462	0.838	8.863	6.229
7	1.423	102.579	0.794	10.535	7.404
8	1.423	112.778	0.738	12.207	8.579

Appendix D: Sample Data Reduction

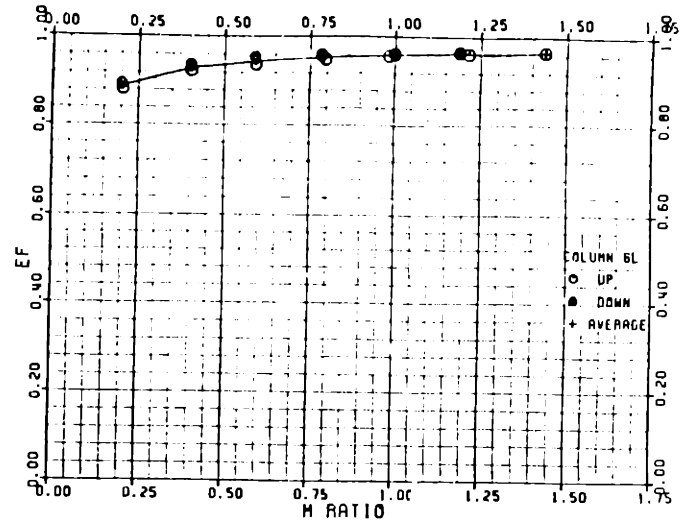
INJECTION ANGLE = 11.5 DEG.

X/S = 0.37



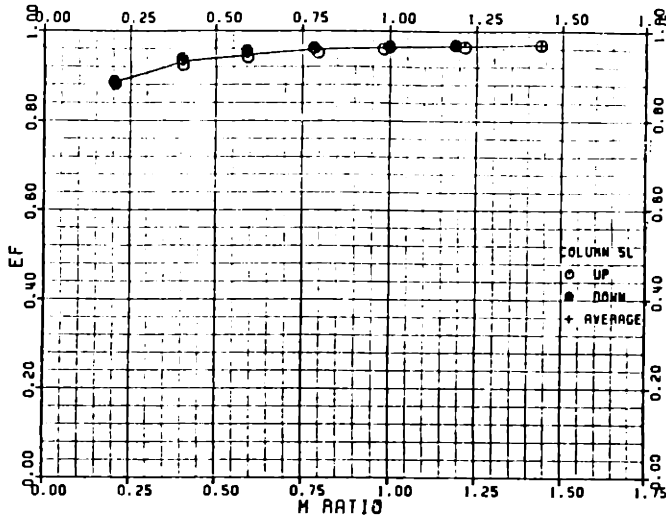
INJECTION ANGLE = 11.5 DEG.

X/S = 0.37



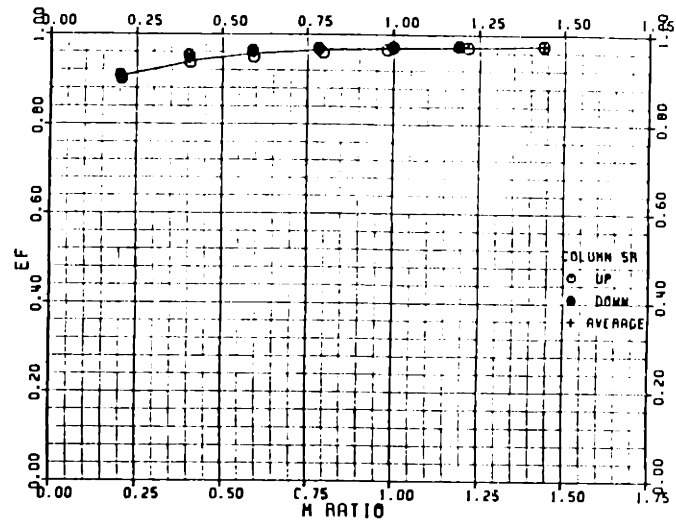
INJECTION ANGLE = 11.5 DEG.

X/S = 0.37



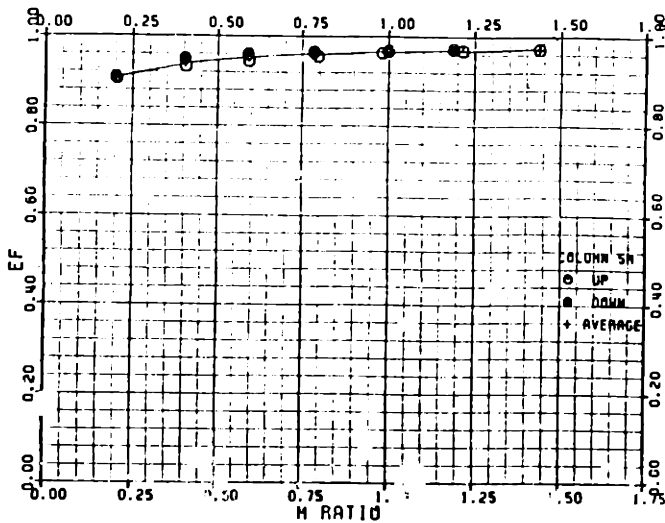
INJECTION ANGLE = 11.5 DEG.

X/S = 0.37



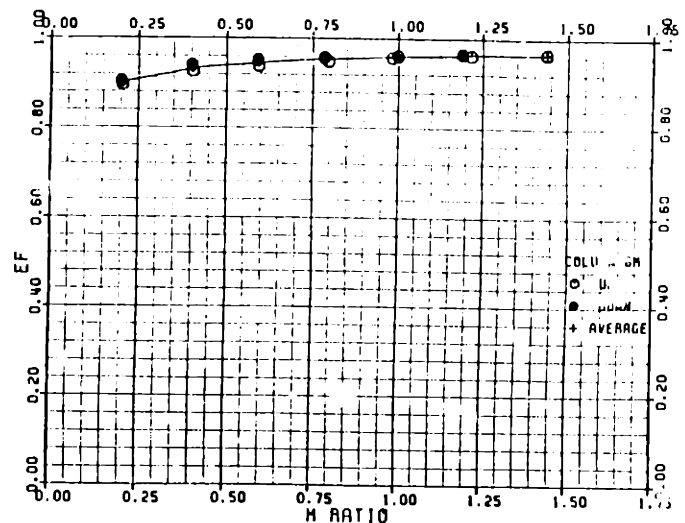
INJECTION ANGLE = 11.5 DEG.

X/S = 0.37



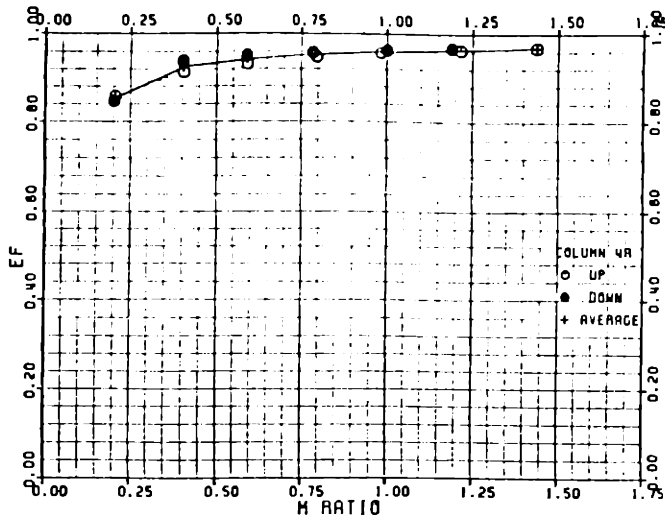
INJECTION ANGLE = 11.5 DEG.

X/S = 0.37



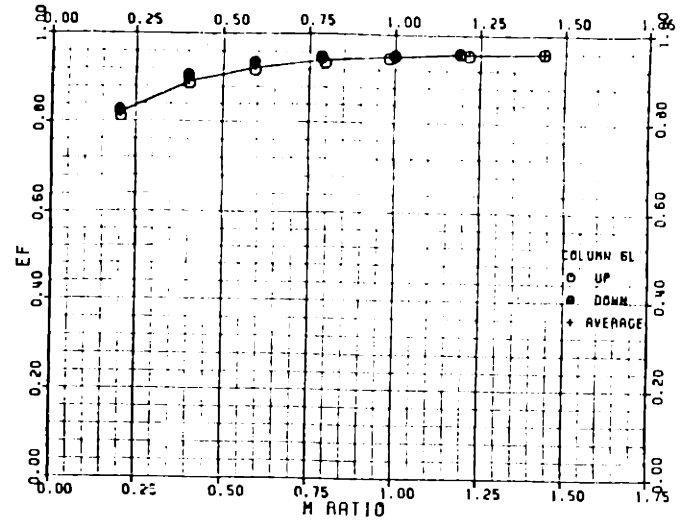
INJECTION ANGLE = 11.5 DEG.

X/S = 1.60



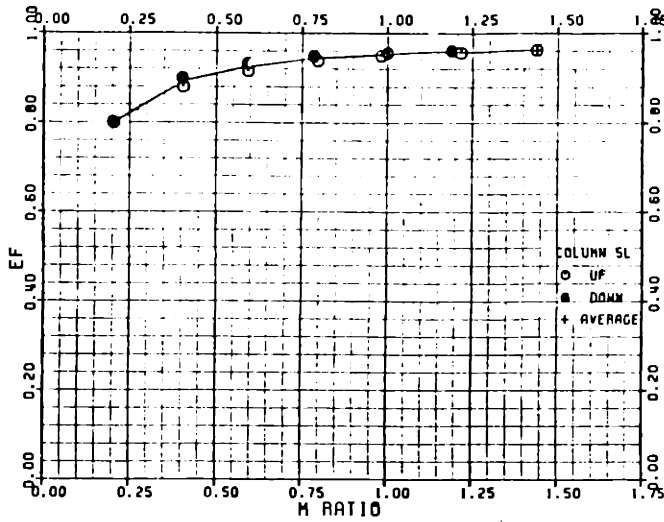
INJECTION ANGLE = 11.5 DEG.

X/S = 1.60



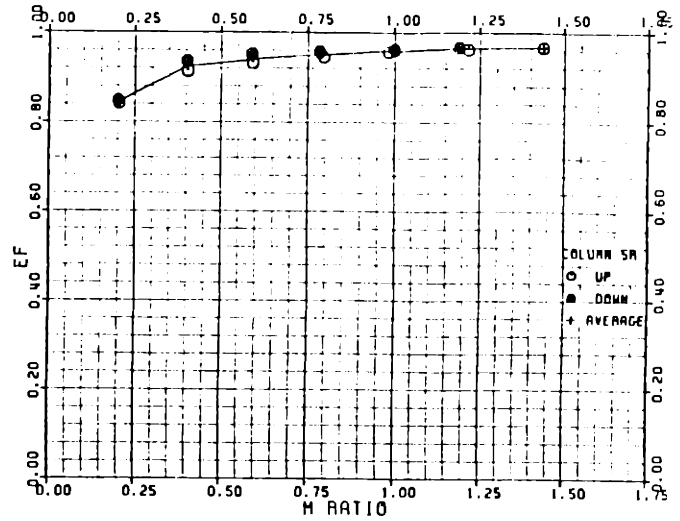
INJECTION ANGLE = 11.5 DEG.

X/S = 1.60



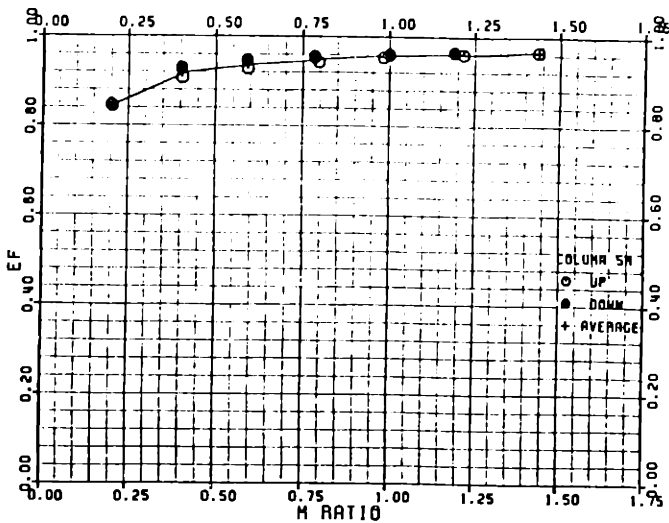
INJECTION ANGLE = 11.5 DEG.

X/S = 1.60



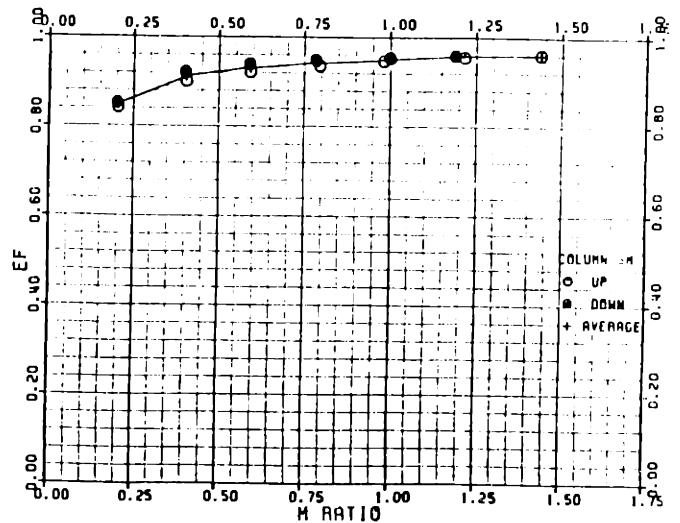
INJECTION ANGLE = 11.5 DEG.

X/S = 1.60



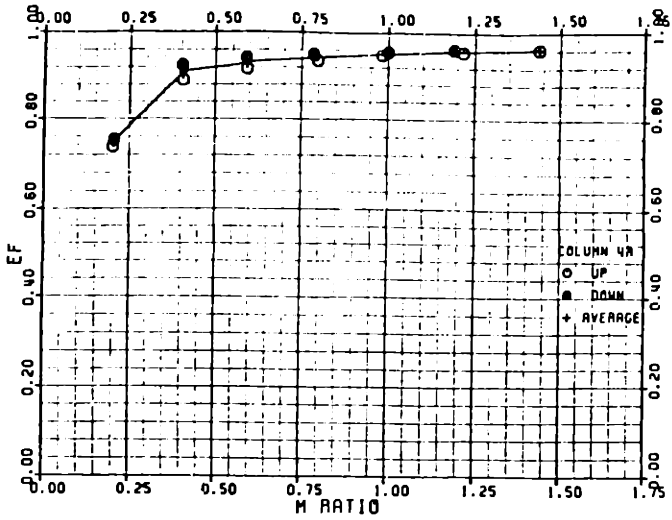
INJECTION ANGLE = 11.5 DEG.

X/S = 1.60



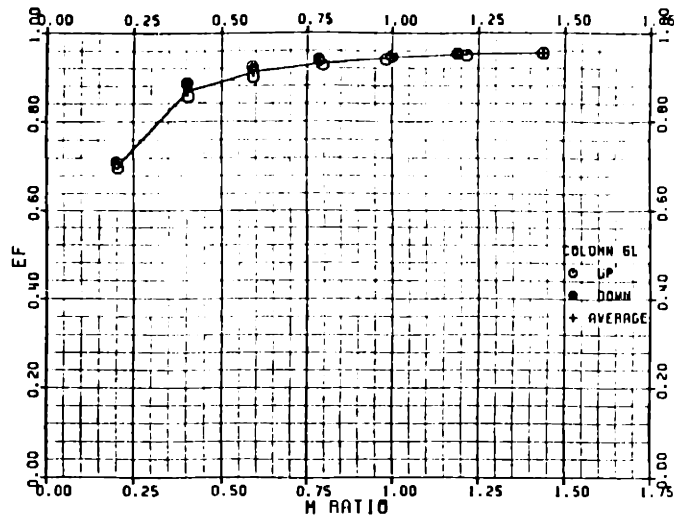
INJECTION ANGLE = 11.5 DEG.

X/S = 2.83



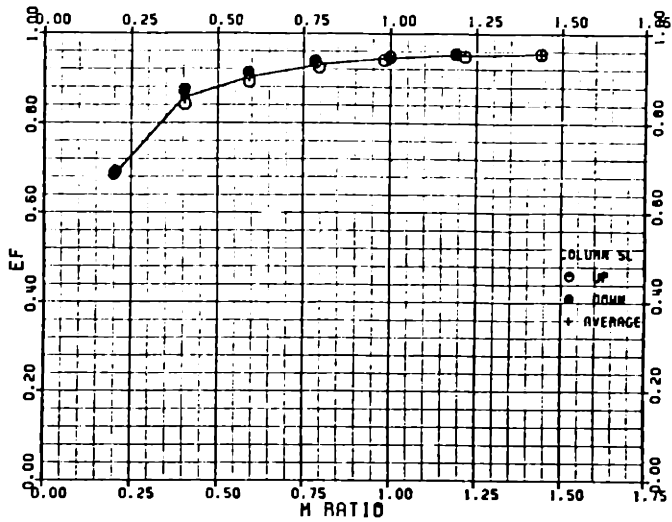
INJECTION ANGLE = 11.5 DEG.

X/S = 2.83



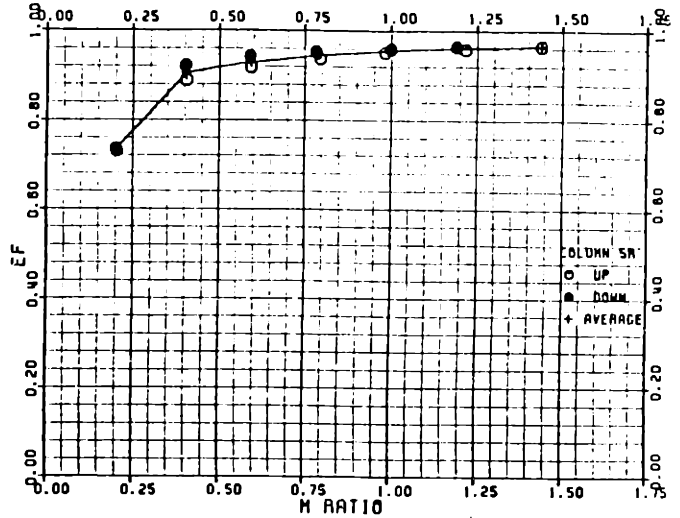
INJECTION ANGLE = 11.5 DEG.

X/S = 2.83



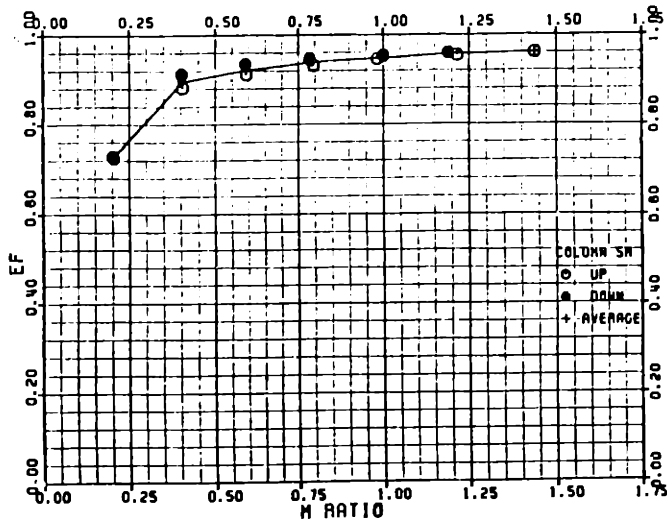
INJECTION ANGLE = 11.5 DEG.

X/S = 2.83



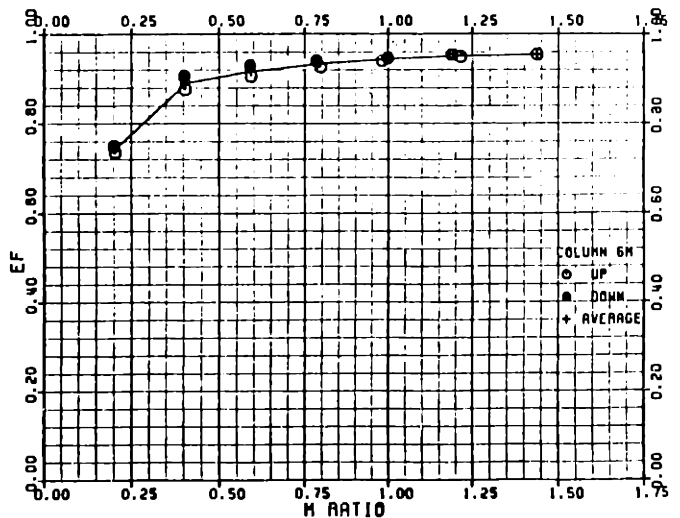
INJECTION ANGLE = 11.5 DEG.

X/S = 2.83



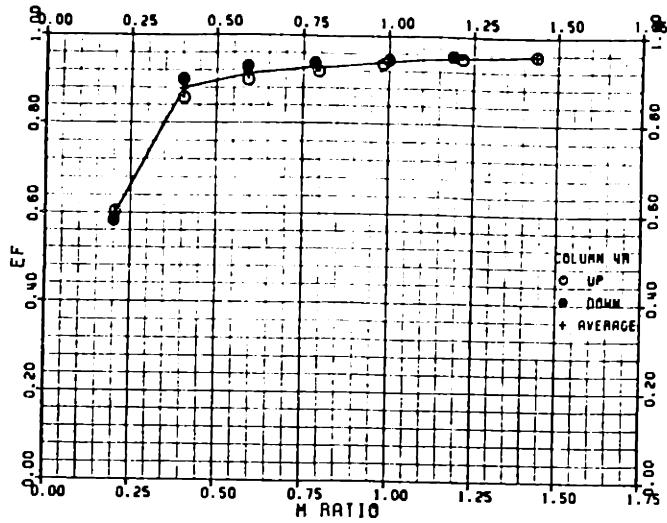
INJECTION ANGLE = 11.5 DEG.

X/S = 2.83



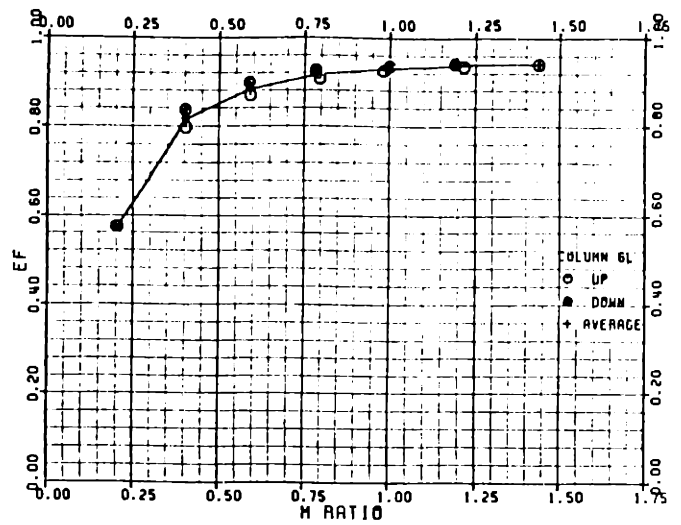
INJECTION ANGLE = 11.5 DEG.

X/S = 4.05



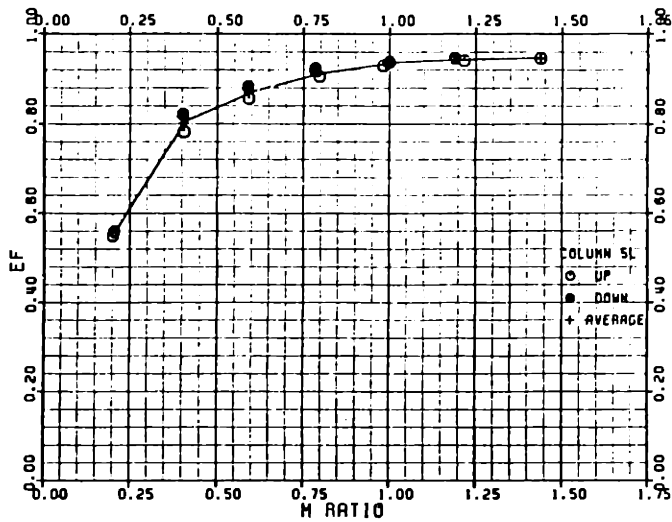
INJECTION ANGLE = 11.5 DEG.

X/S = 4.05



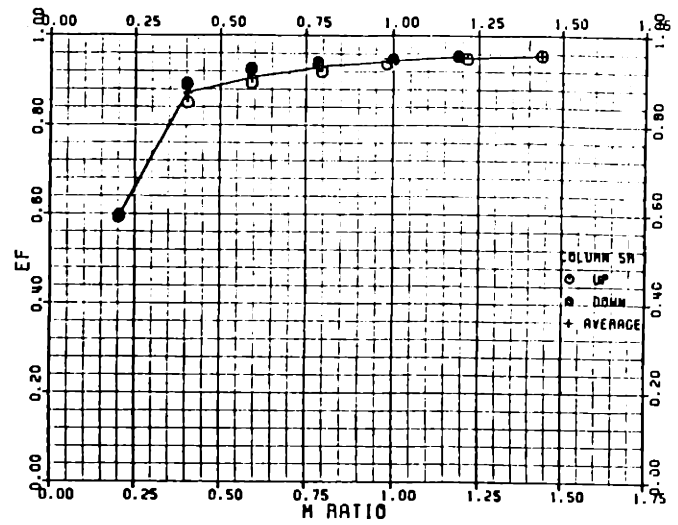
INJECTION ANGLE = 11.5 DEG.

X/S = 4.05



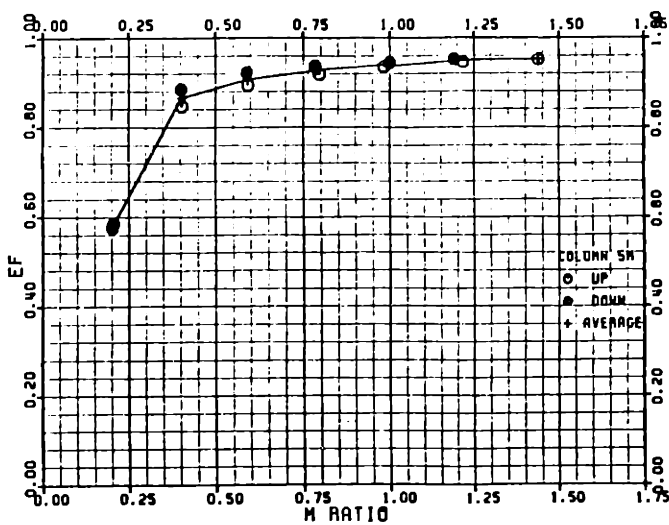
INJECTION ANGLE = 11.5 DEG.

X/S = 4.05



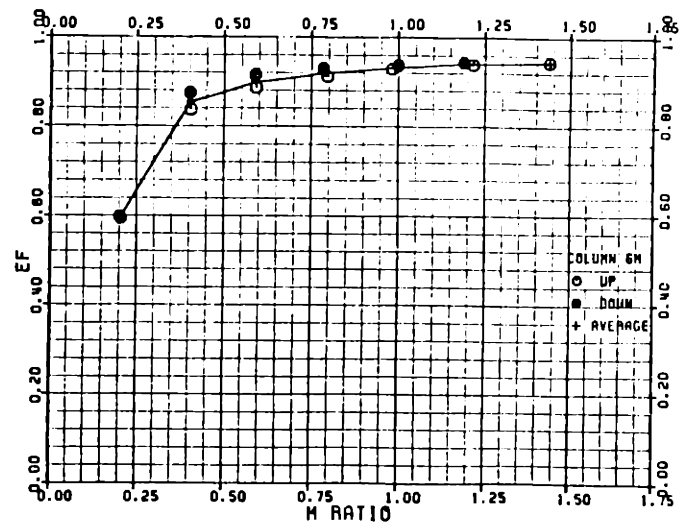
INJECTION ANGLE = 11.5 DEG.

X/S = 4.05



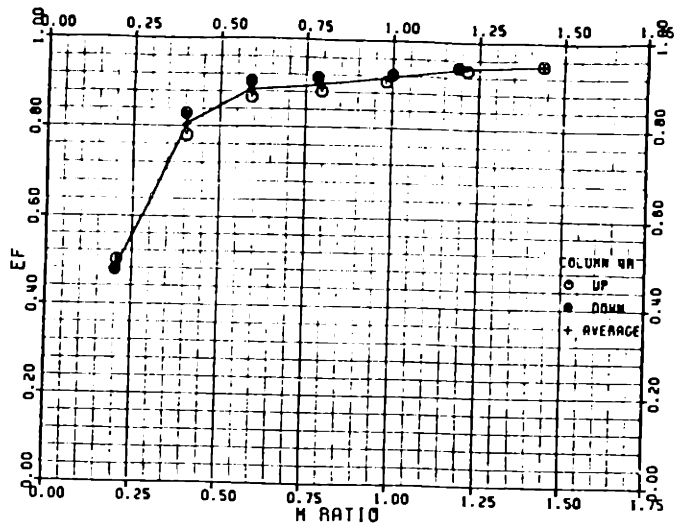
INJECTION ANGLE = 11.5 DEG.

X/S = 4.05



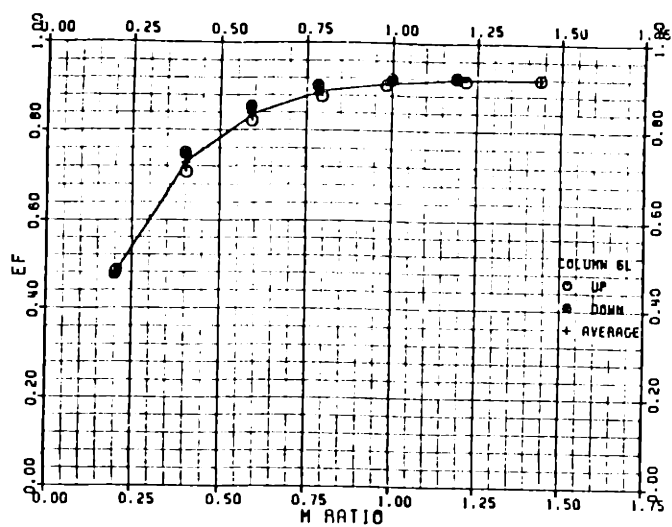
INJECTION ANGLE = 11.5 DEG.

X/S = 5.28



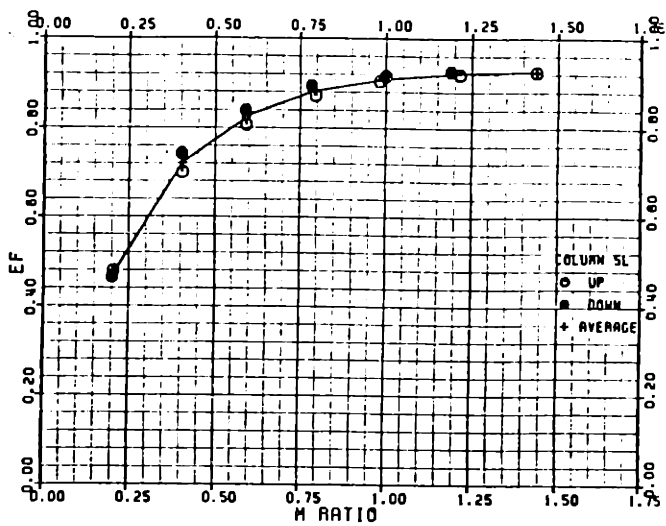
INJECTION ANGLE = 11.5 DEG.

X/S = 5.28



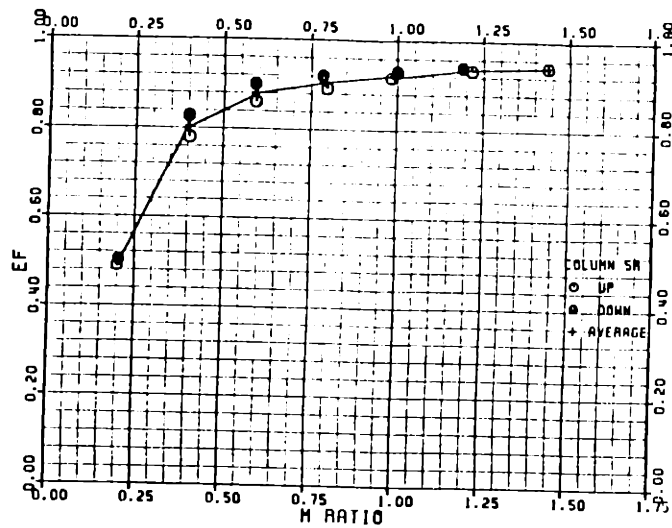
INJECTION ANGLE = 11.5 DEG.

X/S = 5.28



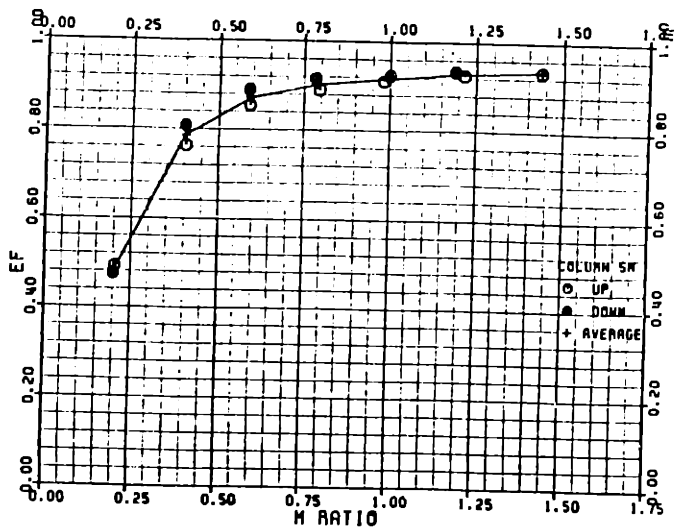
INJECTION ANGLE = 11.5 DEG.

X/S = 5.28



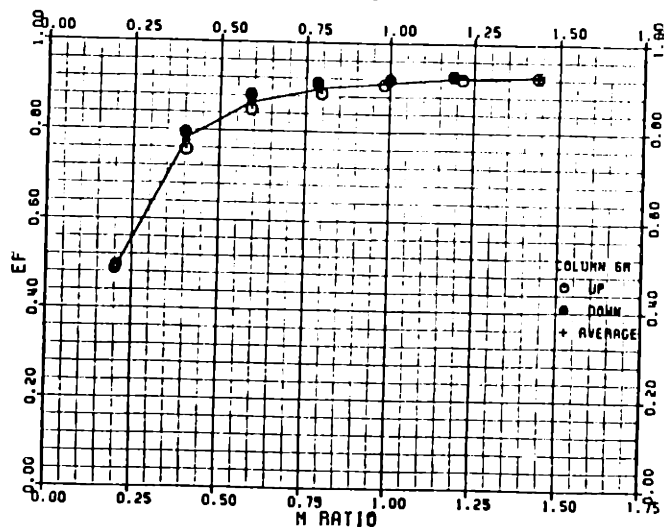
INJECTION ANGLE = 11.5 DEG.

X/S = 5.28



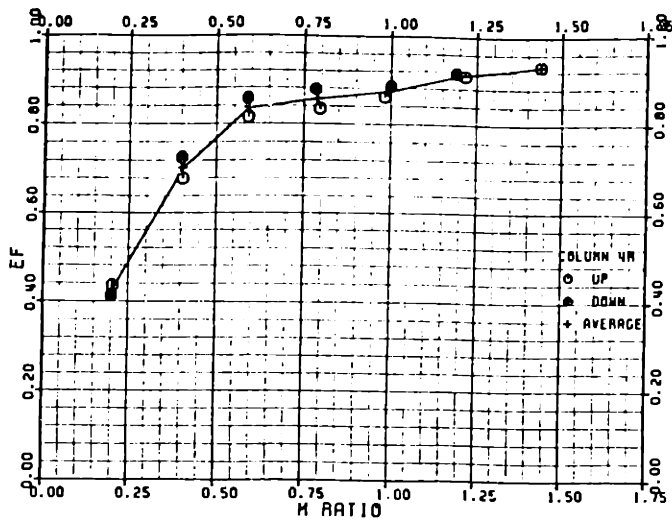
INJECTION ANGLE = 11.5 DEG.

X/S = 5.28



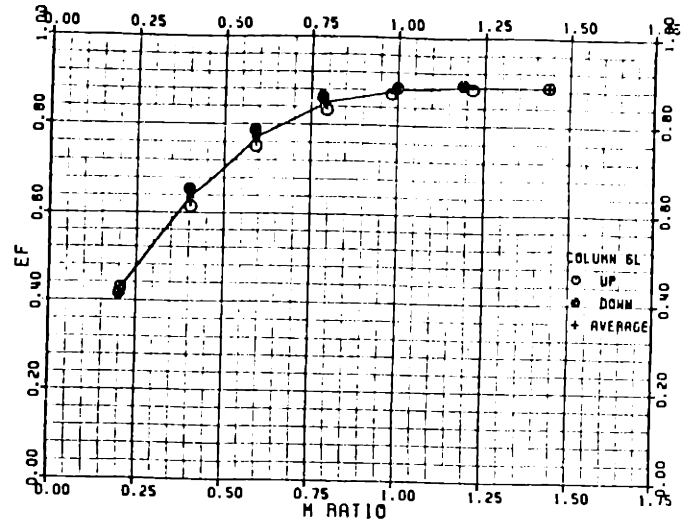
INJECTION ANGLE = 11.5 DEG.

X/S = 6.51



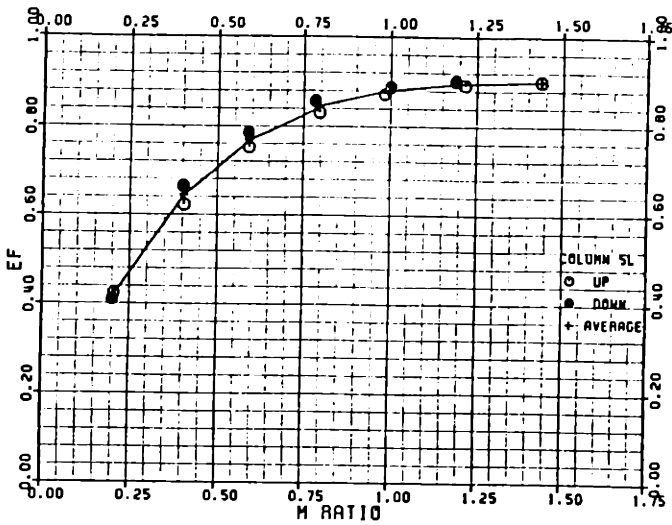
INJECTION ANGLE = 11.5 DEG.

X/S = 6.51



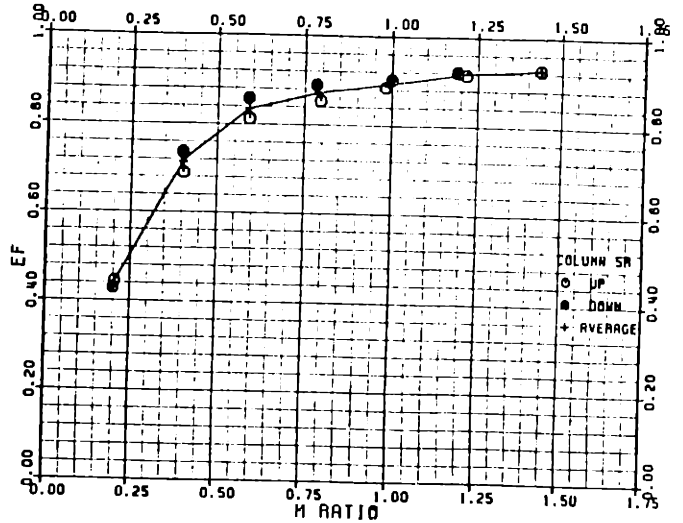
INJECTION ANGLE = 11.5 DEG.

X/S = 6.51



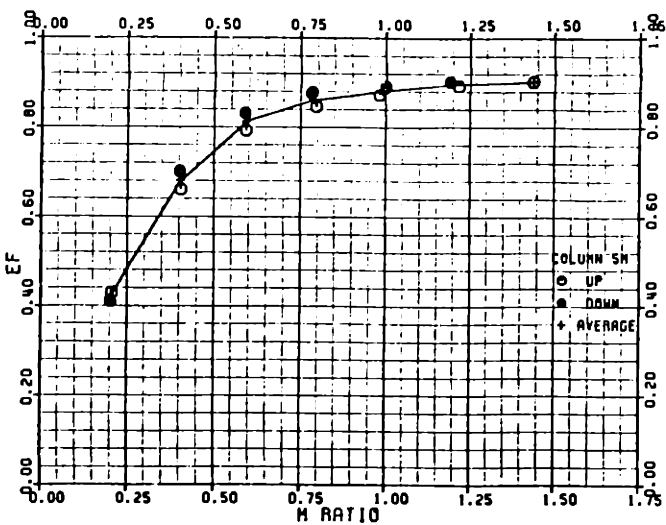
INJECTION ANGLE = 11.5 DEG.

X/S = 6.51



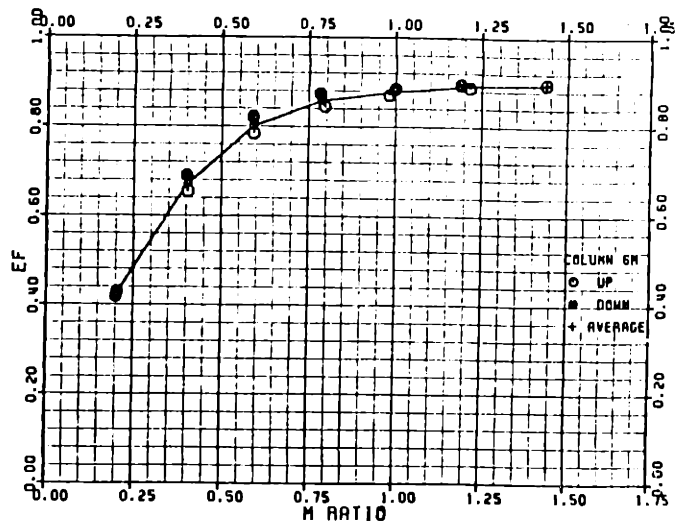
INJECTION ANGLE = 11.5 DEG.

X/S = 6.51



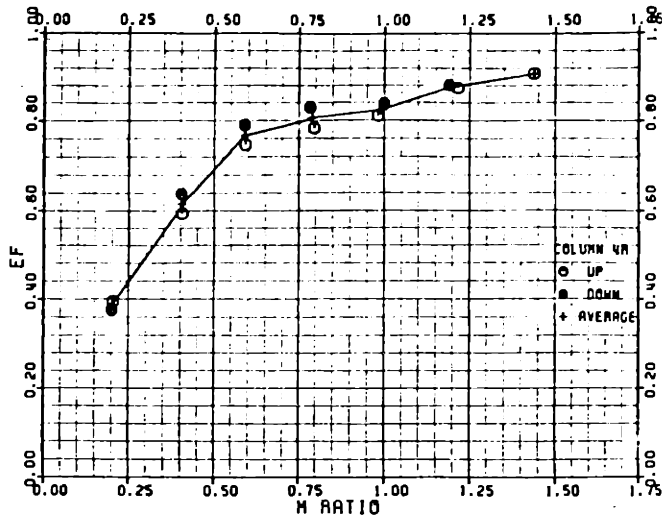
INJECTION ANGLE = 11.5 DEG.

X/S = 6.51



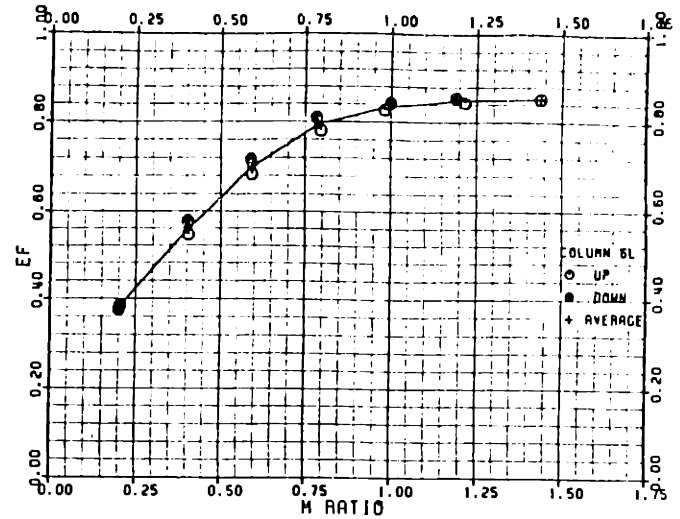
INJECTION ANGLE = 11.5 DEG.

X/S = 7.74



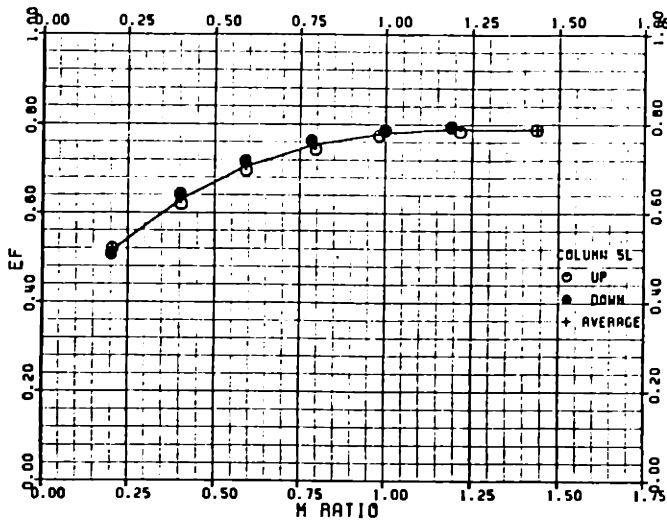
INJECTION ANGLE = 11.5 DEG.

X/S = 7.74



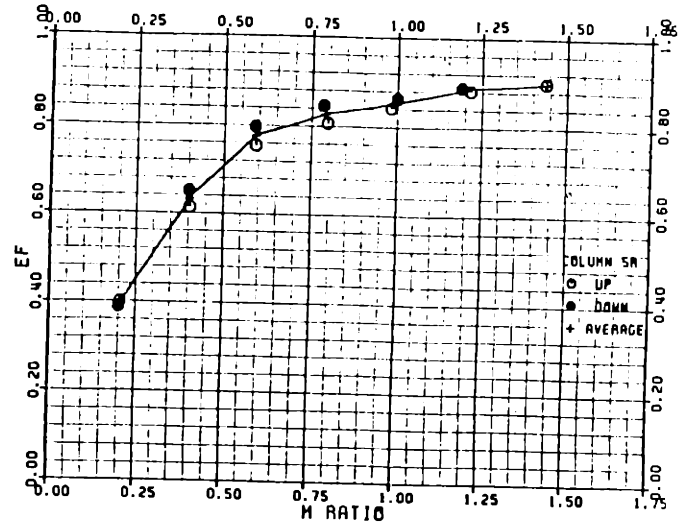
INJECTION ANGLE = 11.5 DEG.

X/S = 7.74



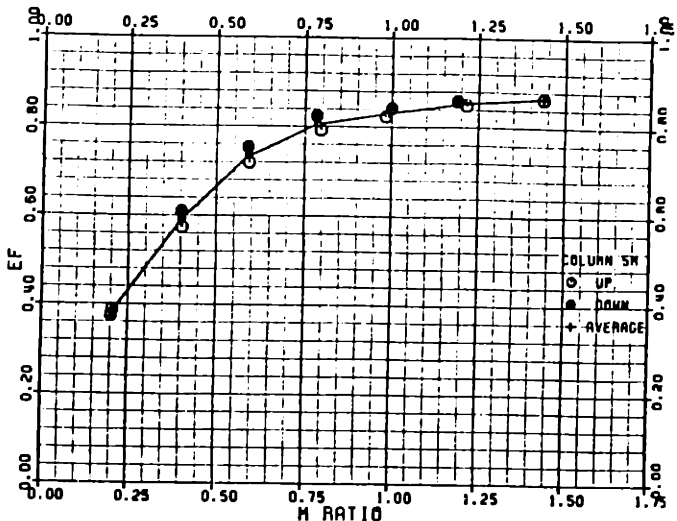
INJECTION ANGLE = 11.5 DEG.

X/S = 7.74



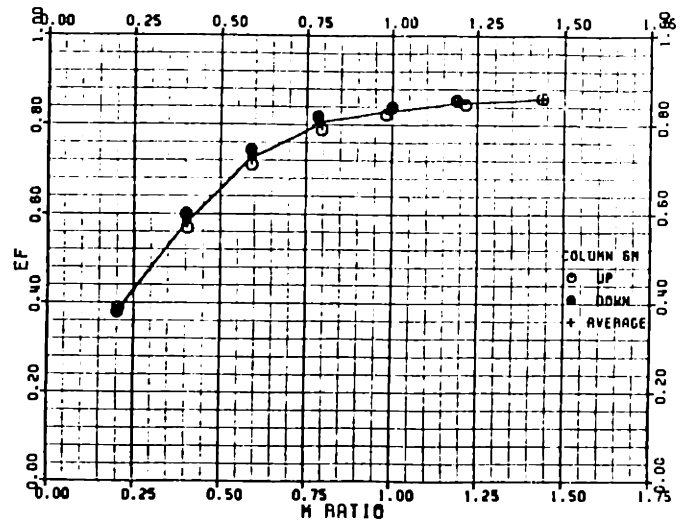
INJECTION ANGLE = 11.5 DEG.

X/S = 7.74



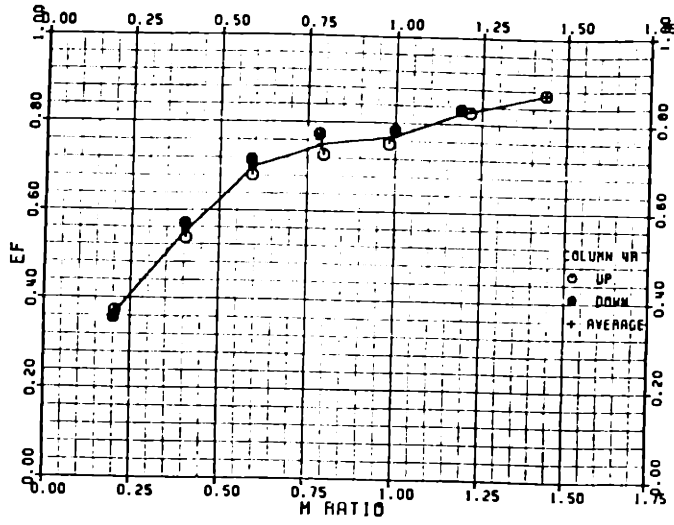
INJECTION ANGLE = 11.5 DEG.

X/S = 7.74



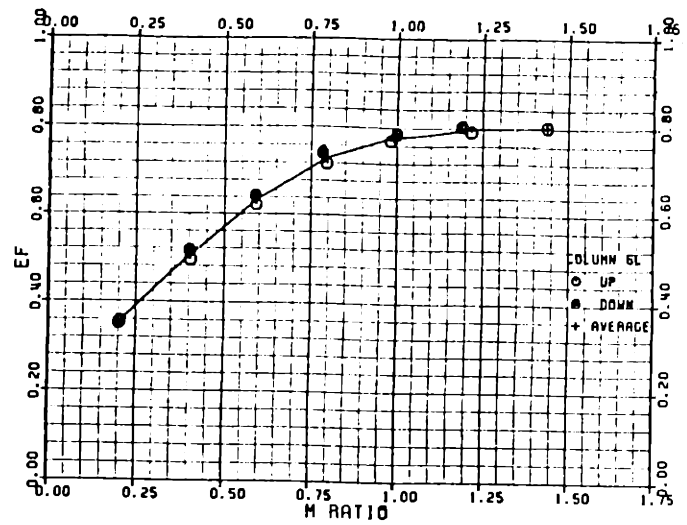
INJECTION ANGLE = 11.5 DEG.

X/S = 8.97



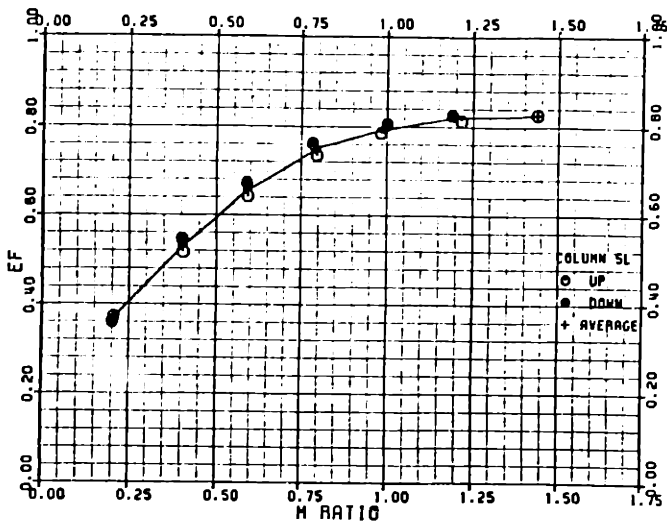
INJECTION ANGLE = 11.5 DEG.

X/S = 8.97



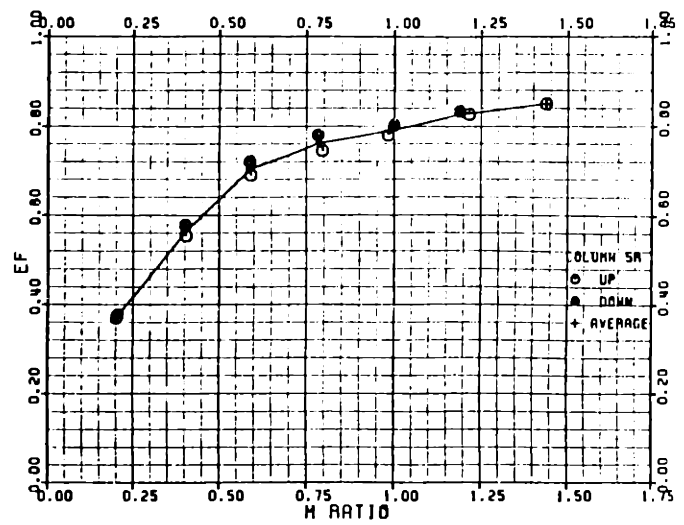
INJECTION ANGLE = 11.5 DEG.

X/S = 8.97



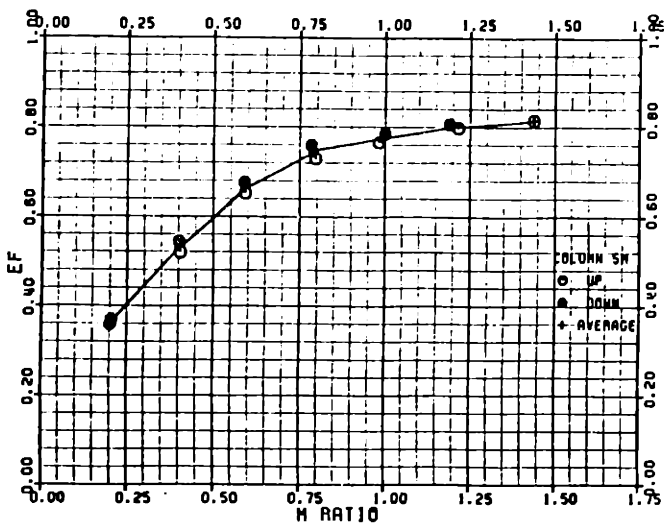
INJECTION ANGLE = 11.5 DEG.

X/S = 8.97



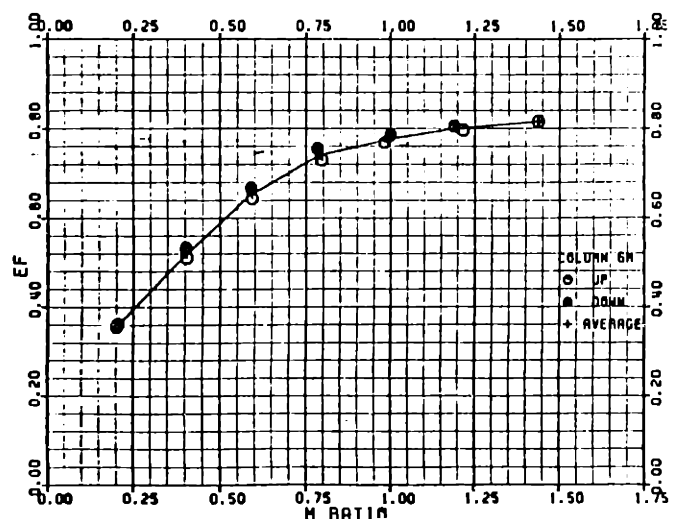
INJECTION ANGLE = 11.5 DEG.

X/S = 8.97



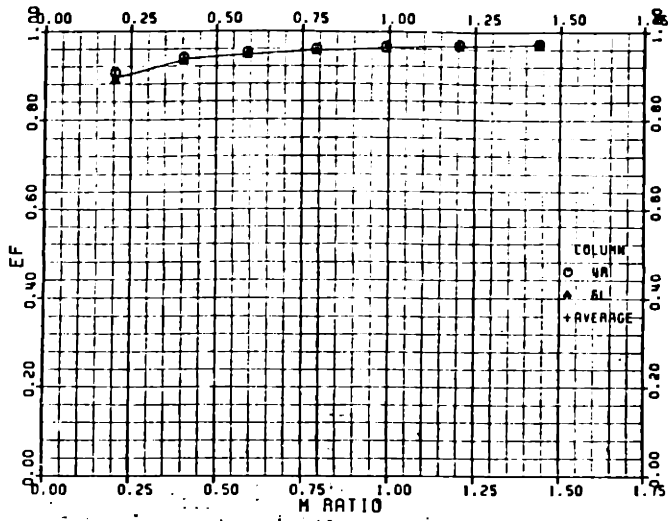
INJECTION ANGLE = 11.5 DEG.

X/S = 8.97



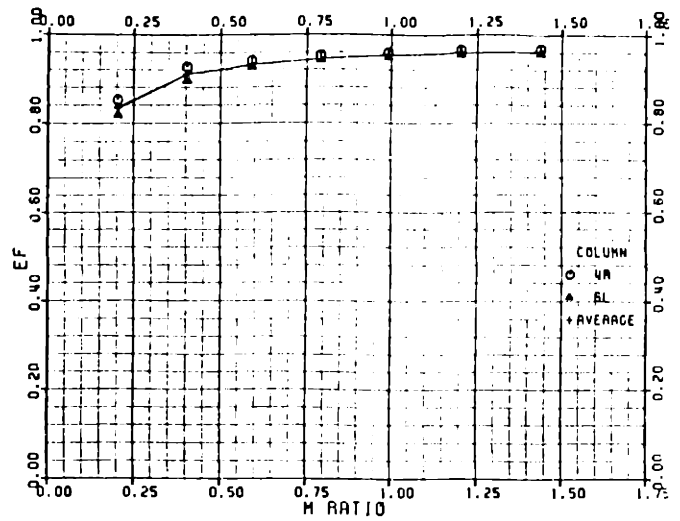
INJECTION ANGLE = 11.5 DEG.

X/S = 0.37



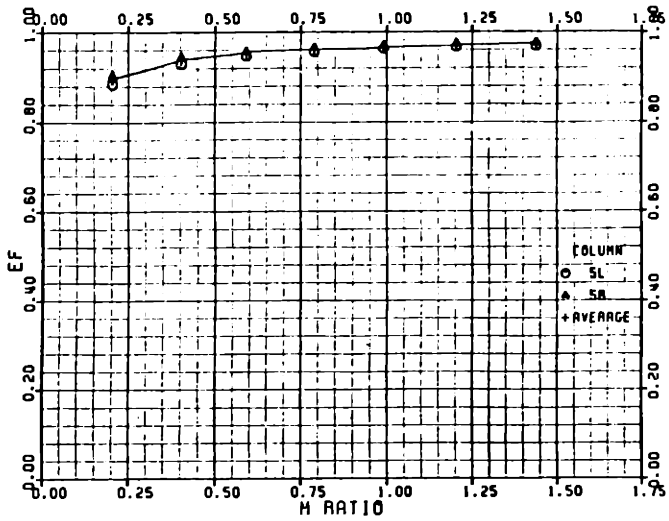
INJECTION ANGLE = 11.5 DEG.

X/S = 1.60



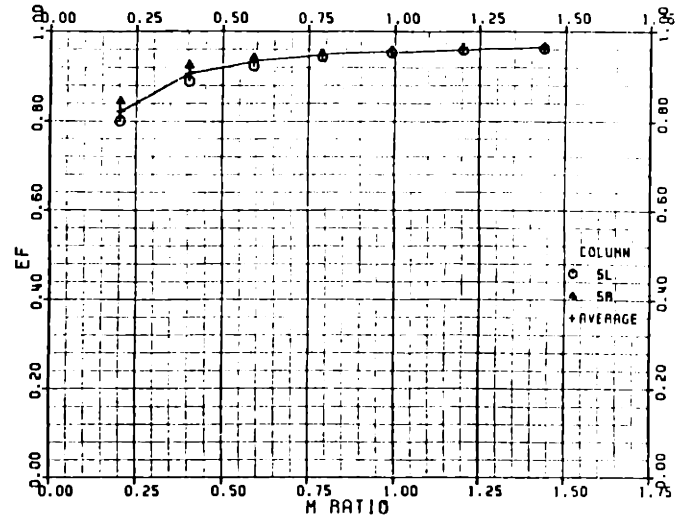
INJECTION ANGLE = 11.5 DEG.

X/S = 0.37



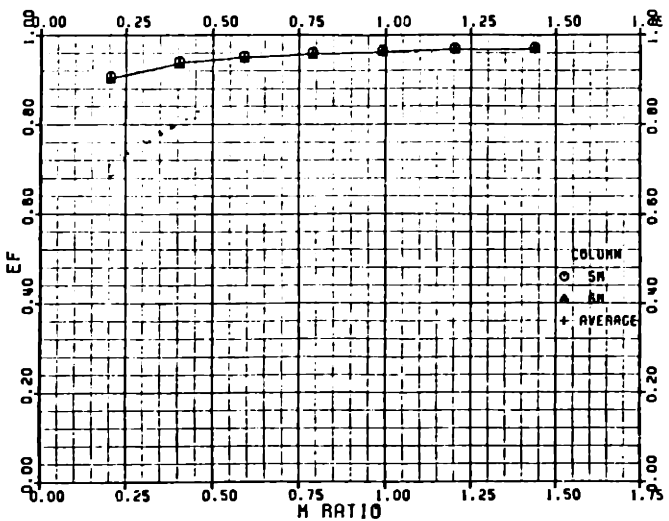
INJECTION ANGLE = 11.5 DEG.

X/S = 1.60



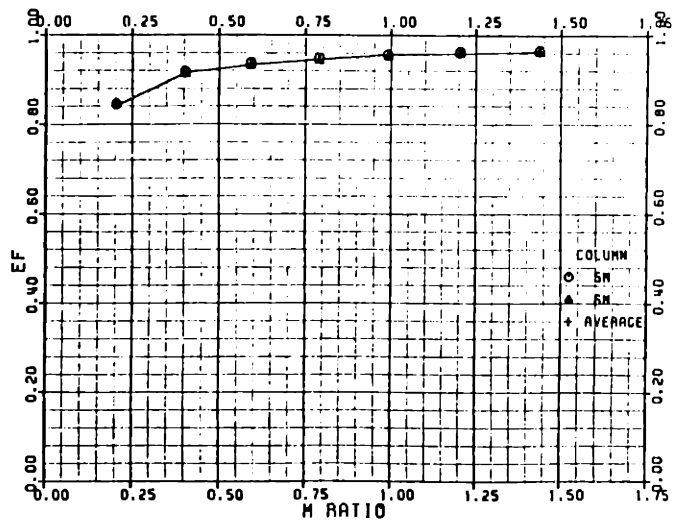
INJECTION ANGLE = 11.5 DEG.

X/S = 0.37



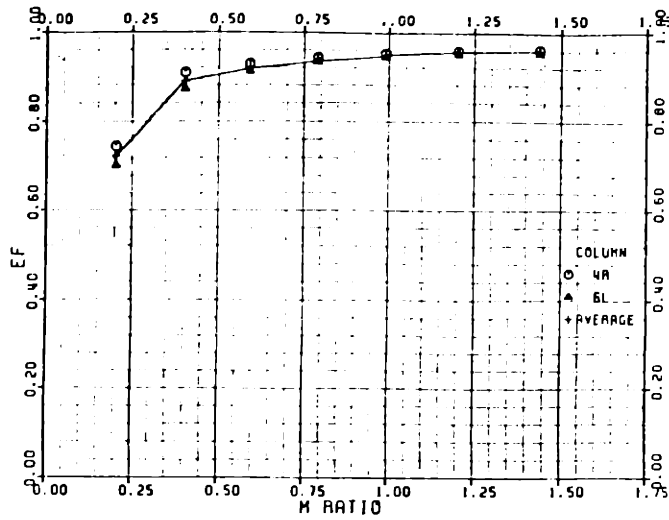
INJECTION ANGLE = 11.5 DEG.

X/S = 1.60



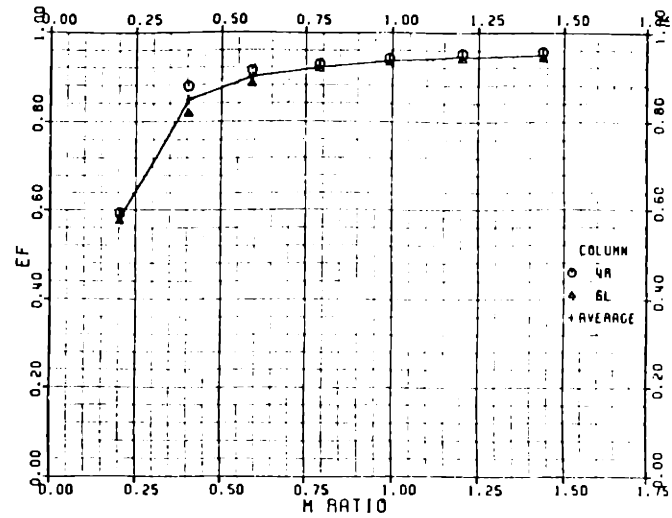
INJECTION ANGLE = 11.5 DEG.

X/S = 2.83



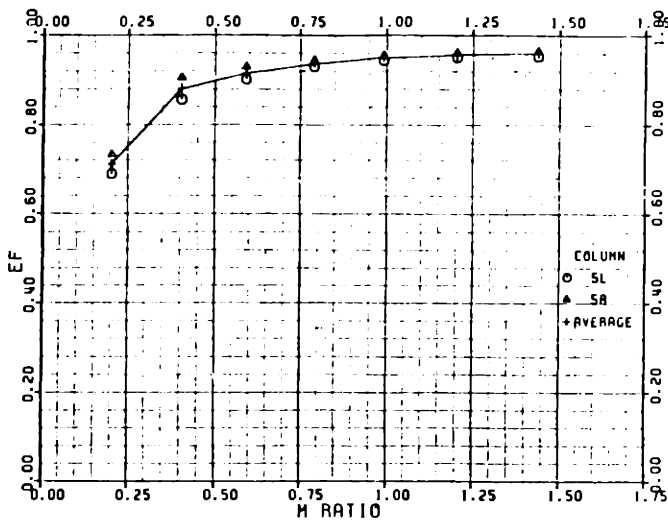
INJECTION ANGLE = 11.5 DEG.

X/S = 4.05



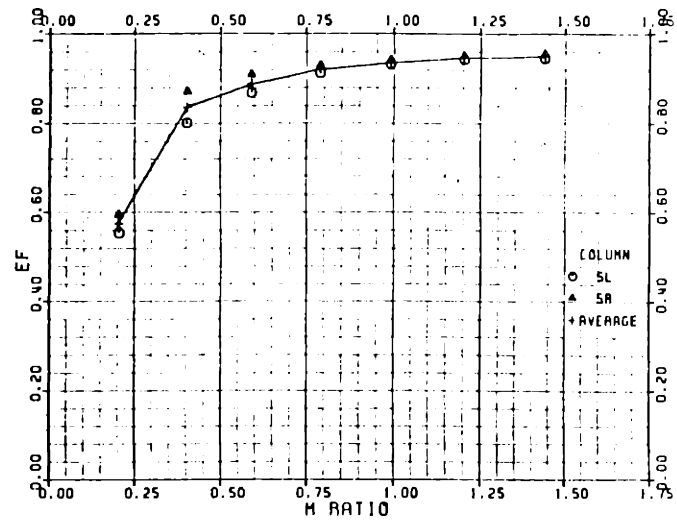
INJECTION ANGLE = 11.5 DEG.

X/S = 2.83



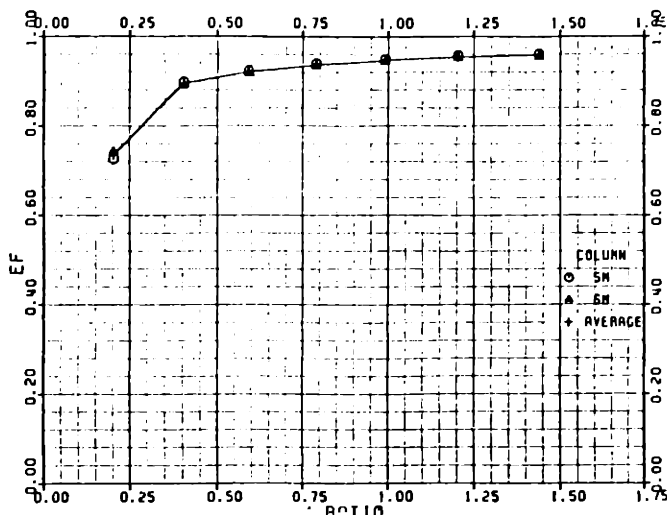
INJECTION ANGLE = 11.5 DEG.

X/S = 4.05



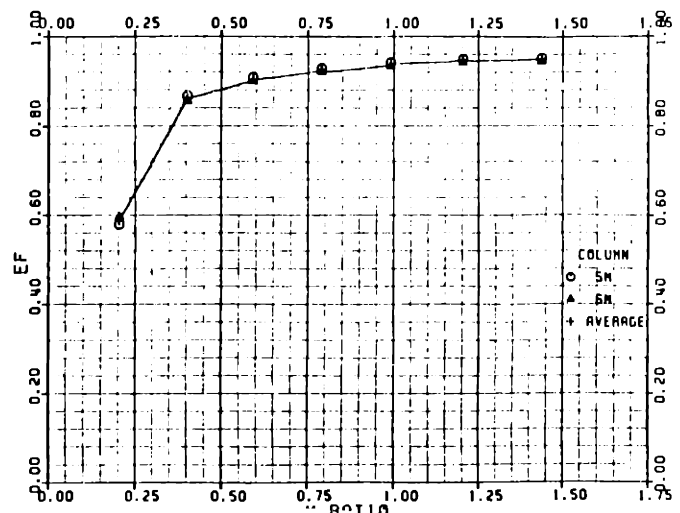
INJECTION ANGLE = 11.5 DEG.

X/S = 2.83



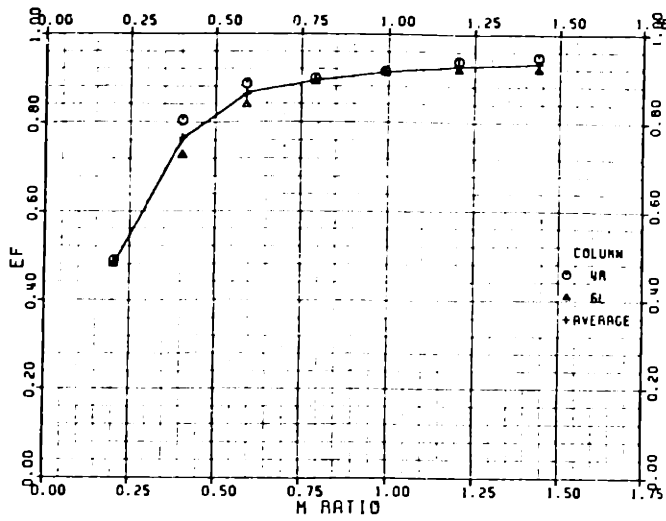
INJECTION ANGLE = 11.5 DEG.

X/S = 4.05



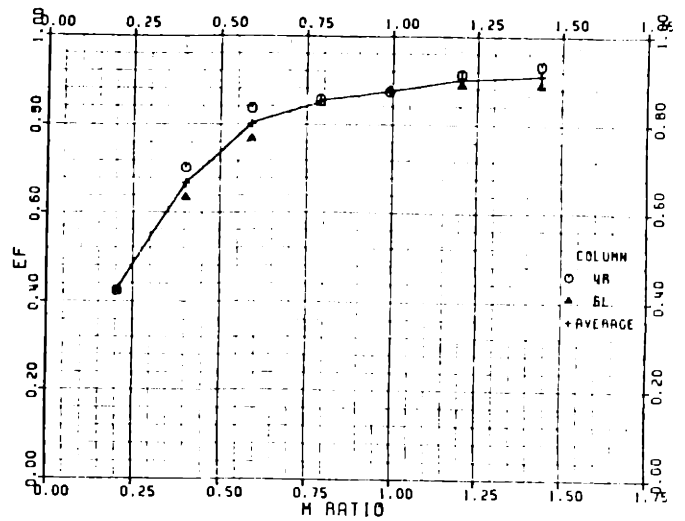
INJECTION ANGLE = 11.5 DEG.

X/S = 5.28



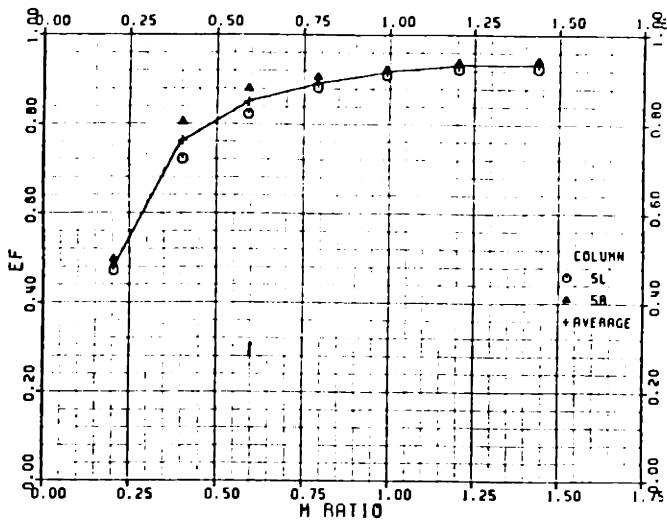
INJECTION ANGLE = 11.5 DEG.

X/S = 6.51



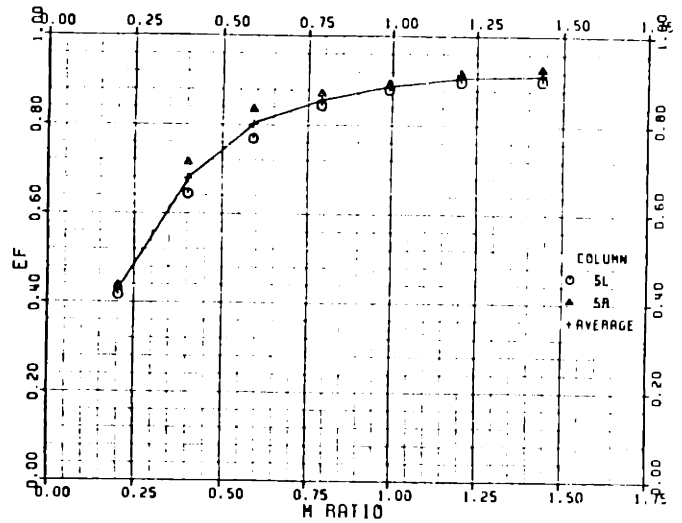
INJECTION ANGLE = 11.5 DEG.

X/S = 5.28



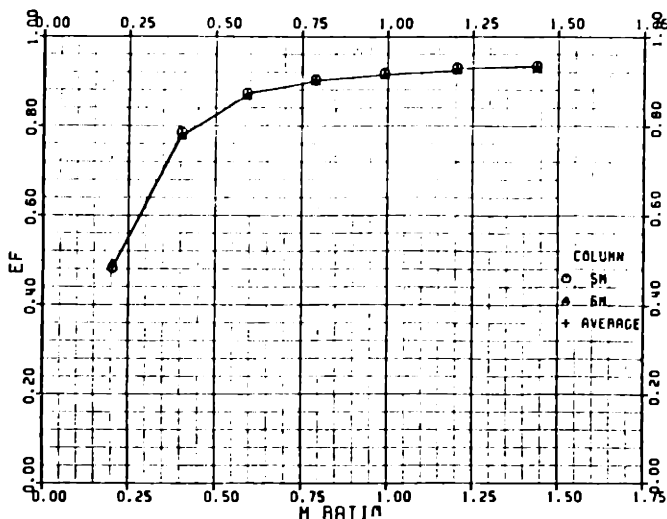
INJECTION ANGLE = 11.5 DEG.

X/S = 6.51



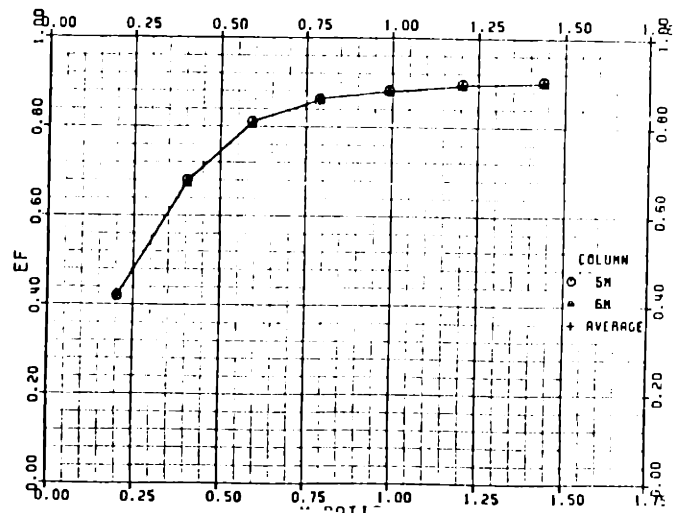
INJECTION ANGLE = 11.5 DEG.

X/S = 5.28



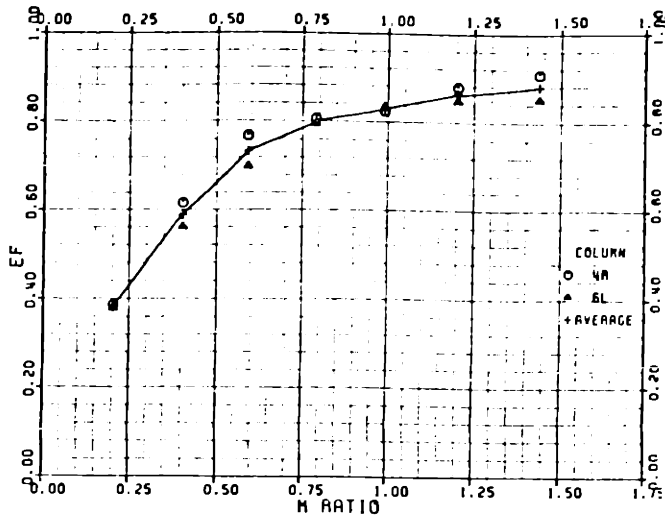
INJECTION ANGLE = 11.5 DEG.

X/S = 6.51



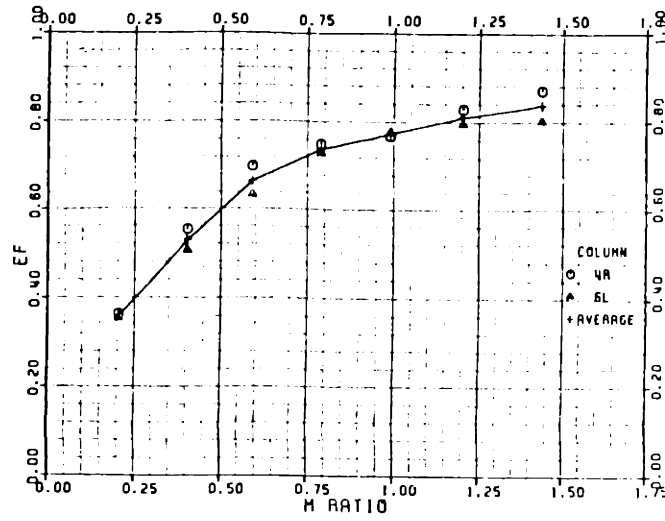
INJECTION ANGLE = 11.5 DEG.

X/S = 7.74



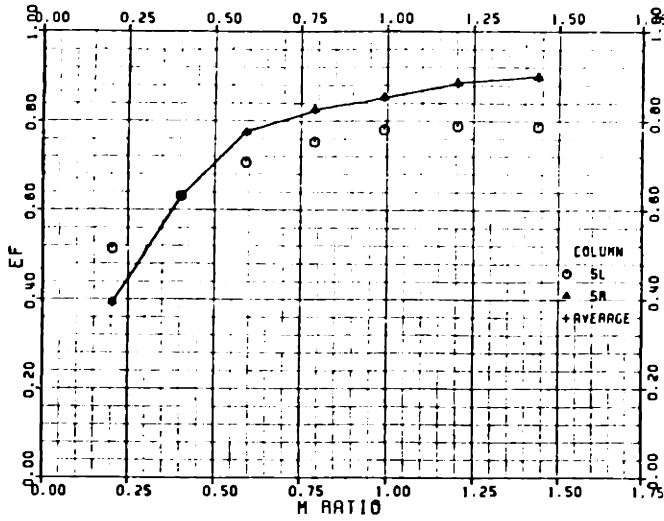
INJECTION ANGLE = 11.5 DEG.

X/S = 8.97



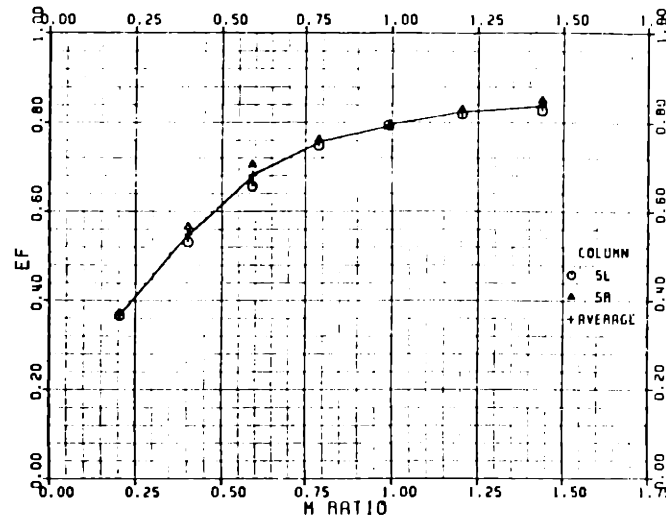
INJECTION ANGLE = 11.5 DEG.

X/S = 7.74



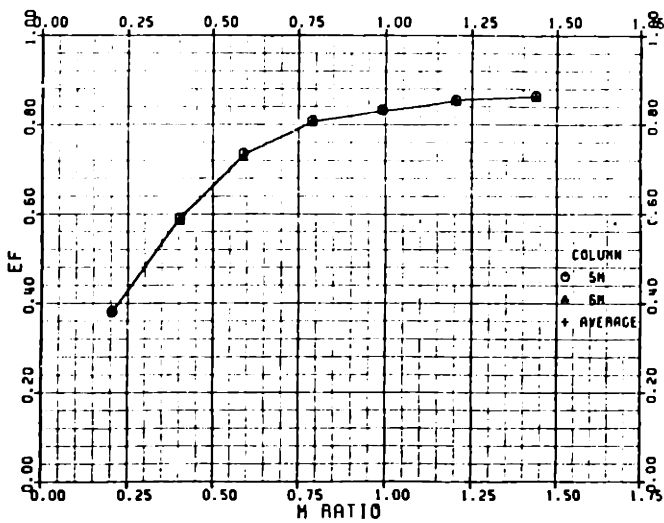
INJECTION ANGLE = 11.5 DEG.

X/S = 8.97



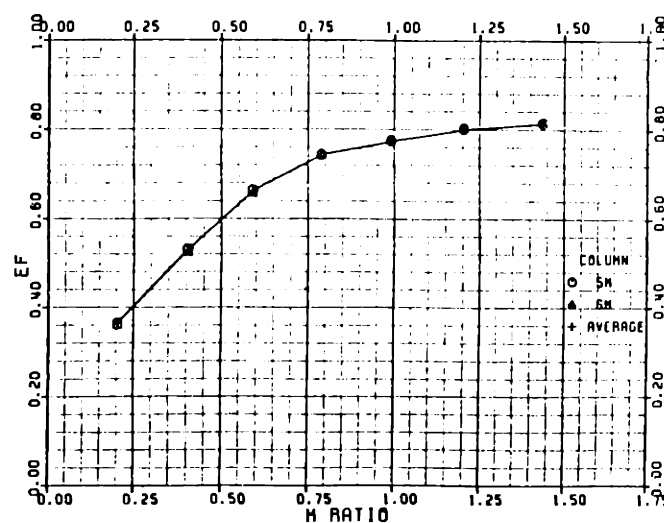
INJECTION ANGLE = 11.5 DEG.

X/S = 7.74

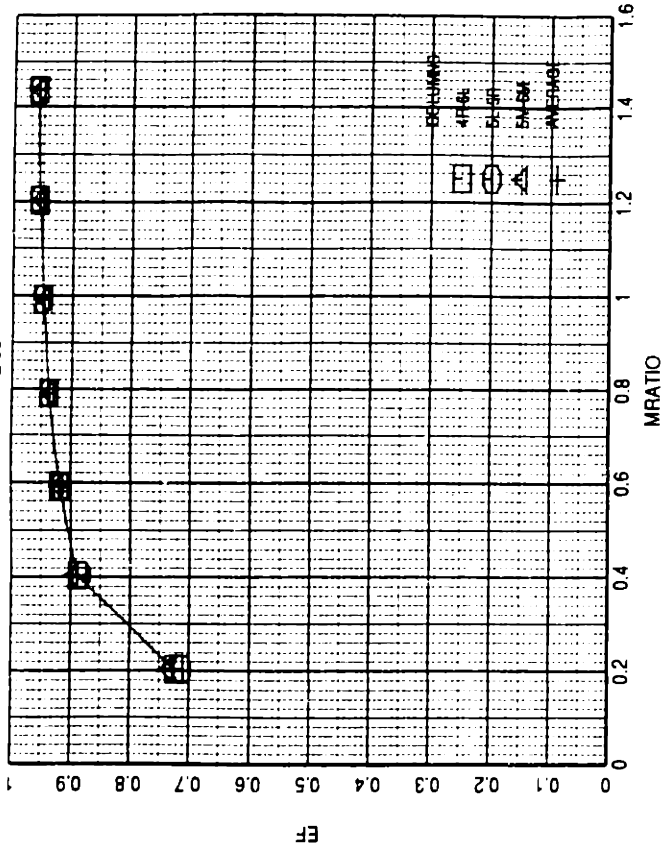


INJECTION ANGLE = 11.5 DEG.

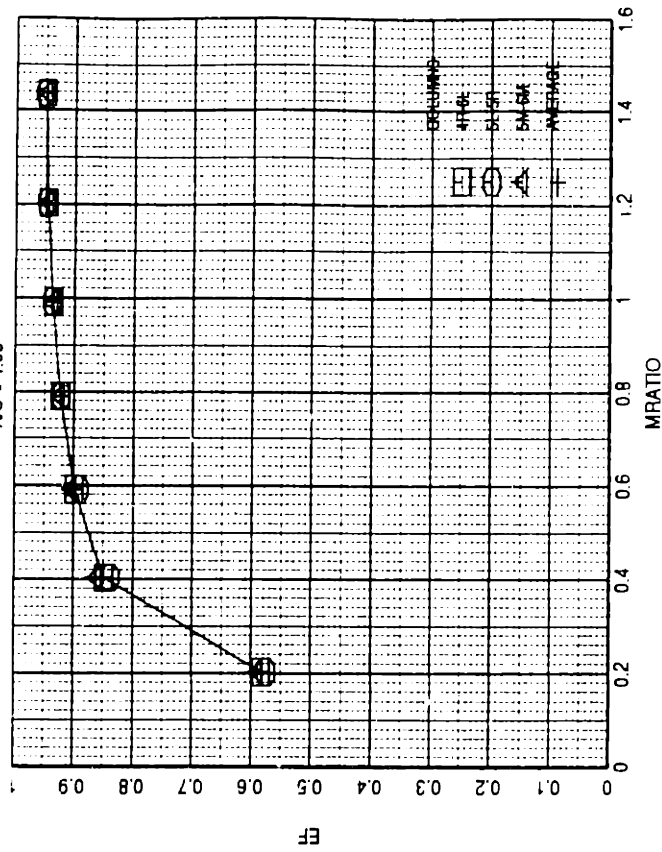
X/S = 8.97



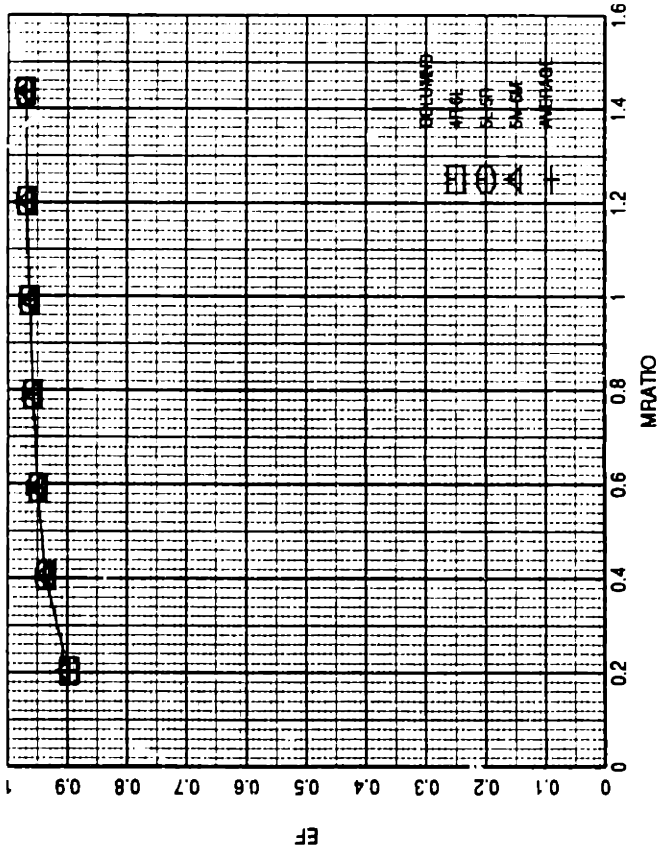
INJECTION ANGLE = 11.5 DEG.
X/S = 2.83



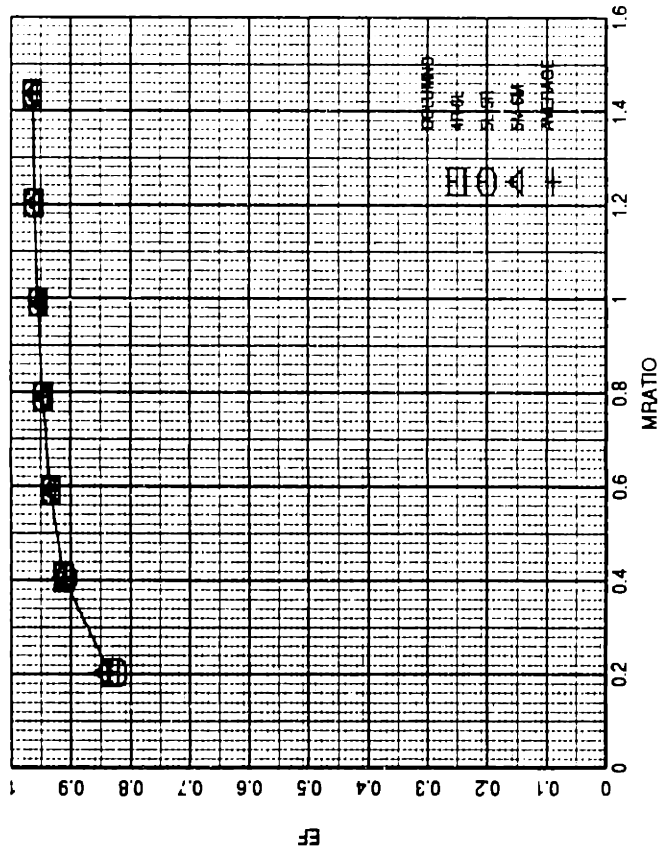
INJECTION ANGLE = 11.5 DEG.
X/S = 4.05



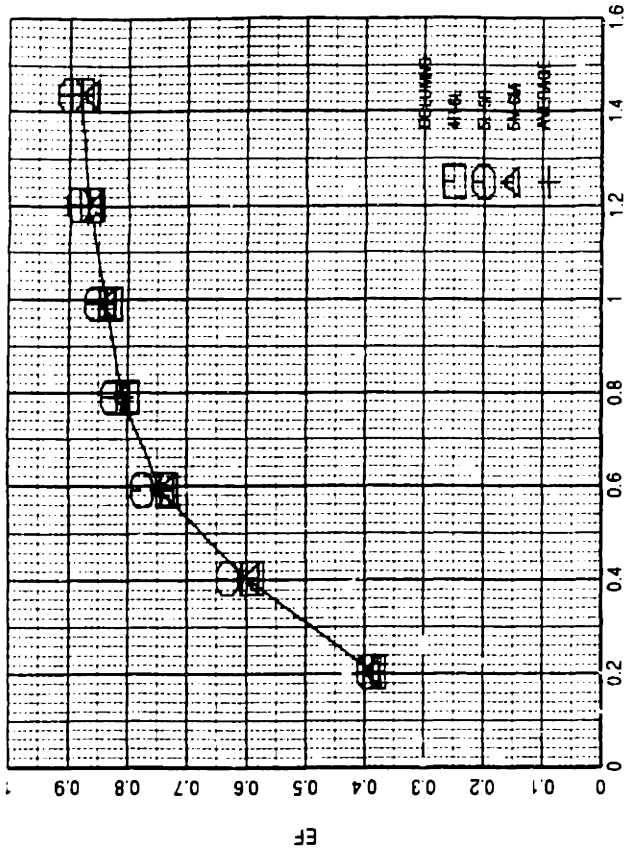
INJECTION ANGLE = 11.5 DEG.
X/S = 0.37



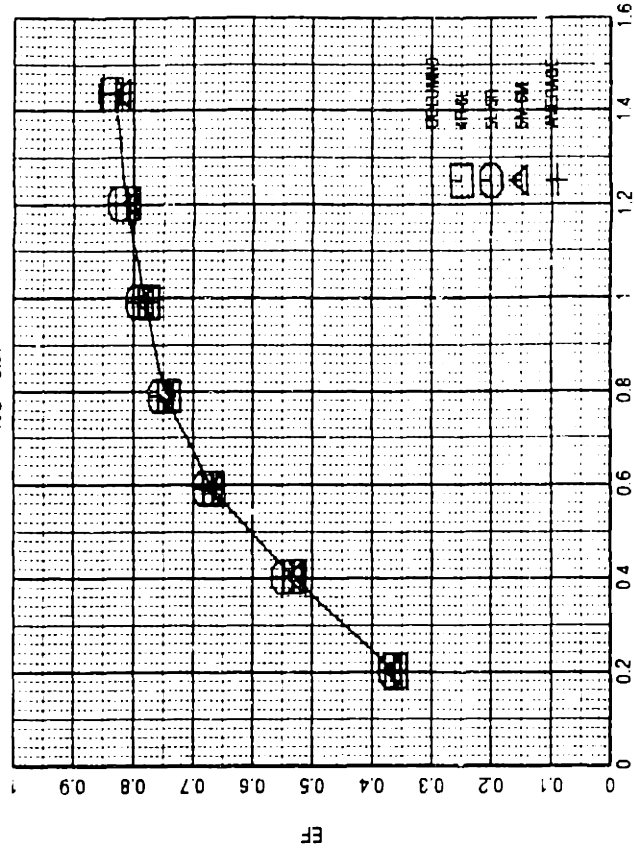
INJECTION ANGLE = 11.5 DEG.
X/S = 1.60



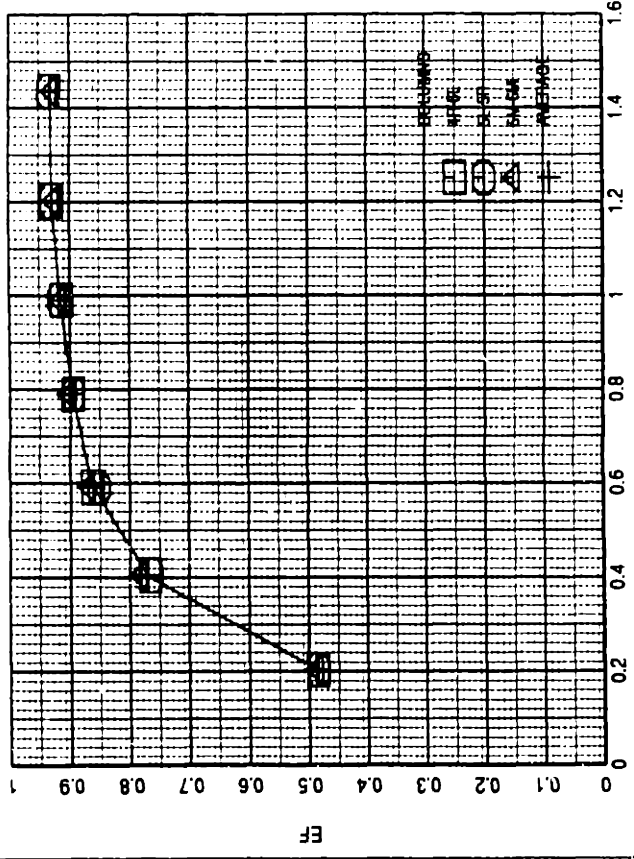
INJECTION ANGLE = 11.5 DEG.
X/S = 7.74



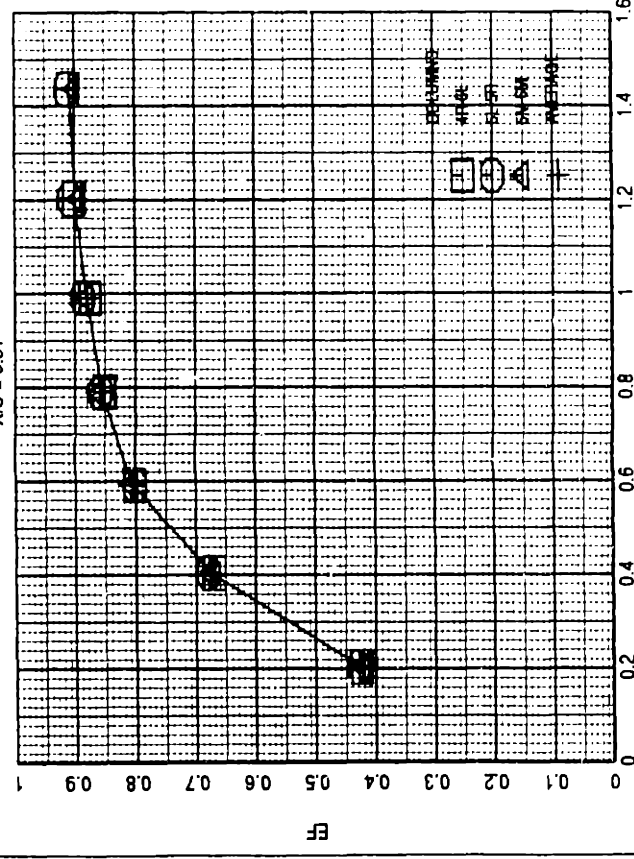
INJECTION ANGLE = 11.5 DEG.
X/S = 8.97



INJECTION ANGLE = 11.5 DEG.
X/S = 5.28



INJECTION ANGLE = 11.5 DEG.
X/S = 6.51



INJECTION ANGLE = 11.5 DEG.

